Receptor protein-tyrosine phosphatases controlling activity of the oncoprotein FLT3 ITD

Dissertation
zur Erlangung des akademischen Grades
Doctor rerum naturalium (Dr. rer. nat.)

vorgelegt dem Rat der Medizinischen Fakultät
der Friedrich-Schiller-Universität Jena

vorgelegt von M. Sc. Anne Kresinsky
geboren am 13.05.1990 in Elsterwerda

Gutachter:

1. PD Dr. rer. nat. habil. Jörg Paul Müller, Universitätsklinikum Jena
2. Apl. Prof. Dr. rer. nat. habil. Frank-Dietmar Böhmer, Universitätsklinikum Jena
3. Prof. Dr. med. habil. Carsten Müller-Tidow, Universitätsklinikum Heidelberg

Tag der öffentlichen Verteidigung: 15.01.2019

Table of Contents

Abbreviations

aa	Amino acid
AKT	Protein kinase B
AML	Acute myeloid leukemia
APS	Ammoniumpersulfate
BCR	B cell receptor
BFU	Burst forming unit (erythroid progenitor colony forming units)
BM	Bone marrow
BSA	Bovine serum albumin
C/EBPalpha	CCAAT/estradiol-binding protein alpha
CAR	Chimeric Antigen Receptor
CFU	Colony forming unit
CFU GEMM	CFU of multipotential granulocyte, erythroid, macrophage, megakaryocyte precursors
CFU GM	CFU of granulocyte/macrophage precursors
CLP	Common lymphoid progenitor
CMML	Chronic myelomonocytic leukemia
CMP	Common myeloid progenitor
DAB	3, 3` diaminobenzidine
DEP-1	Density enhanced phosphatase 1 (synonyms: Ptprj, CD148)
DNMT3a	DNA (cytosine-5)-methyltransferase 3 alpha
DPI	Diphenyleneiodonium
DUSP	Dual-specific protein tyrosine phosphatases
EDTA	Ethylenediaminetetraacetic acid
EPO	erythropoietin
ER	Endoplasmatic reticulum
ERK1/2	Extracellular signal-regulated kinase 1/2
ETO	Eight-Twenty one oncoprotein
FBS	Fetal bovine serum
FDA	Food and Drug Administration
FL	FLT3 ligand
FLK2	Fetal liver kinase 2
FLT3	FMS like tyrosine kinase
FN-III	fibronectin type III repeat
FW	Forward
GAP	GTPase activating protein
G-CSF	Granulocyte colony stimulating factor
GFP	Green fluorescent protein
GMP	Granulocyte/macrophage progenitor
GMPL	Granulocyte-monocyte-lymphoid progenitor
Grb2	Growth factor receptor-bound protein 2
hiFBS	Heat inactivated fetal bovine serum
HSC	Hematopoietic stem cell
IDH2	Isocytratdehydrogenase 2
IHC	Immunohistochemistry
IL-3	interleukin 3
IL-6	interleukin 6
inv	Inversion
ITD	Internal tandem duplication
JAK	Janus kinase family
JMD	Juxtamembrane domain
ko	Knockout
Lin^-	Lineage negative
LMPP	Lymphoid-primed MPP

LSK cells	Lin^- $Sca\text{-}1^+$ $c\text{-}kit^+$ cells
MAPK	Mitogen-activated protein kinase
MEP	Megakaryocyte/erythrocyte progenitor
MLL	Myeloid-lymphoid or mixed-lineage leukemia
MPN	Myeloprolifeative neoplasm
MPO	Myeloperoxidase
MPP	Multipotent progenitors
MS	Multiple Sclerosis
NDS	Normal donkey serum
NK cells	Natural killer cells
Nox4	NADPH oxidase 4
NP 40	Tergitol-type NP-40
NPM1	Nucleophosmin gene 1
NRPTP	Non-receptor protein tyrosine phosphatase
OB	Osteoblast
OC	Osteoclast
PBS	Phosphate buffered saline
PCR	Polymerase chain reaction
PEI	Polyethylenimine
PNK	Polynucleotide kinase
PP14	Placental protein 14
PTK	Protein tyrosine kinase/ kinases
PTP	Protein tyrosine phosphatase/phosphatases/phosphatases
Ptprc	Protein tyrosine phosphatase receptor-like c
Ptprj	Protein tyrosine phosphatase receptor-like j
RBC	Red blood cells
REV	Reverse
ROS	Reactive oxygen species
RPTP	Receptor-like protein tyrosine phosphatase/phosphatases
RTK	Receptor tyrosine kinase/kinases
RUNX1	Runt-related transcription factor 1
SCF	stem cell factor
SCID	Severe combined immune deficiency
SDS	Sodiumdodecylsulfate
SEM	Standard error of the mean
SFK	Src family kinases
SNP	Single nucleotide polymorphisms
STAT 5	Signal transducer and activator of transcription 5
t	Translocation
TBS-T	TBS-Tween
TCR	T cell receptor
TEMED	Tetramethylethylen diamin
TET2	Ten Eleven Translocation 2
TKD	Tyrosine kinase domain
TKI	Tyrosine kinase inhibitor/inhibitors
TMD	Transmembrane domain
WBC	White blood cells
Y	Tyrosine residue

Zusammenfassung

In etwa 25 % der Patienten mit akuter myeloischer Leukämie (AML) treten interne Duplikationen (ITD) in der juxtamembranen Domäne des Rezeptors auf, die zu einer konstitutiv aktiven Kinase mit veränderter Signalaktivität führen. Trotz der Entwicklung und Zulassung von kleinen Tyrosinkinase-Inhibitoren (TKI), die FLT3 ITD inaktivieren, bleibt AML eine Erkrankung mit schlechter klinischer Prognose. Bei AML-Patienten treten häufig Rückfälle auf, welche teilweise auf zusätzliche erworbene Mutationen von FLT3 ITD zurückzuführen sind und zu einer Resistenzbildung der Kinase gegen TKI beitragen. Die 5-Jahres-Überlebensrate beträgt lediglich 40 - 50 %. Daher sind alternative Behandlungsstrategien von FLT3 ITD-positiven AML-Patienten wichtig.
Unsere Arbeitsgruppe hat die regulierende Rolle der Rezeptor-Protein-Tyrosin-Phosphatasen (RPTP) Ptprj/DEP-1 und Ptprc/CD45 auf das FLT3-Wildtypprotein in Modellzellsystemen gezeigt. Darüber hinaus zeigen Array-Daten, dass ein niedriges Expressionslevel von Ptprj oder Ptprc zu einer schlechteren Prognose von FLT3 ITD-positiven AML-Patienten führt.

Um die regulatorische Funktion von Ptprj und Ptprc auf die FLT3 ITD-Aktivität *in vitro* weitergehend zu untersuchen, wurden die Ptprj bzw. Ptprc Gene in dem Modellzellsystem 32D muFLT3 ITD inaktiviert. Die in dieser Arbeit dargestellten Ergebnisse deuten auf eine Beeinflussung beider RPTP auf die Aktivität von FLT3 ITD hin. Die größten Effekte in Hinblick auf die Inaktivierung der RPTP wurden in Bezug auf die Src-Aktivität beobachtet. Gegenwärtig kann nicht differenziert werden, ob die Beeinflussung der FLT3 ITD Aktivität direkt oder indirekt erfolgt. Es lässt sich vermuten, dass neben spezifischen Effekten auf FLT3 ITD noch weitere physiologische Funktionen durch die beiden RPTP beeinflusst werden.

Um die Rolle von Ptprj und Ptprc auf FLT3 ITD *in vivo* zu untersuchen, wurden $Ptprj^{-/-}$ bzw. $Ptprc^{-/-}$ in $FLT3^{ITD/ITD}$ Mäusen inaktiviert. $FLT3^{ITD/ITD}$ $Ptprj^{-/-}$ Mäuse zeigten eine drastische Verkürzung der Lebensdauer, Leukozytose, einer drastisch verringerte B-Zellpopulation und eine Infiltration myeloischer Zellen in peripheren Organen, was zu Splenohepatomegalie und anormaler Organarchitektur führte. $FLT3^{ITD/ITD}$ $Ptprj^{-/-}$ Mäuse zeigten weiterhin eine stärker ausgeprägte myeloproliferative Neoplasie mit extramedullärer Hämatopoese, als für $FLT3^{ITD/ITD}$ Mäuse gezeigt. Die erhöhte FLT3 Phosphorylierung in $FLT3^{ITD/ITD}$ $Ptprj^{-/-}$ Mäusen zeigte, dass der beobachtete Phänotyp auf eine erhöhte FLT3 ITD-Aktivität zurückgeführt werden kann.

Die Inaktivierung des Ptprc Gens in $FLT3^{ITD/ITD}$ Mäusen führte zu einer dramatischen Verkürzung der Lebensdauer, einem ähnlichen hämatologischen Phänotyp wie in $FLT3^{TD/ITD}$ $Ptprj^{-/-}$ Mäusen sowie zur Entwicklung einer schweren Monozytose. Außerdem wurde eine Leukozytose mit anämischen Merkmalen, und ein Mangel an Lymphozyten sowie Thrombozyten beobachtet. Eine myeloproliferative Neoplasie, welche durch starke Infiltration myeloischer Zellen in periphere Organe gekennzeichnet war, führte zu einer Splenohepatomegalie und einer Nephromegalie. Darüber hinaus wurden signifikant erhöhte Mengen an hämatopoetischen Vorläufer- und Stammzellen sowie Megakaryozyten in den peripheren Organen gefunden, was wiederum auf eine extramedulläre Hämatopoese hindeutet. Die phänotypischen Veränderungen waren mit einer erhöhten onkogenen Signalaktivität von FLT3 ITD und der Aktivierung des nachgeschalteten Zielproteins STAT5 verbunden. Diese Daten zeigten, dass Ptprc die FLT3 ITD-Signalaktivität *in vivo* beeinflusst. Darüber hinaus zeigten histopathologische und computertomographische (CT) Untersuchungen der $FLT3^{ITD/ITD}$ $Ptprc^{-/-}$ Mäuse einen unerwarteten Knochenphänotyp wie verkürzte Knochenlänge, reduzierte Knochendichte, erhöhtes Knochenvolumen und erhöhter Oberflächenrauheit sowie ektopische Knochenbildung in peripheren Organen was in keiner der Kontrolltiere festgestellt wurde. Diese Beobachtungen deuten auf eine bisher unerwartete Rolle von FLT3 ITD (und vermutlich FLT3) bei der Regulierung der Knochenentwicklung und des Knochenumbaus hin.

Zusammenfassend konnte die regulierende Rolle von Ptprj und Ptprc auf die onkogene FLT3 ITD-Aktivität *in vivo* nachgewiesen werden. Ähnliche physiologische Effekte in Antwort auf die Inaktivierung von Ptprj oder Ptprc in vitro und in vivo deuten auf eine ähnliche Wirkungsweise der beiden Membran-gebundenen Proteintyrosin-Phosphatasen hin.

Summary

Activating internal tandem duplication (ITD) mutations in the juxtamembrane domain of FLT3 leading to constitutively active kinase with altered signaling quantity were identified in about 25 % of acute myeloid leukemia (AML) patients. Despite development and approval of small tyrosine kinase inhibitors (TKI), targeting FLT3 ITD, AML remains a disease with poor clinical prognosis. AML patients frequently relapse partially due to additional acquired mutations on FLT3 ITD resulting in resistance of kinases to TKI. The 5-year survival rate is only 40-50 %. Alternative treatment strategies of FLT3 ITD-positive AML patients are urgently needed.
Recently our research group observed an attenuating role of receptor protein-tyrosine phosphatases (RPTP) Ptprj/DEP-1 and Ptprc/CD45 on FLT3 wild type protein in model cell systems. In addition, array data demonstrated that low level of Ptprj and Ptprc, respectively result in poor prognosis of FLT3 ITD positive AML patients.

To get further inside in the regulatory function of Ptprj and Ptprc on FLT3 ITD activity *in vitro*, Ptprj or Ptprc genes were inactivated in the model cell system 32D muFLT3 ITD cells. The results presented in this thesis suggest that both RPTP influence the activity of FLT3 ITD. The greatest effects in terms of inactivation of RPTP were observed in terms of Src activity. At present it cannot be differentiated whether the FLT3 ITD activity is directly or indirectly influenced. It can be assumed that in addition to specific effects on FLT3 ITD, other physiological functions are influenced by the two RPTP.

To study the role of Ptprj and Ptprc on FLT3 ITD *in vivo* $Ptprj^{-/-}$ or $Ptprc^{-/-}$ was inactivated in $FLT3^{ITD/ITD}$ mice. $FLT3^{ITD/ITD}$ $Ptprj^{-/-}$ mice demonstrated drastically shortened life span, leukocytosis, drastically decreased B cell population and infiltration myeloid cells in peripheral organs, leading to splenohepatomegaly and aberrant organ architecture. $FLT3^{ITD/ITD}$ $Ptprj^{-/-}$ mice showed a further pronounced myeloproliferative neoplasm with extramedullary hematopoiesis as demonstrated for $FLT3^{ITD/ITD}$ mice. Increased FLT3 phosphorylation in $FLT3^{ITD/ITD}$ $Ptprj^{-/-}$ mice indicated that the observed phenotype is due to increased FLT3 ITD activity.
Inactivation of Ptprc gene in $FLT3^{ITD/ITD}$ mice resulted in drastically shortened life span, similar hematopoietic phenotype like in $FLT3^{ITD/ITD}$ $Ptprj^{-/-}$ and development of severe monocytosis. In addition, leukocytosis with anemic features, lack of lymphocytes and platelets were observed. Myeloproliferative neoplasm was characterized by severe infiltration of myeloid cells in peripheral organs which resulted in splenohepatomegaly as well as nephromegaly. Furthermore, significantly increased amount of hematopoietic

progenitor and stem cells and surprisingly megakaryocytes were observed in peripheral organs indicating extramedullary hematopoiesis. Phenotypic alterations were associated with increased oncogenic signaling of FLT3 ITD and activation of downstream target STAT5. These data demonstrated that Ptprc affects FLT3 ITD signaling activity *in vivo*. In addition, histopathology and computed tomography (CT) revealed unexpected bone phenotype with shortened bone length, reduced bone density, increased bone volume and increased surface roughness along with ectopic bone formation in peripheral organs in $FLT3^{ITD/ITD}$ $Ptprc^{-/-}$ mice but in none of the control animals. These observations suggest a previously unexpected role of FLT3 ITD (and presumably FLT3) to regulate bone development and remodelling.

Taken together, regulatory role of Ptprj and Ptprc on oncogenic FLT3 ITD activity could be demonstrated *in vivo*. Similar *in vitro and in vivo* physiologic effects in response of inactivation of Ptprj or Ptprc indicate similar mode of action of both membrane bound PTP.

1. Introduction

1.1 Hematopoietic system

The mammalian hematopoietic system contains more than ten different mature cell types deriving from a common progenitor, the hematopoietic stem cell (HSC). The process of blood cell differentiation – hematopoiesis – is a dynamic and hierarchical process to maintain self-renewal capacity of HSC as well as to generate progeny of fully functional mature hematopoietic cells throughout lifetime (Seita and Weissman 2010). By undergoing specific differentiation HSC lose their self-renewal capacity. First HSC differentiate into multipotent progenitors (MPP) which can still differentiate into all lineages but have lost their self-renewal capacity. MPP perform then lineage restricted differentiation into either common myeloid (CMP) or common lymphoid progenitors (CLP) (Reya et al. 2001). From CMP evolve megakaryocyte-erythrocyte progenitors (MEP), granulocyte-macrophage progenitors (GMP) and mast cells. GMP will differentiate into basophil, neutrophil or eosinophil granulocytes or into monocytes which subsequently differentiate into macrophages and myeloid dendritic cells. MEP develop into erythrocytes or megakaryocytes which differentiate into platelets. B cells, T cells, natural killer (NK) cells and lymphoid dendritic cells, the so called lymphoid lineage, mature from CLP (Figure 1) (Giebel and Punzel 2008).

Imbalances in regulation of hematopoiesis e.g. caused by genetic alterations of HSC or progenitors lead to hematopoietic malignancies like leukemia or myeloproliferative neoplasms (MPN). These disorders can be classified by cellular origin – myeloid or lymphoid – or by progression of disease – chronic or acute (Sell 2005).

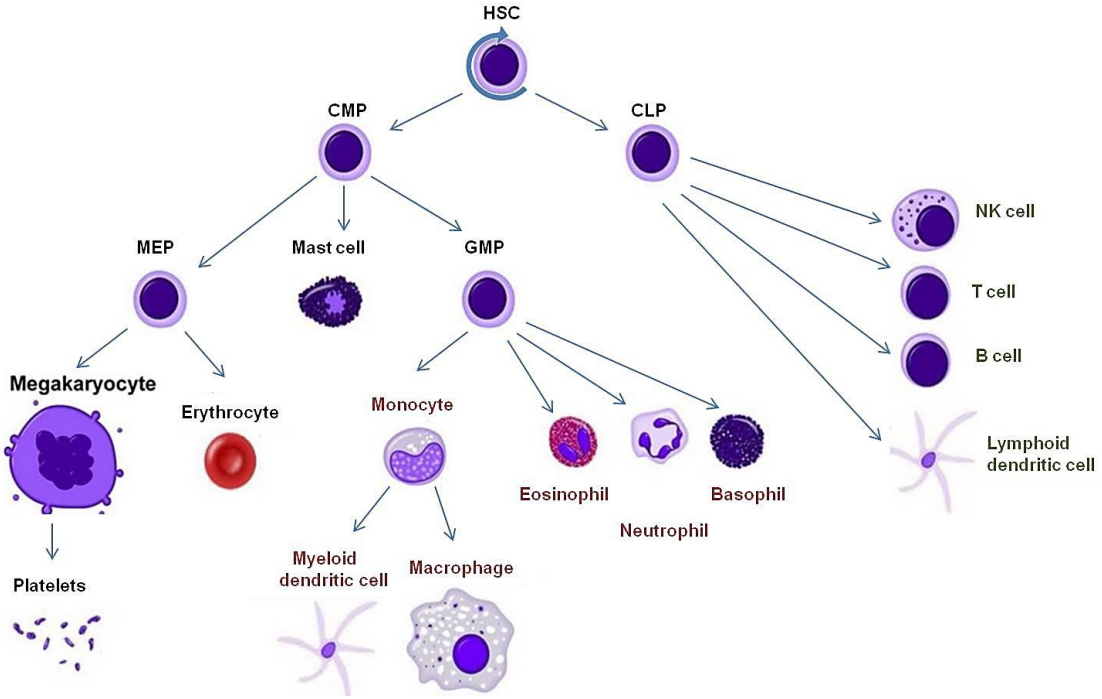

Figure 1. Hierarchy of hematopoietic system. Hematopoietic stem cells (HSC) balance self-renewal and differentiation to maintain blood production throughout life time. HSC differentiate into lineage specific common myeloid progenitor (CMP) or common lymphoid progenitor (CLP). CLP differentiate into lymphoid cells (cell types labeled in green) including natural killer (NK) cells, B cells, T cells and lymphoid dendritic cells. CMP differentiate either into megakaryocyte-erythrocyte progenitors (MEP), mast cells or granulocyte-macrophage progenitors (GMP). The myeloid differentiated lineage (cell types labeled in red) arisen from GMP is composed of eosinophil, basophil and neutrophil granulocytes as well as monocytes which further differentiate into macrophages and myeloid dendritic cells. MEP differentiate into erythrocytes or megakaryocytes subsequently producing platelets. Figure adapted from Stirewalt & Radich (Stirewalt and Radich 2003).

1.2 Acute myeloid leukemia (AML)

1.2.1 General aspects of AML

AML is a phenotypically and genetically heterogeneous disease of hematopoietic myeloid progenitor cells characterized by uncontrolled proliferation and impaired function due to undifferentiated phenotype (Fröhling et al. 2005). These abnormal progenitor (blast) cells accumulate in the bone marrow and peripheral organs, leading to displacement of mature functional hematopoietic cells and organ failure. Symptoms of AML are fatigue, weakness, hepatomegaly, splenomegaly, fever, increased infection susceptibility and bleeding (Liesveld 2010, Döhner et al. 2015). AML has a very drastic progression leading to death within one year without treatment (Estey and Döhner 2006, Schlenk et al. 2008). Poor prognosis for AML especially for patients at age 65 and older has been described. AML is a disease of mainly elderly people but also occurs in children. The median age at diagnosis is 68 years (Figure 2). The median age at death is 72 years (Howlader N 2017) (Figure 2). It is the most common myeloid leukemia with a prevalence of 4.2 cases per 100 000 adults (Liesveld 2010). AML can be acquired by

several risk factors like ionizing radiation or benzene (smoking) (Kane et al. 1999). In 10 - 15 % AML evokes as a secondary disease after cytotoxic chemotherapy (Smith et al. 2003).

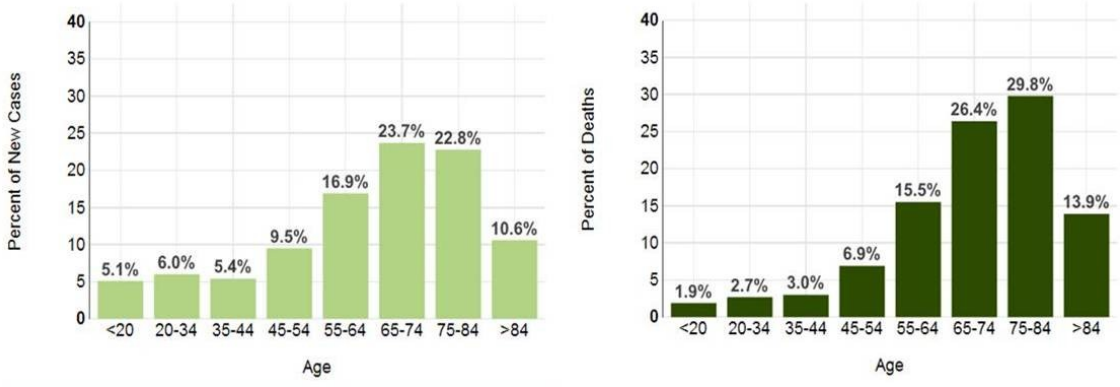

Figure 2. Age-dependent new cases and deaths of AML patients. Percentage of newly diagnosed AML cases (upper panel) and percentage of deaths (lower panel) are presented in relation to age. Figure from https://seer.cancer.gov/statfacts/html/amyl.html (visited 28.03.2018)

In 2008 AML has been classified by world health organization (WHO) in molecular groups according to chromosome aberrations (e.g. reciprocal translocations, inversions, insertions, deletions, trisomies, and monosomies) (Vardiman et al. 2009). More recent screening of 1540 AML patients has demonstrated that roughly 50 % of patients do not fit into this classification although carrying driver mutations (Papaemmanuil et al. 2016). Thus, a new classification of AML was performed including genomic issues. 11 new subgroups of AML have been evaluated partly corresponding to WHO classification (Papaemmanuil et al. 2016). Additionally so called diver mutations have been found in AML patients affecting treatment and survival.

Molecular characterization of leukemia has demonstrated that genetic alterations in the leukemia clone frequently fall into two classes: Those affecting transcription factors interfering with hematopoietic differentiation (e.g. AML1-ETO, RUNX1, CEBPA, MLL, Hox genes) and mutations affecting genes involved in signal transduction conferring proliferative and survival advantage to cells (e.g. activating mutations of FLT3 and c-Kit). This has favored a two-hit model of leukemogenesis. The collaboration of these two classes of genetic alterations is necessary for malignant transformation of hematopoietic progenitor cells (Kelly and Gilliland 2002, Fröhling et al. 2005, Schlenk et al. 2008, Schessl et al. 2005, Pinheiro et al. 2007). Mouse experiments have demonstrated that just one type of mutation affecting either proliferation or differentiation is sufficient to cause MPN but will not result in AML (Downing 2003). Recent genetic studies have demonstrated that another group of mutations targeting epigenetic modifications (e.g. TET2, IDH2, DNMT3a) also contributes to AML development and outcome (Lagunas-Rangel et al. 2017).

1.2.2 Therapeutic strategies for AML

Due to the fact that AML is a heterogeneous group of disorders, different treatment strategies are inevitable. In young AML patients (< 60 years), intensive chemotherapy is often used with Cytarabine and Anthracyclines leading to 25 - 75 % cure. Allogenic bone marrow transplantation represents an alternative treatment. Since only less than 10 % of older patients will survive such a harsh therapy, alternative treatment strategies are urgently needed (Estey and Döhner 2006, Schlenk et al. 2008). Supporting chemotherapy by inhibition of receptor tyrosine kinases (RTK) which are involved in tumor progression via tyrosine kinase inhibitors (TKI) has been demonstrated as alternative therapy. These small-molecule inhibitors have been first used for inhibition of BCR-ABL fusion protein tyrosine receptor in chronic myeloid leukemia (Druker et al. 2001). All TKI interact with the ATP-binding site of TKD and competitively inhibit ATP binding. Thereby, TKI prevent receptor phosphorylation and activation of downstream signaling. Small inhibiting molecules targeting RTK e.g. FLT3 exist in first and second generation. First generation TKI like Midostaurin (PKC412) lack specificity for FLT3, and also target other RTK and downstream targets of FLT3. This increases cytotoxicity but also increases off target effects. Midostaurin has been approved by the Food and Drug Administration in April 2017 (Levis 2017). Combined with chemotherapy Midostaurin has been introduced as new AML treatment strategy (Stone et al. 2017). Second generation TKI like Quizartinib (AC220) mainly targeting FLT3 have less off target effects and are in phase III of clinical trials. Because epigenetic modifications have been demonstrated to be linked to AML hypomethylating agents have been tested in AML patients. In older patients, the use of hypomethylating agents has improved median and short-term overall survival but has not translated into improved cure rates, which remain disappointingly low (Dombret and Gardin 2016).

1.3 Receptor-type tyrosine kinases

1.3.1 General aspects on receptor-type tyrosine kinases

Balanced protein tyrosine phosphorylation is essential to regulate several cellular processes including differentiation, cell growth, migration, survival and apoptosis (Cohen 2002, Hendriks and Pulido 2013). Besides, reversible phosphorylation plays a pivotal role in intracellular communication, e.g. PI3K/AKT pathway, Ras/ERK1/2 and SFK pathway. Signal transfer is tightly regulated by activity of protein tyrosine kinases (PTK), resulting in phosphorylation and activity of protein tyrosine phosphatases (PTP), dephosphorylating substrate proteins carrying a phosphorylated tyrosine residue. PTK can be subgrouped into two classes: cytoplasmic and transmembrane receptor-type

tyrosine kinases (RTK). RTK were subgrouped on basis of amino acid (aa) sequence homologies (Ullrich and Schlessinger 1990, Robinson et al. 2000). All RTK consist of an extracellular domain to interact with ligands e.g. growth factors, hormones and cytokines, a membrane spanning part and an intracellular domain with protein tyrosine kinase activity and a C-terminal domain. Within all classes of mammalian RTK the consensus sequence the in kinase domain is conserved. Activation of RTK is induced by ligand binding accompanied by conformational alterations in the extracellular domain. RTK catalyzes trans-autophosphorylation of their tyrosine residues within their polypeptide chains (Ullrich and Schlessinger 1990). Several gene encoding RTK have been identified as proto-oncogenes, particularly for EGFR, PDGFR β (Golub et al. 1994), c-KIT (Beghini et al. 2000) and FLT3 (Drexler 1996, Lyman and Jacobsen 1998).

1.3.2 FMS-like tyrosine kinase 3

1.3.2.1 Structure and expression profile of FLT3

FMS-like tyrosine kinase 3 (FLT3) also designated as fetal liver kinase 2 (FLK2) or CD-marker antigen 135 (CD135) has been independently cloned by two groups using murine fetal liver cells or placental cells (Matthews et al. 1991, Rosnet et al. 1991). FLT3 belongs to class III RTK. Murine FLT3 has been identified to share 86 % sequence identity of protein level with human FLT3. Human FLT3 encodes two splicing forms: a 993 aa and a 952 aa long form. Murine FLT3 encodes a 1000 aa long protein. It is comprised of five immunoglobulin-like domains in the extracellular domain, a single transmembrane domain (TMD), a juxtamembrane domain (JMD) and a split tyrosine kinase domain linked by a kinase-insert, followed by a C-terminal domain (Agnes et al. 1994, Griffith et al. 2004, Takahashi 2011, Small et al. 1994) (Figure 3). The most frequent mutations of FLT3 are internal tandem duplications (ITD) in the JMD of FLT3 resulting in ligand-independent constitutive active kinase (Figure 3).

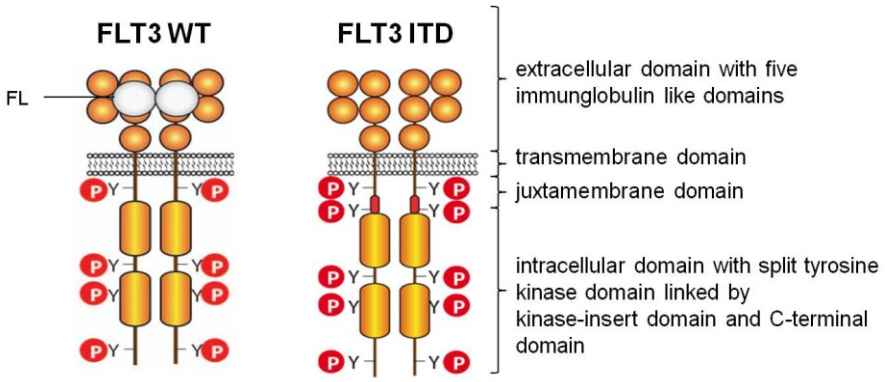

Figure 3. Wild type FLT3 and oncogenic FLT3 ITD. FLT3 consists of five extracellular immunoglobulin-like domains, a transmembrane domain, a juxtamembrane domain and a split tyrosine kinase domain linked by a kinase-insert domain, and a C-terminal domain. FLT3 WT dimerizes upon ligand binding of FLT3 ligand (FL). FLT3 ITD has an ITD mutation in the JMD resulting in ligand-independent dimerization and constitutive active kinase (modified according to (Müller et al. 2012))

FLT3 expression slightly differs in man and mouse. In humans FLT3 expression occurs at low level in HSC and CMP and at high levels in CLP and GMP but not in mast cells (Hjertson et al. 1996) and MEP (Kikushige et al. 2008). Murine FLT3 expression has been demonstrated in CLP (Kikushige et al. 2008). For the myeloid lineage controversial results have been obtained concerning the expression of FLT3. While Kikushige and colleagues have demonstrated FLT3 expression in all progenitors of granulocyte / macrophage pathway including CMP and GMP, Boyer and colleagues have demonstrated a lack of FLT3 expression on CMP (Kikushige et al. 2008, Boyer et al. 2011). Furthermore, FLT3 is expressed in lymphoid organs such as liver, spleen, thymus and placenta but probably just because of invasion of FLT3-expressing hematopoietic cells and not due to organ FLT3 expression itself (Rosnet et al. 1993). FLT3 WT is expressed at high levels in cells of most AML patients (Gilliland and Griffin 2002, Carow et al. 1996, Rosnet et al. 1996).

1.3.2.2 FLT3 activation, signaling and function in hematopoiesis

Biogenesis of FLT3 comprises synthesis in the ER and subsequent transit to Golgi compartment and finally to cell membrane, with accompanying changes in glycosylation pattern (Schmidt-Arras et al. 2005). The immature high-mannose form of FLT3 (130 kDa) is located in the endoplasmic reticulum (ER) (Schmidt-Arras et al. 2005) or ER near compartments (Koch et al. 2008). Mature FLT3 (150 kDa) is highly glycosylated and membrane associated.

Wild type FLT3 receptor is localized in the cell membrane in a monomeric form. This inactive state conformation of the receptor prevents dimerization by steric inhibition. The phosphoryl acceptor site of the tyrosine kinase domain is blocked by the JMD (Stirewalt and Radich 2003). Upon ligand binding of FLT3 ligand (FL) dimerization of FLT3 is promoted and subsequent activation of intrinsic kinase activity occurs resulting in trans-autophosphorylation of tyrosine residues. Of special importance for this thesis are in particular phosphorylation sites Y589 and Y591 in the JMD (Verstraete and Savvides 2012, Griffith et al. 2004). The phosphorylated receptor serves as a docking site for several intracellular signaling molecules including the p85 subunit of phosphatidyl-inositol 3-kinase (PI3K), phospholipase C-γ (PLC-γ), SH2 (Src homology domain 2) containing proteins, growth factor receptor-bound protein 2 (Grb2), extracellular signal-regulated kinase 1/2 (ERK1/2), Fyn kinase (Src family kinase), protein kinase B (AKT) and Src-like non-receptor kinases (Rosnet et al. 1996, Dosil et al. 1993, Zhao et al. 2000, Levis et al. 2006, Chougule et al. 2016, Schmidt-Arras et al. 2009). FLT3–mediated phosphorylation of these adapter proteins results in activation of PI3K/AKT pathway which is involved in cell cycle progression and Ras-Raf-ERK1/2

signaling cascade that regulates mitosis and proliferation (Dosil et al. 1993). Only minor effects of FLT3 on activation of signal transducer and activator of transcription 5 a (STAT5a) and STAT5b have been demonstrated (Zhang et al. 2000, Rocnik et al. 2006).

FLT3 plays a pivotal role in hematopoietic development. In normal hematopoiesis FLT3 is known to promote proliferation, survival and differentiation of MPP and CLP (Hudak et al. 1995). Its expression is associated with loss of self-renewal potential of HSC (Adolfsson et al. 2001). Interestingly, mice deficient for FLT3 demonstrated normal mature hematopoietic populations, disruption of FLT3 led to deficiencies in primitive hematopoietic progenitors. In addition, the positive role of FLT3 on MPP and lymphoid differentiation, especially B cells was demonstrated (Mackarehtschian et al. 1995). However, several studies demonstrated that FLT3 function is cell-type specific and dependent on growth factors and cytokines (Hudak et al. 1995, Hirayama et al. 1995, Gabbianelli et al. 1995, Haylock et al. 1997). Deregulated activity of FLT3 has been shown to lead to disrupted cellular homeostasis and has been involved in leukemogenesis. Activating internal tandem duplication (ITD) mutations of FLT3 has been found in about 25 % of AML patients (see chapter 1.3.3). Other FLT3 mutations found in leukemia and hematopoietic malignancies are point mutations in the activation loop of tyrosine kinase domain (predominantly D835Y), represented in 5 % of AML cases (Abu-Duhier et al. 2001, Yamamoto et al. 2001, Meshinchi and Appelbaum 2009, Gilliland and Griffin 2002) and ITD mutations in the tyrosine kinase domain (Breitenbuecher et al. 2009). FLT3 ITD mutations contribute to growth factor independent growth, resistance to apoptosis as well as resistance to tyrosine kinase inhibitors (TKI) in chemotherapy (Fröhling et al. 2007, Gilliland and Griffin 2002, Kayser et al. 2009).

1.3.3 FLT3 ITD

1.3.3.1 Altered signaling quality and transforming capacity of oncogenic FLT3 ITD

In 1996 ITD mutations in the JMD of FLT3 have been first reported in AML patients (Nakao et al. 1996). These mutations are localized mainly between exon 14 and 15 of the JMD. Their length varies from 3 to 1236 base pairs from case to case (Stirewalt and Radich 2003, Schnittger et al. 2002, Gilliland and Griffin 2002). The ITD mutation in the JMD abrogates its inhibitory function of this domain for the TKD. Thus, ITD mutations of FLT3 results in ligand-independent dimerization and tyrosine autophosphorylation (Kiyoi et al. 1998) leading to constitutive active tyrosine kinase (Griffith et al. 2004) (Figure 3).

While FLT3 WT predominantly occurs in its 150 kDa complex glycosylated form, FLT3 ITD predominantly exists in the high-mannose form (Schmidt-Arras et al. 2005). Impaired maturation is dependent on kinase activity. It has been demonstrated that because of

complex formation with chaperone calnexin FLT3 ITD trafficking is impaired and receptor is retained in the ER or ER near compartments (Schmidt-Arras et al. 2005, Koch et al. 2008). Constitutively active FLT3 ITD contributes to growth factor-independent proliferation and drives aberrant phosphorylation of STAT5, which is tightly associated with strong transforming potential (Stirewalt and Radich 2003, Mizuki et al. 2000, Hayakawa et al. 2000). FLT3 ITD also promotes the production of reactive oxygen species (ROS) by activation of a STAT5-Nox4 axis consequently resulting in genomic instability and reversible inactivation of PTP (Jayavelu et al. 2016, Sallmyr et al. 2008). The SFK Fyn and Src have been reported to interact with FLT3 and contribute to STAT5 driven transformation (Chougule et al. 2016, Leischner et al. 2012). Additionally, FLT3 ITD suppresses CCAAT/estradiol-binding protein alpha (C/EBPalpha) and PU.1, transcription factors that promote myeloid differentiation (Choudhary et al. 2005, Mizuki et al. 2003).

Transgenic mouse models were established to analyze *in vivo* the molecular pathways that play an important role for generation of leukemia with physiologic aberrancies of FLT3. FLT3 ITD knockin mice developed a fully penetrating MPN closely resembling human chronic myelomonocytic leukemia (CMML) (Lee et al. 2007). FLT3 ITD-expressing bone marrow (BM) and spleen cells showed enhanced phosphorylation of FLT3 and STAT5 (Lee et al. 2007). Heterozygous $FLT3^{+/ITD}$ knockin mice developed MPN, characterized by splenomegaly, leukocytosis, and myeloid hypercellularity but did not develop leukemia-like disease. The disease progressed to mortality by 6 to 20 month (Li et al. 2008). Increased levels of granulocytes / monocytes and dendritic cells have been observed. Moreover, a decreased fraction of B lymphocytes has been demonstrated. Activation of FLT3 downstream signaling through STAT5 has been showed by increased expression of STAT5 targets (Chu et al. 2012). Depletion of functional HSC was completely reversible upon treatment with the TKI Sorafenib inhibiting oncogenic FLT3 ITD kinase activity. Loss of wild type allele contributed to myeloid expansion and disease aggressiveness in FLT3 ITD background. Thus, these mouse models revealed that FLT3 ITD alone was capable of developing MPN but no leukemia. Similar results were observed in BM transplantation studies (Kelly et al. 2002). Additional cooperating events, e.g. expression of NUP89-HOXD13 fusion gene, appear to be required to initiate progress to acute leukemia (Greenblatt et al. 2012).

1.3.3.2 Clinical impact of FLT3 ITD

FLT3 ITD is the most common FLT3 mutation and occurs in about 25 % of AML cases (Schlenk et al. 2008, Papaemmanuil et al. 2016). It is associated with poor prognosis, increased relapse and short survival of patients after chemotherapy and transplant

(Fröhling et al. 2005, Kiyoi and Naoe 2006, Olesen et al. 2005). A number of inhibitors of FLT3 signaling have been identified and are in clinical trial to improve clinical outcome of AML patients with FLT3 activating mutation (described in chapter 1.2.2).

Chimeric Antigen Receptor (CAR) T cell therapy is another recent treatment strategy for leukemia. The therapy resulted in long term remission in acute lymphoblastic leukemia (leukemia and lymphoma society 2018). FLT3-CAR T cells has been demonstrated to effectively target FLT3 expressing AML blasts as well as FLT3 expressing cell lines. It has been shown that combinatorial treatment of immunotherapy with TKI treatment increased FLT3 surface expression especially in FLT3 positive AML cells and thus, enhanced recognition of malignant cells by CAR T cells (Reiter et al. 2018, Jetani et al. 2018, Wang et al. 2018).

Another promising AML treatment strategy may be the use of monoclonal FLT3 antibodies. An Fc-optimized antibody directed to FLT3 (termed 4G8SDIEM) has been shown to induce strikingly enhanced cellular toxicity in FLT3 expressing cell lines and AML blasts (Hofmann et al. 2012). Last year, the biotechnology company SYNIMMUNE presented the first Fc-optimized FLT3 directed antibody (FLYSYN) which is used for phase I clinical studies in AML patients (Steiner 2017).

1.4 Protein-tyrosine phosphatases

Dysregulation of tyrosine phosphorylation processes can result in uncontrolled growth, undifferentiated phenotype, impaired apoptosis and increased migration which are characteristics of neoplastic and metastatic diseases. Aberrant PTP signaling is frequently linked to human diseases including cancer, diabetes, as well as cardiovascular, autoimmune and neuropsychiatric disorders (Östman et al. 2006, Tonks 2006, Julien et al. 2011, Hendriks and Pulido 2013, Böhmer et al. 2013a, Alonso et al. 2004, Tautz et al. 2013). Thus, PTP may have the potential to be used as important drug targets and molecular markers in the clinic. Within the PTK family several PTK were identified to have an oncogenic potential. Since PTP counter the activity of PTK it has been assumed that PTP act mainly as tumor suppressors. However, PTP can also activate PTK function. By dephosphorylation of inhibitory tyrosine residues PTP can activate PTK which potentially lead to increased proliferation and activation of known cancer pathway, e.g. Src. The activity of PTK and PTP is a dynamic process which may also result in mutual activation (Fournier et al. 2016).

Most PTP have a catalytic cysteine in their PTP domain. They can be grouped into 3 classes. Class I consists of 111 PTP and represent the biggest class of PTP. It is further subclassified into classical PTP and dual-specific protein phosphatases (DUSP) representing the two biggest subgroups and 4 further groups with few members only (Alonso et al. 2016). The classical PTP are further subdivided into 20 receptor-like

protein tyrosine phosphatases (RPTP) and 17 non-receptor protein tyrosine phosphatases (NRPTP). 13 out of these 20 RPTP contain two conserved intracellular catalytic domains. The membrane proximal domain D1 harbors the catalytic activity and the membrane distal domain D2 as well as the C terminal domain has regulatory function (Barnea et al. 2016). Intracellular and extremely variable extracellular segments are linked by a transmembrane domain (Alonso et al. 2004, Fischer et al. 1991, Alonso et al. 2016). Some RPTP, e.g. Ptprj, have a single intracellular catalytic domain only (Östman et al. 1994).

The majority of PTP are post-translationally modified whereby RPTP are mainly glycosylated. N- and O- linked carbohydrates are linked to the extracellular domain of RPTP. Glycosylation is the prerequisite for surface localization and prop
er maturation of the proteins. Furthermore the catalytic cysteine of the PTP domain of class I and class II PTP is highly susceptible to reversible oxidation by ROS, which leads to inactivation of PTP activity (Alonso et al. 2004).

1.4.1 Receptor protein-tyrosine phosphatase J (Ptprj)

1.4.1.1 Structure and expression profile of Ptprj

Receptor protein-tyrosine phosphatase J, also designated as HPTP-η, CD148 or density enhanced phosphatase 1 (DEP-1) is encoded by the Ptprj gene. In 1994 two separate groups characterized Ptprj in WI-38 human embryonic lung fibroblasts cell line (Östman et al. 1994) or in the human leukemic cell line F36O (Honda, Inazawa et al. 1994). In humans the gene is located at the short arm of chromosome 11 (11p11.2). Human Ptprj is composed of a 970 aa long extracellular domain comprised of eight fibronectin-type III-like (FN-III) domains, a transmembrane domain of 25 aa and an intracellular region of 342 aa containing a single phosphatase domain with intrinsic phosphatase activity (Figure 4) (Östman et al. 1994, Honda et al. 1994). An alternative splice variant of human Ptprj exists, called sPtprj with 539 aa corresponding to the N-terminus of Ptprj extracellular domain. 1996 murine and rat homologues of Ptprj have been identified, exhibiting the same structure as the human Ptprj. Murine Ptprj reveals 71 % sequence identity of the entire protein compared to human Ptprj.

Surface localized Ptprj is highly glycosylated at several residues and has a molecular weight of 180 - 230 kDa in all species. Unglycosylated Ptprj has a molecular weight of 148 kDa (de la Fuente-Garcia et al. 1998).

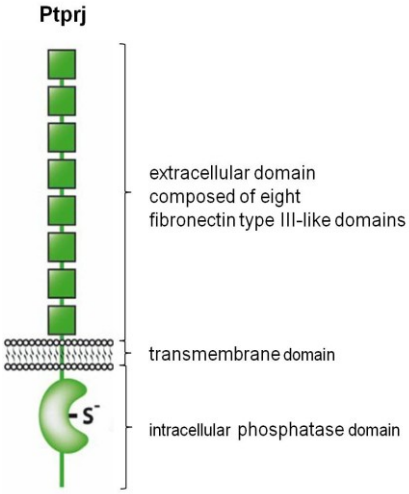

Figure 4. Schematic drawing of Ptprj. Ptprj is a transmembrane PTP consisting of an extracellular domain composed of eight fibronectin-type III-like domains, a transmembrane domain and an intracellular part with phosphatase domain (according to (Müller et al. 2012)).

High expression levels of murine Ptprj were found in brain, kidney, spleen, liver, intestines and low level in all other tissues (Kuramochi et al. 1996, Honda et al. 1993).
Initial studies on adherent cell lines demonstrated a density-dependent increase of Ptprj with highest expression level before the saturation of culture had been reached (Östman et al. 1994, Keane et al. 1996). It was shown that Ptprj is involved in VE-cadherin mediated cell contact inhibition in endothelial cells by dephosphorylation of VEGFR and inhibition of proliferative ERK1/2 pathway (Grazia Lampugnani et al. 2003). Flow cytometric analyses demonstrated Ptprj expression on all human hematopoietic lineages with higher intensity on granulocytes than on monocytes and lymphocytes, on peripheral blood lymphocytes, including CD4 and CD8 positive T cells, B cells, platelets, NK cells, mature thymocytes, dendritic cells and microglia (Schneble et al. 2017). However, a low expression level of Ptprj has been demonstrated in cell lines of B and T cell origin (de la Fuente-Garcia et al. 1998, Gaya et al. 1999).

1.4.1.2 Ptprj mode of action

Both, positive and negative regulation of different signal transduction pathways in hematopoietic cells, have been described for Ptprj including platelets (Senis et al. 2009, Mori et al. 2012), T cells (de la Fuente-Garcia et al. 1998, Tangye et al. 1998), B cells (Skrzypczynska et al. , Zhu et al. 2008), macrophages (Zhu et al. 2008) and myeloid cells (Jayavelu et al. 2016, Arora et al. 2011, Godfrey et al. 2012). Inhibited breast cancer and colon carcinoma growth have been reported due to increased Ptprj expression, introducing Ptprj as tumor suppressor gene with a regulatory function on cell growth (Keane et al. 1996, Balavenkatraman et al. 2006). Loss of the short arm of chromosome 11, including Ptprj gene, has been detected in various tumors like breast cancer, cell carcinoma of bladder, hepatoblastoma and hepatocellular carcinoma (Ruivenkamp et al. 2002). Loss of heterozygosity of Ptprj as well as single nucleotide

polymorphisms (SNP) have been demonstrated in thyroid tumors where Ptprj is downregulated compared to normal thyroid tissues (Iuliano et al. 2004). Low levels or loss of Ptprj have been also observed in colon, mammary and lung cancer (Trapasso et al. 2000), inflamed tissues and high grade carcinomas (Autschbach et al. 1999). Furthermore, Ptprj has been indicated as a candidate for the mouse colon cancer susceptibility locus, Scc1 (Ruivenkamp et al. 2002).

Besides tumor suppressor functions of Ptprj further studies indicate pro-tumorigenic functions of Ptprj. *In vivo* studies in Ptprj$^{-/-}$ mice revealed an essential role of Ptprj in tumor-associated angiogenesis and introduced stroma derived Ptprj as a promoter of tumor progression (Fournier et al. 2016). In addition, an alternative splicing variant of Ptprj (sPtprj), was shown to have pro-angiogenic activity in HUVEC cells. It has been demonstrated that sPtprj is upregulated in glioblastoma, one of the most angiogenic tumors (Bilotta et al. 2017).

1.4.1.3 Substrates of Ptprj

Within others known substrates Ptprj phosphorylates growth factor receptors and PTK like PDGFβ (Kovalenko et al. 2000); VEGFR2 (Chabot et al. 2009), MET (Palka et al. 2003), Lyn (Skrzypczynska et al.), Fyn (Schneble et al. 2017), ERK1/2 (Sacco et al. 2009), FLT3 WT as well as FLT3 ITD (Arora et al. 2011, Godfrey et al. 2012). An interplay of VEGFR2 and Ptprj which leads to activation of Ptprj and subsequently dephosphorylation of Src kinase (Spring et al. 2012, Fournier et al. 2016, Le Pera et al. 2016). Src activity is regulated by two phosphorylation sites: an inhibitory tyrosine and an autophosphorylation site. Originally identified in chicken activating tyrosine residue is at position 416 and inhibitory tyrosine residue 527 (Cooper et al. 1986, Weijland et al. 1996). In mouse Src activity is regulated by tyrosine residues 424 (activating) and 535 (inhibitory) whereas in humans it is regulated by tyrosine residues 419 (activating) and 530 (inhibitory). Autophosphorylation of Y416 is dependent on previous dephosphorylation of the inhibitory Y527. Phosphorylation sites of Src differ slightly in different organisms. Upon Src activation subsequent AKT activation was demonstrated (Chabot et al. 2009). Taken together Ptprj is an important regulator of several cancer pathways such as Ras/ERK1/2, Src and PTEN/PI3K/AKT pathway and shows up mainly as a tumor suppressor gene.

1.4.1.4 Phenotype of Ptprj$^{-/-}$ mice

At organismic level inactivation of Ptprj in mice by in frame replacement of intracellular domain with enhanced green fluorescent protein (GFP) resulted in severe developmental consequences, defects of vascularization and early mortality (Takahashi et al. 2003). Mice lacking Ptprj expression in all cells of hematopoietic origin displayed normal life span but partially impaired B cell development (Zhu et al. 2008). Total genetic ablation of Ptprj is reported to result in normal growth, viability, fertility and development and does not predispose to spontaneous tumorigenesis (Trapasso et al. 2006).

1.4.1.5 Role of Ptprj on FLT3 and FLT3 ITD

In 2011 Ptprj has been identified to negatively regulate FLT3 WT signaling and activity *in vitro* (Arora et al. 2011). Is was also shown that Ptprj directly interacts with FLT3 WT (Böhmer et al. 2013b). Downrregulation of Ptprj resulted in increased AKT and ERK1/2 phosphorylation. Overexpression of Ptprj resulted in decreased phosphorylation of AKT and ERK1/2 phosphorylation. Moreover, it has been shown that FLT3 was hyperphosphorylated in murine myeloblast-like 32D cell line expressing murine FLT3 WT protein (named subsequently 32D muFLT3 WT) cells but not in 32D cell line transduced with murine oncogenic FLT3 ITD (named subsequently 32D muFLT3 ITD (Grundler et al. 2005)) and MV4-11 cells. *In vitro* investigations on FLT3 ITD revealed high ROS levels that oxidize catalytic cysteine of Ptprj and thus impair phosphatase activity. Quenching of cellular ROS levels reactivated Ptprj leading to dephosphorylation of FLT3 ITD in cells *in vitro* (Godfrey et al. 2012). The origin of high ROS levels in cells overexpressing FLT3 ITD and in FLT3 ITD positive primary AML samples has been identified in NADPH oxidase 4 (Nox4), a downstream target of activated STAT5 in oncogenic FLT3 ITD signaling pathway (Jayavelu et al. 2016).

Gene expression study of 285 adults with AML (Valk study GEO accession GSE1159 (Valk et al. 2004)) revealed a negative correlation of Ptprj downregulation and patient survival in FLT3 ITD positive AML patients (Figure 5A). Patients carrying FLT3 ITD mutation and low levels of Ptprj showed a close to significant lower overall survival probability than patients carrying FLT3 ITD with high expression of Ptprj. To the contrary, high Ptprj expression level in AML patients bearing FLT3 WT showed decreased overall survival probability compared to FLT3 WT AML patients with low Ptprj expression level (Figure 5B). These data may indicate an important role of Ptprj in development of FLT3 ITD-driven AML.

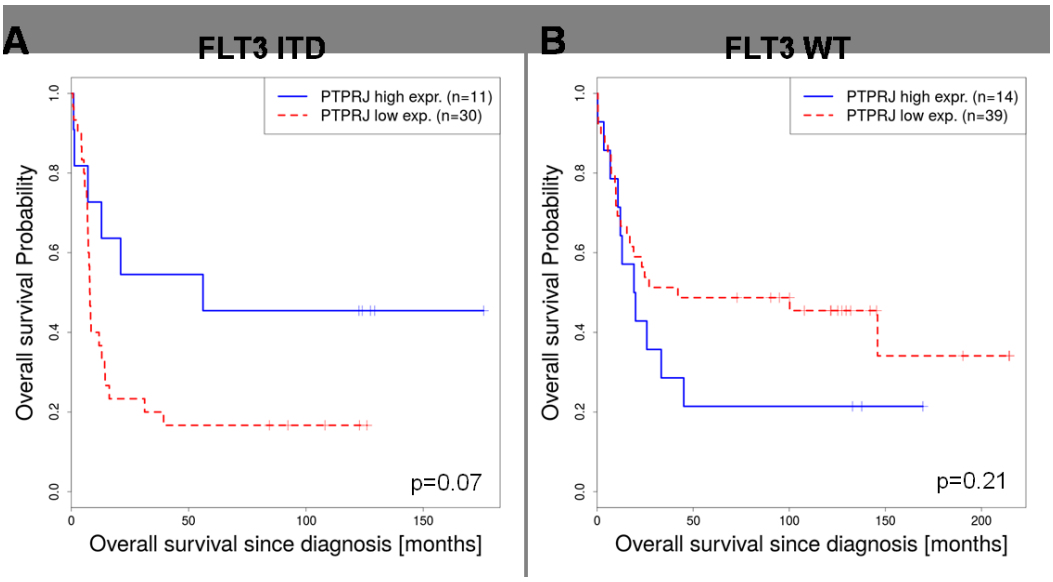

Figure 5. Ptprj expression affects prognosis of AML patient. Overall survival of AML patients (GEO accession GSE1159 (Valk et al. 2004)) with low (red, dotted) and high (blue) PTPRJ expression in FLT3 ITD and FLT3 WT background. Survival curves of AML FLT3 ITD positive (A, cutoff = 33.3, p = 0.07) and FLT3 WT patients (B, cutoff = 34.9, p = 0.21) are presented.

1.4.1.6 Ptprj as clinical target

The tumor suppressor role of Ptprj has been identified in several human cancers as mentioned above. Preclinical models of human thyroid and pancreatic tumors have demonstrated the possibility of using Ptprj as a therapeutic target (Iuliano et al. 2003, Trapasso et al. 2004). In addition, activation of tumor suppressor function of Ptprj by agonists showed beneficial effects in clinical trials. Paduano et al. identified a Ptprj agonist peptide from a random peptide phage that activates Ptprj by binding, leading to reduced ERK1/2 phosphorylation, proliferation and increased apoptosis (Paduano et al. 2012). Ortuso and colleagues discovered another Ptprj agonist peptide (PTPRJ-pep19.4) and revealed that the peptide inhibits proliferation in breast cancer cells as well as ERK1/2 phosphorylation but has no effect on normal breast cells (Ortuso et al. 2013). Thrombospondin1 and Syndecan-2 have been identified as naturally occurring ligands of Ptprj. Increased PTP activity has been demonstrated upon Thrombospondin1 binding (Takahashi et al. 2012, Whiteford et al. 2011). In combination with bone morphogenic protein 4 (BMP4) Thrombospondin1 inhibited tumor angiogenesis and suppressed growth of solid tumors (Tsuchida et al. 2014).

1.4.2 Receptor protein-tyrosine phosphatase C (Ptprc)

1.4.2.1 Structure and expression profile of Ptprc

In the middle of 1970s, Ptprc was identified by two independent groups characterizing the functionally important 'leukocyte specific antigen' (Trowbridge et al. 1975, Fabre and Williams 1977). In 1988 CD45 was identified as first RPTP based on aa sequence homology with PTP1B and PTP activity in CD45-containing cell fractions (Charbonneau et al. 1988, Tonks et al. 1988). CD45, encoded by the Ptprc gene, is also designated as lymphocyte common antigen (L-CA), T200, B220, or Ly-5. Ptprc consists of a variable, isoform-specific extracellular domain of 391-552 aa, a membrane spanning domain of 21 aa and a 704 aa large intracellular part consisting of a tandem phosphatase domain (D1 and D2, each 300 aa) and a C-terminal domain (about 80 aa) (Thomas et al. 1985). In mammals the Ptprc gene consists of 35 exons. Exons 4(A), 5(B), 6(C) and 7 are involved in alternative mRNA splicing and generate RA, RB and RC isoforms of Ptprc. Due to alternative splicing several theoretical splicing variants are possible but just 6 has been observed in reasonable levels, in particular isoform E3_8, (lacking exons 4-7, no O-linked glycosylation), CD45RO (lacking exons 4-6), CD45RB (carrying exon 5), CD45RAB (carrying exons 4 and 5), CD45RBC (carrying exons 5 and 6) and CD45RABC (carrying exons 4-6) (Holmes 2006).

Among all Ptprc isoforms the extracellular part consists of 3 membrane proximal FN-III domains and a cysteine-rich domain followed by variable N-terminal end. The FN-III domains are highly N-glycosylated and important mediators of CD45 stability and maturation to the cell surface (Sato et al. 1993, Pulido and Sanchez-Madrid 1992). Since the majority of O-glycosylation of CD45 can be found in the alternatively spliced region encoded by exon 3 to exon 8, different CD45 isoforms vary extensively in their O-glycosylation patterns (Figure 6) (Trowbridge and Thomas 1994, Thomas et al. 1985).

Within different species (human, mouse, rat) the cytoplasmic domain of Ptprc exhibits 90 % sequence identity whereas in the extracellular part these proteins share 50 % sequence identity only (Thomas et al. 1987). Ptprc has been detected in all higher mammals so far, in chicken and lower vertebrates as horn shark (*Heterodontus francisci*) and hagfish (*Myxini),* indicating that Ptprc is evolutionary conserved (Matthews et al. 1990).

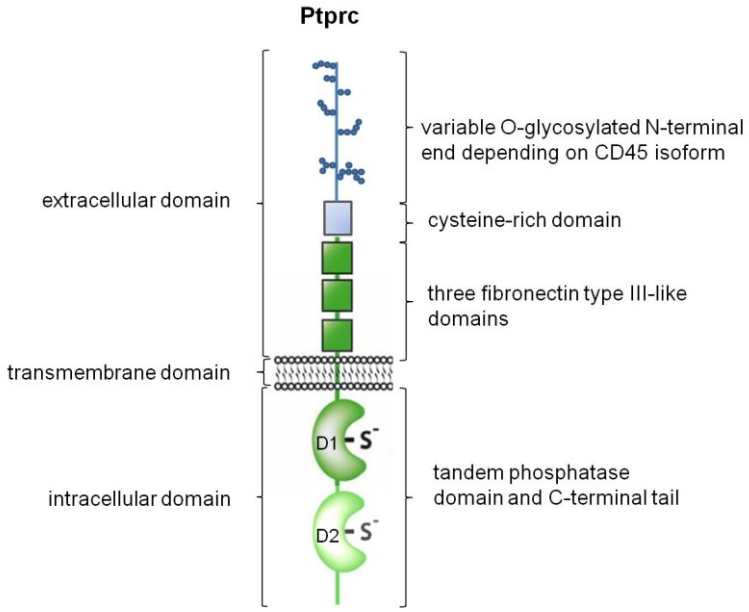

Figure 6. Schematic drawing of Ptprc. Ptprc is composed of a variable glycosylated extracellular domain with cysteine-rich domain and three FN-III domains, a transmembrane domain and an intracellular domain with tandem phosphatase domain and C-terminal tail (modified according to (Müller et al. 2012)).

Isoforms have been expressed in cell type specific and differentiation-dependent manner in all nucleated hematopoietic cells but not on mature erythrocytes and platelets (Hall et al. 1988, Trowbridge et al. 1991, Thomas 1989). In addition, Ptprc has been detected in cells of hematopoietic origin like osteoclasts and microglia (Tan et al. 2000, Boyle et al. 2003, Shivtiel et al. 2008). It represents 5 - 10 % of all cell surface proteins of B and T cells. Due to isoform specific expression Ptprc has a molecular weight of 180-220 kDa. In B cells the highest 220 kDa form is expressed whereas in immature thymocytes the 180 kDa form has been predominantly found. Furthermore, Ptprc has been demonstrated to be one of the most abundantly expressed PTP in primary AML cells as well as in AML cell lines (Arora et al. 2012).

1.4.2.2 Ptprc mode of action

The intracellular part of Ptprc comprises a tandem phosphatase domain. In the membrane proximal D1-domain (Figure. 6) phosphatase activity has been demonstrated whereas in membrane distal D2-domain not (Figure 6). Sequence and mutagenesis studies have revealed that the aa proline (pro1517), serine (ser1523), alanine (ala1524), glycine (gly1525) and arginine (arg1528) surrounding the catalytic cysteine (cys1522) match the PTP consensus motive (V/I)HCSAG(V/I)GR(T/S)G and are essential for PTP activity in D1. In D2, in the sequence VHCRDGSQQTG 5 aa varied from the consensus sequence. By insertion of D2 sequence in D1 the PTP activity was abrogated (Streuli et al. 1990). Deletion of the D2 domain also suppressed PTP activity, indicating a regulatory function of D2 itself or of the C-terminal domain. Regulation of PTP activity by dimerization of CD45 has also been demonstrated (Majeti et al. 1998). Dimer formation is more likely for the small CD45RO isoform than for the highly glycosylated CD45RABC

isoform, depending on charged carbohydrate residues (Xu and Weiss 2002). Localization in membrane subdomains has also been demonstrated to play an important role in Ptprc activity due to the accessibility of specific substrates and phosphorylation (Wang et al. 1999). Transient oxidation has also been reported to regulate Ptprc activity (Singh et al. 2005). However, own studies indicated no ROS mediated inactivation of Ptprc in FLT3 ITD expressing AML cells, as opposed to other PTP in these cells (Godfrey et al. 2012).

So far, a number of Ptprc ligands have been identified but most of them are not binding exclusively to Ptprc. Some of the ligands are only present under certain clinical conditions like an ongoing infection or in pregnancy and there seems to be no natural extracellular ligand that can be found in all healthy adults. pUL11, a transmembrane protein of the cytomegalovirus RL11 (CMV RL11) family, has been identified as CD45 ligand (Gabaev et al. 2014). Interaction of pUL11 with CD45 led to impaired T cell receptor (TCR) signaling and inhibited T cell development. Another ligand which has been identified is placental protein 14 (PP14), a glycoprotein expressed by endometrial deciduas during the first and second trimesters of pregnancy (Morrow et al. 1994). Because of its lectin-like properties it binds to CD45 and thereby leads to dimerization and inactivation of CD45 PTP activity.

1.4.2.3 Ptprc substrates and signaling

Ptprc is capable to dephosphorylate C-terminal and kinase domain phosphotyrosines in several SFK. Thereby the consequences of Ptprc action depend on site of phosphorylation and on the subcellular localization relative to its substrate (Gupta and DeFranco 2003, Thomas and Brown 1999). Dephosphorylation of SFK C-terminal phosphotyrosines e.g. pY505 of Lck activates the kinases whereas dephosphorylation of phosphotyrosines in the kinase domain, e.g. pY394 of Lck inhibit kinase activity. It has been demonstrated that Ptprc acts on C-terminal tyrosine of Lyn, Src, Fyn and Hck. Thereby the kinases were kept in a primed, slightly active state to get fully activated after antigen receptor stimulation (Stone et al. 1997, Trowbridge and Thomas 1994). Controversially, studies in Ptprc ko cells revealed no change in overall activity of the Lck and Fyn (Majeti et al. 1998). Conclusively, Ptprc acts as a positive and negative regulator of SFK (regulatory mechanism as described for Src in chapter 1.4.1.3).

Moreover Ptprc targets janus kinase family (JAK) receptors and therefore negatively regulates cytokine receptor signaling involved in differentiation, proliferation and antiviral immunity of hematopoietic cells (Irie-Sasaki et al. 2001). Ptprc plays an important role for innate immunity. It is furthermore required for TCR and B cell receptor (BCR) mediated signaling (Justement et al. 1991, Desai et al. 1994). In mice, CD45 knockout could not

fully unmask the role of CD45 in B cells due to the expression of the receptor protein tyrosine phosphatase CD148 (Autschbach et al. 1999). Mice genetically inactivated for CD45 and CD148 show a very early block in B-cell development. Thus, CD45 and CD148 share a certain level of functional redundancy in B cells and the myeloid lineage (Zhu et al. 2008). However, more recent work has demonstrated that there are other non-overlapping functions of Ptprc and Ptprj in B cells. Ptprj was more important for B1 BCR signaling than Ptprc (Skrzypczynska et al. 2016, Zikherman et al. 2012).
In conclusion, Ptprc has a positive role in regulating TCR signal transduction in mature and immature T cells. CD45 regulates both, positive and negative selection of B cells (Cyster et al. 1996).

1.4.2.4 Consequences of Ptprc inactivation

Three distinct Ptprc knockout mouse strains were created lacking either exon 6 (Kishihara et al. 1993), exon 9 (Byth et al. 1996) or exon 12 (Mee et al. 1999). Consistent in all Ptprc ko mice B cell development appeared normal. In mice lacking Ptprc exon 6 low remaining levels of CD45 were still detected due to the fact that some CD45 isoforms skip the mutated exon 6 by alternative splicing. A block of early thymocyte development, block of T cell development at transition of immature $CD4^+$ $CD8^+$ double positive cells to mature $CD4^+$ or $CD8^+$ T cells and strikingly, reduced amounts of T cells in peripheral lymphoid organs have been observed. Furthermore, reduced cytotoxic cell response after challenge with lymphocytic choriomeningitis virus (LCMV) has been demonstrated in Ptprc ko mice (Kishihara et al. 1993, Byth et al. 1996, Mee et al. 1999). Genetic inactivation of Ptprc was associated with reduced homing and reduced G-CSF mobilization of progenitor cells. Moreover, mice inactivated for Ptprc had less primitive cells in the BM but increased numbers of these cells in the spleen, yet with reduced homing and repopulation potential (Shivtiel et al. 2008). Interestingly, reduced bone turnover and impaired bone remodeling processes resembling a mild osteopetrosis have been observed in Ptprc ko mice. Moreover, an abnormal pattern of trabecular distribution has been demonstrated in femurs of Ptprc ko mice (Shivtiel et al. 2008).

1.4.2.5 Clinical impact of Ptprc

Ptprc plays a significant role in B and T cell development, autoimmune diseases and cancer as well as in infectious diseases including fungal infections. Loss of function mutations and a SNP at nucleotide 77, precisely C77G, were associated with disease development and virus susceptibility, reviewed in Hendriks & Pubilo 2013 and Rheinländer 2018 (Hendriks and Pulido 2013, Rheinländer et al. 2018).

Ptprc ko mice and humans develop severe combined immune deficiency (SCID) with defective T and B cell development and function (Tchilian et al. 2001b, Roberts et al. 2012, Kung et al. 2000). A causative role of Ptprc in multiple sclerosis (MS) has been proposed (Nakahara et al. 2005). The C77G SNP has been detected to be associated with MS in several families (Jacobsen et al. 2000). This SNP does not result in change of aa sequence but blocks the alternative splicing of exon 4 (Thude et al. 1995). However, results of subsequent, much larger studies rather argue against an association between this Ptprc C77G SNP and MS (Szvetko et al. 2009). Interestingly, during these studies the C77G SNP has been found at a much higher frequency in hepatitis C virus-infected patients than in healthy controls (Dawes et al. 2006). Furthermore this SNP has been correlated to increased risk of HIV infection (Tchilian et al. 2001a).

An attenuating role of Ptprc on FLT3 WT has been demonstrated (Arora et al. 2011, Stopp 2009). Studies on the question if Ptprc is also negatively controlling the activity of mutated FLT3 ITD activity are still pending. Gene expression study of blasts from 285 adults with AML (GEO ID GSE1159 (Valk et al. 2004), Figure 7A) and from BM or peripheral blood of 163 untreated AML patients with normal karyotype (GEO ID GSE12417 (Metzeler et al. 2008), Figure 7B) revealed negative correlation of diminished Ptprc activity and patient survival in FLT3 ITD mutated AML patients. In AML patient carrying FLT3 WT receptor no correlation has been observed between Ptprc activity and patient survival (Figure 7). Thus, it is tempting to speculate, that Ptprc negatively regulate FLT3 ITD activity, contributing to patient survival.

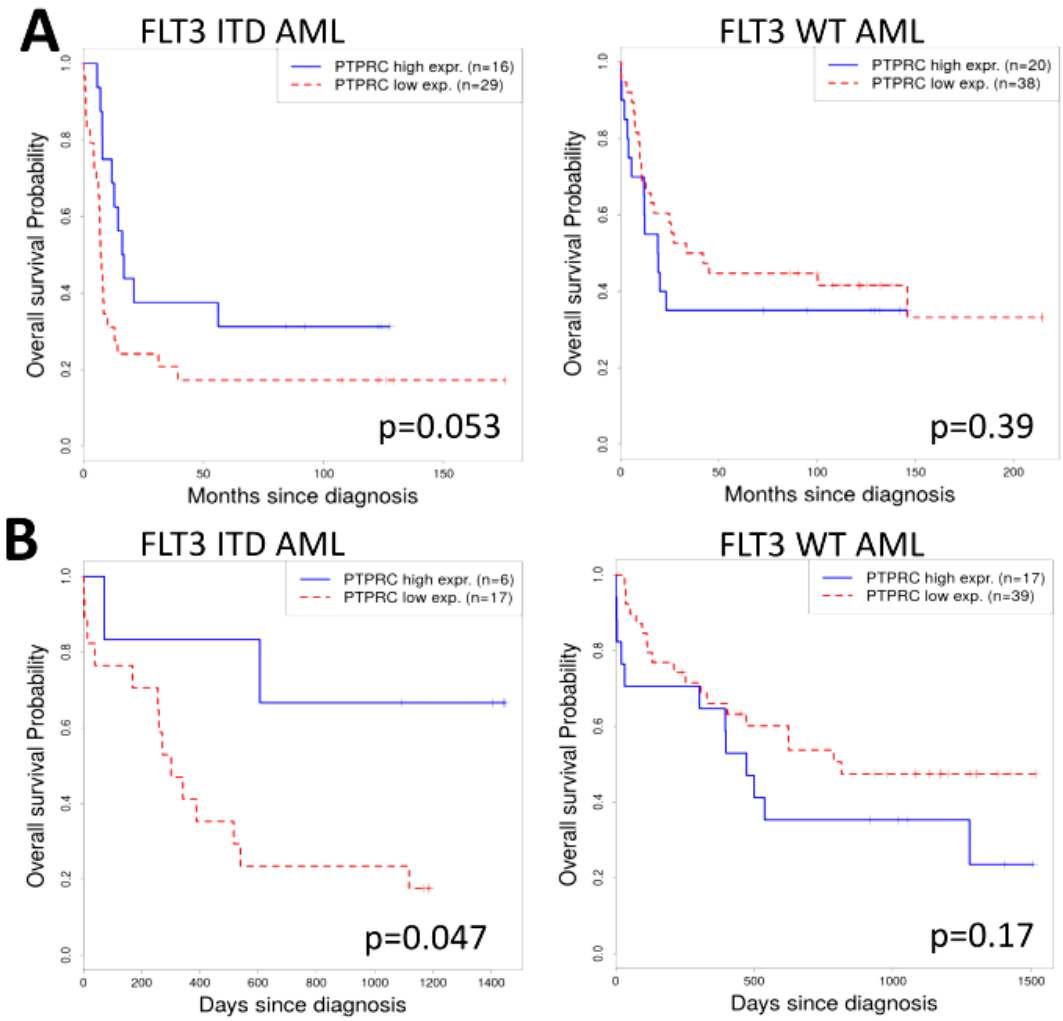

Figure 7. PTPRC expression is inversely correlated to survival of FLT3 ITD positive AML patients. Overall survival of patients with low (red, dotted) and high (blue) PTPRC expression is depicted. Data are based on data sets of Valk (Valk et al. 2004) (GEO-ID GSE1159, A) and Metzeler (Metzeler et al. 2008) (GEO ID GSE12417, B). Survival curves of AML FLT3 ITD positive (left) and FLT3 WT (right) patients as well as p values are presented.

2. Aims of the study

Despite development and approval of small tyrosine kinase inhibitors (TKI) targeting FLT3 ITD, AML patients frequently relapse partially due to additional acquired mutations on FLT3 ITD resulting in resistance of kinases to TKI.

Recently, our research group demonstrated an inhibitory role of Ptprj/DEP-1 and Ptprc/CD45 on FLT3 WT in a model cell system (Arora et al. 2011). In addition, counteracting activity of Ptprj on FLT3 ITD was also demonstrated *in vitro* (Godfrey et al. 2012). Accompanying array data revealed that the survival of normal karyotype FLT3 ITD positive AML patients with low level of Ptprj or Ptprc, respectively was shorter than in patients with high level of the particular phosphatase (Valk et al. 2004, Metzeler et al. 2008).

The purpose of this dissertation is therefore the deeper assessment of the role of Ptprj and Ptprc in regulating the oncogenic activity of AML-related oncoprotein FLT3 ITD *in vitro* and *in vivo*. For this aim, the following goals are to be addressed:

I) Assessing the effect of complete inactivation of Ptprj, Ptprc or both in model cell systems *in vitro*. By using CRISPR/Cas9 system genes encoding Ptprj and/or Ptprc shall be inactivated in 32D muFLT3 ITD myeloid progenitor cells to investigate the effects on FLT3 ITD activity as well as downstream signaling.

II) Study the role of Ptprj and Ptprc on FLT3 ITD-driven myeloproliferative disease *in vivo.* FLT3 ITD knockin mice ($FLT3^{ITD/ITD}$) expressing the oncoprotein under control of its endogenous promoter shall be mated to either $Ptprj^{-/-}$ or $Ptprc^{-/-}$ mice to obtain homozygous $FLT3^{ITD/ITD}$ $Ptprj^{-/-}$ and $FLT3^{ITD/ITD}$ $Ptprj^{-/-}$ mice. These double mutated mice shall be analyzed regarding organ weight and architecture, hematopoiesis, blood cell composition in BM and peripheral organs and further possible physiological phenotypes. Moreover, FLT3 ITD phosphorylation shall be investigated in $FLT3^{ITD/ITD}$ mice genetically inactivated for RPTP as well as potentially abrogated downstream signaling of oncogenic FLT3 ITD (Figure 8).

The identification of natural antagonists of FLT3 ITD might provide new strategies for treatment of FLT3 ITD-driven AML because activation of FLT3 ITD counterparts should lower FLT3 ITD activity and its transforming potential.

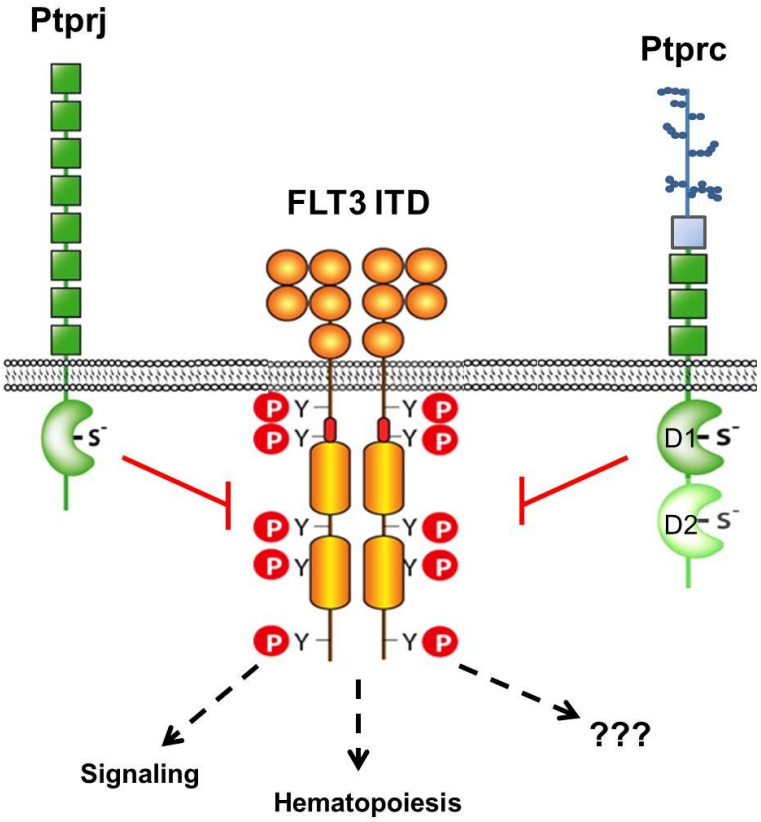

Figure 8. Schematic presentation of proposed actions of Ptprj and Ptprc on oncogenic FLT3 ITD. The potential antagonistic activity of Ptprj and Ptprc on oncogenic FLT3 ITD activity will be investigated. Especially FLT3 ITD phosphorylation and downstream signaling will be analyzed. In addition, physiological effects in hematopoiesis shall be checked as well as potential further effects.

3. Material

3.1 Cell work

3.1.1 Cell lines

Table 1: Used and generated cell lines

Cell line	Description	Plasmid backbone	Origin/Source
32D muFLT3 ITD	murine myeloblast-like cell line, transduced with FLT3 ITD-GFP	pMSCV-IRES-GFP	provided by Dr. Justus Duyster and Dr. Rebecca Grundler, Munich, Germany (Grundler et al. 2005)
32D muFLT3 ITD Ptprj ko	32D muFLT3 ITD cells with CRISPR mediated Ptprj knockout (clone 1)	lentiCRISPRv2	generated within the scope of this project
32D muFLT3 ITD Ptprc ko I	32D muFLT3 ITD cells with CRISPR mediated Ptprc knockout (clone 1)	pX330-mCherry$_{mut}$	
32D muFLT3 ITD Ptprc ko II	32D muFLT3 ITD cells with CRISPR mediated Ptprc knockout (clone 2)	pX330-mCherry$_{mut}$	
32D muFLT3 ITD Ptprj/Ptprc ko I	32D muFLT3 ITD cells with CRISPR mediated double phosphatase knockout of Ptprj and Ptprc	lentiCRISPRv2	
32D muFLT3 ITD Ptprj/ Ptprc ko II	32D muFLT3 ITD cells with CRISPR mediated double phosphatase knockout of Ptprj and Ptprc	lentiCRISPRv2	
32D muFLT3 ITD empty vector	32D muFLT3 ITD cells transduced with non-targeting lentiCRISPRv2 vector	lentiCRISPRv2	
HEK293T	human embryonic kidney cell line	-	Leibnitz Institute DSMZ

3.1.2 Cell culture

Table 2: Medium additives used for cell culture

Additives	Company (Order number)
1,5-dimethyl-1,5-diazaundecamethylenepolymethobromide (Polybrene)	Sigma Aldrich (Tr-1003)
AC220 (Quizartinib)	Sigma Aldrich (kind gift from S. Mahboobi; University of Regensburg)
CellTiter-Blue Reagent	Promega (G8080)
Diphenyleneiodonium chloride (DPI)	Sigma Aldrich(D2926)
Fetal bovine serum (FBS)	PAN BioTech (P40-37500)
IL-3	ImmunoTools (12340032)

Iodonitrotetrazoliumchloride	Sigma Aldrich (I8377)
Penicillin/ Streptomycin solution	Sigma Aldrich (P0781)
PKC412 (Midostaurin)	Selleckchem (S8064)
Polyethylenimine (PEI)	Sigma Aldrich (408727**)**
Puromycin (puromycin dehydrochloride)	Sigma Aldrich (P8833)
Sodium pyruvate	Sigma Aldrich (S8636)

3.1.3 Plasmids

Table 3: Plasmids

Name	Description	Source
pX330-mCherry$_{mut}$	CBh promotor, encodes Cas9-Flag, PCMV promotor, mCherry sequence without BbsI site	kindly provided my Melanie Kahl (Jena, 2014)
lentiCRISPRv2	Lentivector, EFS-NS promotor, encodes Cas9-Flag, Puromycin resistance gene	Addgene (Sanjana et al. 2014)
pPAX2	lentiviral packaging for 2nd generation vectors	Addgene-Trono Lab Packaging and Envelope plasmids
pVSVg	viral envelope	Kindly provided by Carol Stocking, University of Hamburg
pRSV	3rd generation lentiviral packaging plasmid	Addgene-Trono Lab Packaging and Envelope plasmids
pMDL	lentiviral packaging for 3rd generation vectors, (Contains Gag and Pol)	Addgene-Trono Lab Packaging and Envelope plasmids

3.1.4 Enzymes

Table 4: List of enzymes used for CRISPR/Cas9 cloning

Enzyme	Company
BbsI (for pX330-mCherry$_{mut}$ restriction)	New England Biolabs
BsmBI (for lentiCRISPRv2 restriction)	New England Biolabs
Shrimp alkaline phosphatase	New England Biolabs
RNase A	Applichem
Ligase	ZIMET, Akademie der Wissenschaften der DDR
Polynucleotidkinase (PNK)	Fermentas

3.1.5 gRNA

Table 5 List of gRNA oligonucleotides

Name	Sequence 5 ' - 3 '
muPtprj FW	CACCGGCCGCGGCCTTAGACTCGCAGGG
muPtprj REV	AAACCCCTGCGAGTCTAAGGCCGCGGC
muPtprc FW	CACCGCACAAACCCATGGTCATATCTGG
muPtprc REV	AAACCCAGATATGACCATGGGTTTGTGC

3.2 Antibodies

3.2.1 Flow cytometric Antibodies

Table 6: List of antibodies for flow cytometry

Antibody	Clone	Specificity	Label	Company
7AAD	-	mouse	-	BD Pharmingen
Annexin V	-	mouse	FITC	BD Pharmingen
Annexin V	-	mouse	PE	Immunotools
CD11b (Mac-1)	M1/70	mouse	APC	eBioscience
CD135	A2F10.1	mouse	PE	BD Pharmingen
CD148 (Ptprj)	MO86-5	mouse	PE	MBL
CD19	eBio1D3	mouse	FITC	eBioscience
CD19	1D3	mouse	biotin	BD Pharmingen
CD3ε	145-2C11	mouse	PerCP-Cyannine 5.5	eBioscience
CD45	30-F11	mouse	PE	eBioscience
c-Kit (CD117)	2B8	mouse	APC	eBioscience
Gr-1 (Ly6G/Ly6C)	RB6-8C5	mouse	PE	Biolegend
Sca-1 (Ly6A/E)	D7	mouse	PE-Cyannine 7	eBioscience
Streptavidin	-	mouse	PerCP	BD Pharmingen

3.2.2 Western Blot Antibodies

Table 7: List of Antibodies (Western Blot Analysis)*

Antibody	Order number	Size [kDa]	Reactivity	Host	Dilution	Company
β-actin	A5441	42	mouse/ human	Mouse	1 : 5 000	Sigma Aldrich
4G10 (pY)	05-321	-	mouse/ human	Mouse	1 : 1 000	Upstate
AKT	#9272	60	mouse/ human	Rabbit	1 : 1 000	Cell Signaling
CD45	AF114	147	mouse	Goat	1 : 3 620	R&D Systems
SFK (Y416)**	#2101	60	mouse/ human	Rabbit	1 : 1 000	Cell Signaling
DEP-1	AF1934	146	mouse/ human/ rat	Goat	1 : 500	R&D Systems
ERK1/2	#9107	42/44	mouse/ human	Mouse	1 : 5 000	Cell Signaling
pAKT (S473)	#4060	60	mouse/ human	Rabbit	1 : 1 000	Cell Signaling

panFLT3	AF768	130/150***	mouse	Goat	1 : 1 250	R&D Systems
pERK1/2 (T202/Y204) E10	#9106	42/44	mouse/ human	Mouse	1 : 1 000	Cell Signaling
pFLT3 (Y589)	-	130/150***	mouse/ human	Rabbit	1 : 500	Donation from Lars Rönnstrand
pFLT3 (Y591)	#3461	130/150***	mouse/ human	Rabbit	1 : 1 000	Cell Signaling
pSTAT5 (Y694)	ab32364	90	mouse/ human	Rabbit	1 : 1 000	Abcam
cSRC	sc-18	62/59/55	mouse/ human	Rabbit	1 : 1 000	Santa Cruz
STAT5	sc-835	90	mouse/ human	Rabbit	1 : 1 000	Santa Cruz

*Primary antibodies used for Western Blot detection were diluted in 1x TBS-Tween supplemented with 1 % BSA and 0.02 % sodium azide.
**Activating tyrosine residue is indicated as Y416 (as originally indicated in chicken), activating Src tyrosine residues in mouse and human vary (see chapter 1.4.1.3.). Thus, antibodies detecting activating tyrosine residue of Src are commonly named Y416.
***High-mannose and highly glycosylated form of FLT3 kinase.

Table 8 Secondary antibodies (Western Blot)*

Antibody	Host	Order Number	Company
Anti-goat	Donkey	sc-2020	Santa Cruz
Anti-mouse	Goat	074-1806	KPL
Anti-rabbit	Goat	074-1506	KPL

* The secondary antibodies are horseradish peroxidase labeled. They were diluted 1 : 10 000 in TBS-Tween supplemented with 1 % BSA.

3.2.3 Immunohistochemistry Antibodies

Table 9: Antibodies used for Immunohistochemistry

Antibody	Type	Dilution	Host	Order number	Company
AF488 Donkey anti-Rabbit IgG	secondary	1 : 250	Donkey	A21206	Invitrogen
biotin-SP conjugated Donkey anti-Rabbit IgG	secondary	1 : 200	Donkey	711-065-152	Dianova
CD41 (Integrin Alpha2b)	primary	1 : 500	Rabbit	PB9647	Boster Biological Technologies
Myeloperoxidase Ab-1 (MPO)	primary	1 : 150	Rabbit	#DLN-12930	Dianova
pFLT3 (pY591)	primary	1 : 50	Rabbit	#3461	Cell Signaling
pSTAT5 (Y694)	primary	1 : 50	Rabbit	ab32364	Abcam

3.3. Buffers and Solutions

Table 10: Recipes for buffers and solutions

Buffers/ Solutions	Content
10x Electrophoresis buffer	250 mM Tris 2 M Glycin 35 mM SDS
10x Erythrocyte lysis buffer	155 mM NH_4Cl 10 mM $KHCO_3$ 100 nM EDTA
10x TBS-Tween (TBS-T)	50 mM Tris HCl, pH 7.4 500 mM NaCl 0.5 % (v/v) Tween 20
20x PBS	2.74 M NaCl 54 mM KCl 200 mM Na_2HPO_4 36 mM KH_2PO_4 adjust pH 7,4
4 % Paraformaldehyde-Solution	Paraformaldehyde solved in PBS pH 7.4
50x TAE buffer	2 M Tris HCL, pH 8.0 0.05 M EDTA 5.7 % HCl
5x KCM buffer	0.5 M KCl 0.15 M $CaCl_2$ 0.25 M $MgCl_2$
5x Sample buffer (Laemmli)	20 % (v/v) Glycerin 10 % (w/v) SDS 4 mM β-Mercaptoethanol 0.02 % (w/v) Bromphenol blue 200 mM Tris HCl, pH 6.8
Citrate buffer	0.01 M Tri-Sodiumcitrate-Dihydrate
Collecting gel buffer	0.5 M Tris HCl, pH 6.8
DNA sample buffer	50 % Glycerol 10 mM EDTA 0.1 % Bromphenol blue 0.1 % Xylene cyanol
Immunohistochemistry (IHC) Blocking	PBS-T supplemented with 1 % BSA 5 % Normal goat serum (NGS)
Mini prep Solution I	50 mM Glucose 25 mM Tris-HCl, pH 8.0 10 mM EDTA 0.2 mg/ml RNase
Mini prep solution II	0.2 N NaOH 1 % SDS
Mini prep solution III	3.0 M Natriumacetat
PBS-T	PBS with 0,05 % (v/v) Triton X 100

RIPA buffer	50 mM Tris HCl, pH 8.0 150 mM NaCl 1 % (v/v) NP-40 0.5 % (v/v) Deoxycholate 0.1 % (w/v) SDS Freshly add: cOmplete™ (EDTA-free Phosphatase Inhibitor cocktail, Sigma-Aldrich) used 1 : 25 phosSTOP Easy pack (Sigma-Aldrich) used 1 : 10
Separation gel buffer	2 M Tris HCl, pH 8.8
Stripping buffer	62.5 mM mM Tris 100 mM 2-Mercaptoethanol 2 % SDS
Tank blot buffer	48 mM Tris 39 mM Glycin 0.039 % (v/v) SDS 20 % (v/v) Methanol
TE buffer	10 mM Tris HCl pH 7.5 1 mM EDTA

3.4 Staining Solutions

Table 11: Staining solutions for histology

Staining solution	Company
Eosin Y solution alcoholic	Sigma Aldrich, Steinheim, Germany
Hematoxylin solution according to Mayer	Sigma Aldrich, Steinheim, Germany
PAPPENHEIM-staining kit (MAY GRÜNWALD & GIEMSA)	Morphisto GmbH, Frankfurt a. M., Germany
Sour hemealaun according to Mayer	Dr. K. Hollborn & Söhne GmbH & Co. KG; Leipzig, Germany

3.5 Mouse models

Experiments were approved by the committee of the Thuringian State Government on Animal Research (TVA Reg. no. 02-086/14) and performed according to the Protection of Animals Act of the Federal Republic of Germany. The animals were treated in accordance with the declaration of Helsinki and the guiding principles in the care and use of animals.

Table 12: Used and generated mouse models

Strain	Description	Company
C57BL/6	wild type mice with black 6 background	Jackson laboratory, Bar Harbor, Maine, USA
FLT3 ITD	knockin mutation in FLT3 gene leading to internal tandem duplication in juxtamembrane domain and constitutive active kinase	Jackson laboratory (B6.129-$FLT3_{tm1Dgg}$ mice); Bar Harbor, Maine, USA described in (Lee et al. 2007)
$Ptprc^{-/-}$	mice carrying a disrupted exon 9, resulting in introduction of several stop codons downstream of the insertion and thus, knockout mutation in Ptprc gene (Byth et al. 1996).	MRC Harwell (The Mary Lyon Centre, Harwell Science and Innovation Campus, Oxfordshire, OXF0RD, UK)
$Ptprj^{-/-}$	mice carrying a knockout mutation in Ptprj gene	DELTAGEN INC. San Mateo, California, USA
FLT3 ITD $Ptprc^{-/-}$	mice carrying knockin mutation of FLT3 and knockout of Ptprc	generated within the scope of this project
FLT3 ITD $Ptprj^{-/-}$	mice carrying knockin mutation of FLT3 and knockout of Ptprj	generated within the scope of this project

3.6 Reaction Kits, Chemicals and Consumables

3.6.1 Reaction Kits

Table 13: Reaction Kits

Name	Company
First Strand cDNA Synthesis Kit	Thermo Scientific
Maxima SYBR Green/Rox qPCR Master Mix (2x)	Thermo Scientific
Mouse Direct PCR Kit (for Genotyping)	Bimake
Direct Lineage Cell Depletion Kit	Milthenyi Biotec
DNeasy Blood &Tissue Kit	Qiagen
Zymoclean™ Gel DNA Recovery Kit	Zymoresearch
Qiagen Plasmid Midi Kit	Qiagen
Biotin Mouse Lineage Panel	BD Pharmingen
ABC complex kit	Biozol
Bradford Reagent	Sigma Aldrich
2 x M-PCR OPTI™ Mix (Dye Plus)	Bimake
CellTiter-Blue® Cell Viability Assay	Promega

3.6.2 Chemicals

Table 14: Chemicals and reagents

Reagents/Chemicals	Company
Ammoniumpersulfate (APS)	Serva, Heidelberg Germany
Bromphenol blue	Bio-Rad; Hercules, USA
BSA-c	Aurion, Wageningen, Netherlands
Chloroform	Roth, Karlsruhe, Germany
DMSO	Sigma Aldrich, Steinheim, Germany
ECL-Detection solution	Perkin Elmer Life Science; Waltham USA
EDTA	Applichem, Darmstadt, Germany
Ethanol	Nordbrand Nordhausen GmbH, Nordhausen Germany
Fetal bovine serum	Sigma-Aldrich, Steinheim, Germany
Fluoromount-G®	Biozol, Echingen, Germany
Isoflurane CP	CP Pharma, Burgsdorf, Germany
Normal donkey serum (NDS)	Millipore, Billerica, USA
Paraffin	Merck KGaA, Darmstadt Germany
Sodium dodecyl sulfate (SDS)	Applichem, Darmstadt, Germany
TEMED	Promega, Madison, Wisconsin, USA
Tris	Serva, Heidelberg, Germany
Tri-Sodiumcitrate dihydrate	Sigma Aldrich, Steinheim, Germany
Triton X-100	Roth, Karlsruhe, Germany
Tween 20	Serva, Heidelberg, Germany
Xylene	VWR chemicals, Fontenay-sous-Bois, France
β-Mercaptoethanol	Roth, Karlsruhe, Germany
RedSafe	HISS Diagnostics GmbH, Freiburg, Germany
BD Cytofix / Cytoperm	BD Bioscience; Heidelberg, Germany
BD 10 x Perm / Wash buffer	BD Bioscience, Heidelberg Germany
Methylcellulose HSC001	R&D Systems. Minnesota, USA
Methylcellulose M3434	STEMCELL technologies, Vancouver, Cannada
PageRuler™ Prestained protein ladder	Fermentas, Thermo Fisher Scientific, Massachusetts, USA

3.6.3 Consumables

Table 15: Comsumables

Consumables	Company
LS columns (for MACS based cell separation)	Milthenyi Biotec
0.2 µm syringe filter	Sarstedt
PVDF membrane (0.45 pore size)	Ammersham
Amicon ultra 15 centrifugal filter units	Merck Millipore
Whatmann paper	Applichem
Cell culture flasks/plates	Sarstedt and Greiner Bio-One

3.7 Software

Table 16: List of Software

Software	Application	Company
FlowJo 7.6.5	Analyze flow cytometry data	Tree Star Inc. Ashland, OR, USA
ImageJ 1.49 m	Analyze images	Wayne Rasband, NIH, USA
Graphpad Prism 5	Analyze data, prepare graphs and perform statistics	Graphpad Software Inc., La Jolla, CA, USA
Clone Manager Professional 9	Perform in silico cloning	Scientific & Educational Software, Denver, USA
Chomas Version 2.4.4.	Chromatogram viewer	Freeware
Fujifilm LAS4000	Imaging Software	Fujifilm, Düsseldorf, Germany
NIS Elements 5.01	Imaging Software	Nikon, Tokio, Japan
SigmaPlot 13.0	Analyze data, prepare graphs and perform statistics	Systat Software, Inc, San Jose, USA
MultiGauge V3.0	Analyze data	Fujifilm, Düsseldorf, Germany

4. Methods

4.1 DNA work/cloning

4.1.1 Restriction

The restriction mixtures were prepared according to the following recipe:

restriction buffer for specific enzyme	3 µl
restriction enzyme	1.5 µl
DNA/plasmid (1µg)	x µl
ddH_2O	z µl
Σ	30 µl

The restriction mixture was incubated for 1 h. The temperature was adjusted according to the manufacturer's protocol for the used enzyme. To reduce the probability of re-ligation, the plasmids were dephosphorylated by adding 3 µl Shrimp alkaline phosphatase into restriction mixture and incubated for one hour at 37 °C. The digested plasmids were gel purified with Zymoclean™ Gel DNA Recovery Kit following the manufacturer's protocol.

4.1.2 CRISPR/Cas9 oligonucleotide annealing

The gRNA containing oligonucleotides (see Table. 5) were phosphorylated and annealed prior inserting into CRISPR/Cas9 plasmid. Therefore, the following mixture was used:

Oligonucleotide FWD (100 µM)	1 µl
Oligonucleotide REV (100 µM)	1 µl
10 x T4 Ligation buffer	1 µl
ddH_2O	6.5 µl
T4 PNK	0.5 µl
Σ	10 µl

The phosphorylation mixture was incubated at 37 °C for 30 min followed by 95 °C for 5 min. Finally, the temperature was ramped down to 25 °C (5 °C per min) to anneal the sense and antisense oligonucleotides. Annealed oligonucleotides were diluted 1:200 for further utilization.

4.1.3 Ligation

For ligation of digested plasmid and annealed oligonucleotides the following ligation mixture was prepared:

Vector (about 50 ng)	x µl
annealed oligonucleotides	1 µl
10 x T4 Ligation buffer	2 µl
T4 ligase	1 µl
ddH_2O	z µl
Σ	20 µl

Ligation was performed at 16 °C overnight and inactivated at 65 °C for 20 min.

4.1.4 Transformation

Transformation of CRISPR/Cas9 plasmids pX330-mCherry$_{mut}$-gRNA and lentiCRISPRv2-gRNA into *Escherichia coli (E. coli)* was performed via heat shock. Therefore, heat inactivated ligation reaction was mixed with 20 µl 5 x KCM buffer and 70 µl ddH_2O. For transformation 100 µl competent *E. coli* XL-1 blue cells (kindly provided by Annette Böhmer) were mixed with DNA and incubated on ice for 30 min. Heat shock occurred by 10 min room temperature incubation. Transformed *E. coli* cells were suspended in 800 µl LB medium and incubated at 37 °C for 1 h prior to plating on an agar plate containing 100 µg / ml Ampicillin. Plates were incubated at 37 °C overnight.

4.1.5 Plasmid preparation

Depending on required purity and amount of DNA, plasmid preparations were performed in mini or midi scale. For mini prep 2 ml and for midi prep 50 ml LB media containing 100 µg / ml Ampicillin were inoculated with one picked single clone from transformation agar plate. Cultures were incubated at 37 °C overnight with shaking 225 rpm. For mini prep 2 ml bacteria culture were centrifuged and suspended in 100 µl mini prep solution I, followed by 2 min incubation at room temperature. For lysis, 200 µl of mini prep solution II were added to the cell suspension and incubated 5 min at room temperature. 150 µl of mini prep solution III were added, homogenized, incubated on ice for 2 min and centrifuged at 14 000 rpm for 10 min. The supernatant was transferred into a new reaction tube. DNA precipitation was performed by adding 900 µl 96 % ethanol, followed by 5 min incubation and centrifugation (14 000 rpm, 10 min). DNA pellet was washed with 800 µl 70 % ethanol, centrifuged and obtained plasmid DNA pellet was suspended in 50 µl TE buffer. Midi prep was performed using Quiagen Plasmid Midi Kit according to the manufacturer's protocol.

4.2 Cell culture

All eukaryotic cells were cultured in a humidified incubator at 37 °C and an atmosphere of 5 % CO_2. For murine 32D muFLT3 ITD cell line and all prepared 32D muFLT3 ITD PTP ko cell lines RPMI medium with 25mM HEPES and L-Glutamine (Millipore) was used. Cells were cultivated in media supplemented with 10 % heat inactivated (hi) FBS, 1 % Penicillin / Streptomycin solution, 1 % sodium pyruvate and 2 ng/ml IL-3. 4 h before starting signaling experiments cells were starved in RPMI medium without supplements and treated with 0.5 µM DPI, if indicated. The cells were maintained by replacing medium every 2 to 3 days without exceeding a cell density of 1 x 10^6.

For freezing, cells were harvested and suspended in hiFBS containing 10 % DMSO. Cell density was adjusted to 1-2 x 10^6 cells / ml. 1 ml cell suspension was transferred into freezing vials and immediately stored in a Styrofoam storage box at -80 °C. For thawing, cells were rapidly thawed in 37 °C water bath and immediately suspended in 10 ml RPMI medium to dilute DMSO. Cell suspension was centrifuged (500 g, 5 min) and cells suspended into fresh culture medium.

4.3 Transfection of HEK293T cells

1.2 x 10^6 HEK293T cells were seeded into a 10 cm dish one day prior transfection. Packaging plasmids were diluted in 500 µl DMEM media according to the following recipe:

<u>generation II system</u> <u>(for lentiCRISPRv2 derivative plasmids)</u>	
Expression vector	10 µg
pPax2	10 µg
pVSVg	2 µg
<u>generation III system</u> <u>(for pX330-mCherry$_{mut}$ derivative plasmids)</u>	
Expression vector	10 µg
pMDL	10 µg
pRSV	5 µg
pVSVg	2 µg

In 0.5 ml RMPI media Polyethylenamin (PEI, 2.5 µg/µg DNA) and DNA was thoroughly diluted. Medium-DNA and medium-PEI mixture were combined, vortexed immediately and incubated for 30 min at room temperature. Medium of HEK293T cells was exchanged to starvation medium without FBS and DNA-PEI-mixture was added drop-wise to the cells followed by 6 h incubation at 37 °C. Afterwards medium was exchanged to DMEM supplemented with hiFBS and further incubated at 37 °C.

4.4 Transduction of 32D muFLT3 ITD

For generation of CRISPR/Cas9 cell lines two different plasmid backbones were used. First constructs were cloned into BbsI restricted px330mCherry$_{mut}$ comprising mCherry fluorescent marker for selection. For better selection of transduced cells the system was later on changed to BsmBI restricted lentiCRISPRv2 backbone carrying a Puromycin resistance cassette (see Table 1).

The produced virus particles were collected 24, 48 and 72 hours (h) after transfection. The virus containing medium of transfected HEK293T cells was collected and filtered by a 0.2 µm syringe filter to remove cells and cell debris. The medium was replaced with fresh DMEM medium containing 10 % hiFBS. Virus particles were concentrated with the help of Amicon ultra 15 centrifugal filter units by centrifugation at 3 000 rpm for 15 min. 50 000 32D mu FLT3 ITD cells / ml were seeded per well into a 12 well plate. Concentrated virus particles and Polybrene (final concentration 8 µg / ml) were added to 32D cells and plate was gently swirled to homogenize. Plates were centrifuged 1 h at 500 g and incubated at 37 °C and 5 % CO_2 atmosphere overnight. Transductions were repeated after 24 h and 48 h. One day after last transduction the Polybrene containing media was replaced with fresh RPMI media. Two days after infection the transduced cells were ether sorted on mCherry positive cells or selected by 2 µg / ml Puromycin or 15 µg / ml Blasticidin, respectively. The antibiotic selection was maintained at least two days but not longer than one week. Clonal amplification was performed and clones analyzed by flow cytometry or sequencing.

4.5 Polymerase chain reaction (PCR)

4.5.1 Amplification for genotyping

To amplify a specific DNA sequence PCR were used. In this work PCR for genotyping were performed using a 2 x M-PCR OPTI™ Mix (Dye Plus) (Bimake, München, Germany) and a Biometra T-Gradient thermocycler.

Step	**FLT3 ITD / Ptprj**	**Ptprc**
Initial denaturation	95 °C; 5 min	94 °C, 2 min
Cycle	Repeat 32 x	Repeat 30 x
Denaturation	96 °C, 30 sec	94 °C, 45 sec
Annealing	62 °C, 30 sec	60 °C, 45 sec
Elongation	72 °C, 45 sec	72 °C, 45 sec
Final elongation	72 °C, 5 min	72 °C, 5 min

4.5.2 Amplification for sequencing

To validate the created 32D muFLT3 ITD Ptprj and Ptprc ko clones the regions of the targeted genomic DNA was amplified prior. First right annealing temperatures of the primers were determined by a gradient PCR.

Table 16: Primers and sequences used for amplification of chromosomal DNA

Name	Sequence 5 ' - 3 '
Ptprc FW	CTCTGAACAACGGCAAAC
Ptprc REV	CTGCAAAGAGGACCCTTTAC
Ptprj FW	TTACCTGGCCCTGGCGTAGCAAC
Ptprj REV	CTAGCTCGTGGCTCTGGAACAGT

Setup for gradient PCR:

5 x Taq reaction buffer	5 µl
2 mM dNTP	2.5 µl
10 µM FWD	1 µl
10 µM REV	1 µl
DMSO	1 µl
ddH_2O	x µl
Magic-Taq	0.5 µl
Template - DNA (60 ng)	y µl
Σ	25 µl

Afterwards, genomic DNA was amplified with the following PCR program:

Initial denaturation	92 °C	3:00 min	
Denaturation	92 °C	0:30 min	} 35 x
Annealing	x °C	0:30 min	
Elongation	72 °C	1:00 min	
Finale elongation	72 °C	3:00 min	

PCR were carried out in an Eppendorf Thermocycler. Annealing temperature was set to 58 °C for amplification of Ptprc genomic DNA and to 59°C for amplification of Ptprj genomic DNA. The efficiency of amplification was validated by loading 5 µl of the reaction mixed with 1 µl 6 x loading buffer on a 1 % agarose gel.

The amplified PCR fragments were purified with the Zymoclean™ Gel DNA Recovery Kit. The purification with the kit was done according to the manufacturer's protocol. Purified PCR products were sent for sequencing.

4.6 Flow cytometric analysis

4.6.1 Verification of CRISPR/Cas9 ko clones

Clonally amplified cell populations were analyzed for successful knockout of Ptprj and/or Ptprc by flow cytometry. 1 x 10^6 cells were harvested, centrifuged and washed with phosphate buffered saline (PBS). Cells were suspended in 48 µl PBS and 2 µl of

antibodies of Ptprj or Ptprc (see Table 6). Cells were incubated on a spinning wheel at 4 °C for 30 min, washed again and suspended in 300 µl PBS. Stained parental cells (non-transduced 32D muFLT3 ITD) were used as positive and unstained parental cells as negative control.

4.6.2 B and T cell analysis

1 x 10^6 murine primary bone marrow and spleen cells of respective mice were washed two times with PBS and suspended in 40 µl PBS + 1 % hiFBS. 2.5 µl of CD11b-APS, Gr-1-PE, B220-FITC, CD3ε-PerCP, respectively were added to cell suspension prior to 30 min incubation at 4 °C on a spinning wheel. Cells were washed subsequently two times with PBS and analyzed by flow cytometry. The subgating was perfomed as seen in the following figure 9. First via forward scatter and sideward scatter a gate was defined to exclude cell debris. Secondly, obtained cells were analyzed concerning CD11b and Gr-1 expresson. Cells positive for both markers were defined as myeloid differentiated cells including monocytes, granulocytes, dendritic cells but also myeloid suppressor cells. Cells which are negative for both markers were defined as myeloid undifferentiated cells, including lymphocytes, precursors and stem cells. Cells negative for CD11b and Gr-1 were further analyzed for expression of CD19 (representing B cells) and CD3ε (representing T cells).

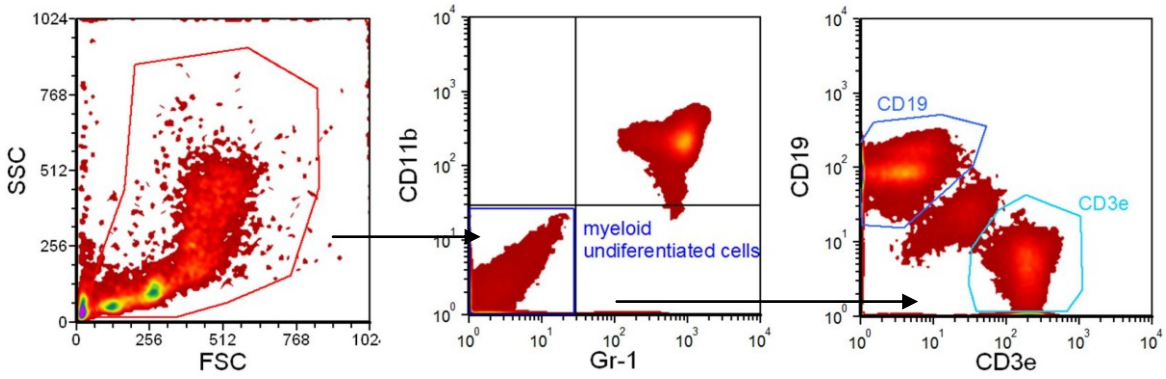

Figure 9. Gating scheme of B and T cell analysis. First, cells were analyzed for surface expression of myeloid markers CD11b and Gr-1. Secondly, cell population which was negative for myeloid differentiation markers was further investigated for CD19 and CD3ε.

4.6.3 Analysis of committed myeloid progenitors and LSK cells

5 x 10^6 murine primary bone marrow and spleen cells of respective mice were washed two times with PBS + 1 % hiFBS and suspended in 50 µl of Biotin Mouse Lineage Panel (BD Bioscience and separately added CD19; ratio 1:25) and incubated at 4°C for 30 min on a spinning wheel. Cells were washed two times washed with PBS + 1 % hiFBS and suspended in 25 µl and 20 µl Streptavidin-PerCP and 2.5 µl of c-kit-APC and Sca-1-PE-Cy7, respectively for additional incubation at 4 °C spinning wheel for 30 min. Then cells were washed two times with PBS + 1 % hiFBS. Furthermore, for FLT3 staining cells

were fixed and permeabelized by suspending them in 200 µl Fixation / Permeabilization buffer (BD Cytofix / Cytoperm) and incubated at 4°C for 30 min. Afterwards, cells were washed with 800 µl 1x BD Perm/Wash buffer. For staining 2.5 µl of PE labelled anti-mouse CD135 antibody were diluted in 47.5 µl 1x BD Perm/Wash buffer and cell pellet was suspended in this solution. Subsequently, cells were incubated for 30 min at 4 °C on spinning wheel and analyzed by flow cytometry. Unstained primary cells of the respective organ were used as negative control and to adjust the gate of lineage negative (Lin^-) cells. All cells which were negative for differentiation markers used in the Biotin Mouse Lineage Panel (BD Pharmingen) were defined as Lin^- cells, representing undifferentiated progenitor cells. Further characterization of these progenitor cells was performed by subgating as seen in the following figure 10. First, via forward scatter and sideward scatter a gate was defined to exclude cell debris. Secondly, in obtained cell population lineage negative cells were defined and further analyzed for expression of c-Kit and Sca-1. Cells which were Lin^-, Sca-1^- and c-Kit^+ were defined as committed myeloid progenitors. Lin^-, Sca-1^+ and c-Kit^+ cells were defined as LSK cells, containing HSC and MPP. Myeloid progenitors and LSK cells were further investigated for FLT3 expression.

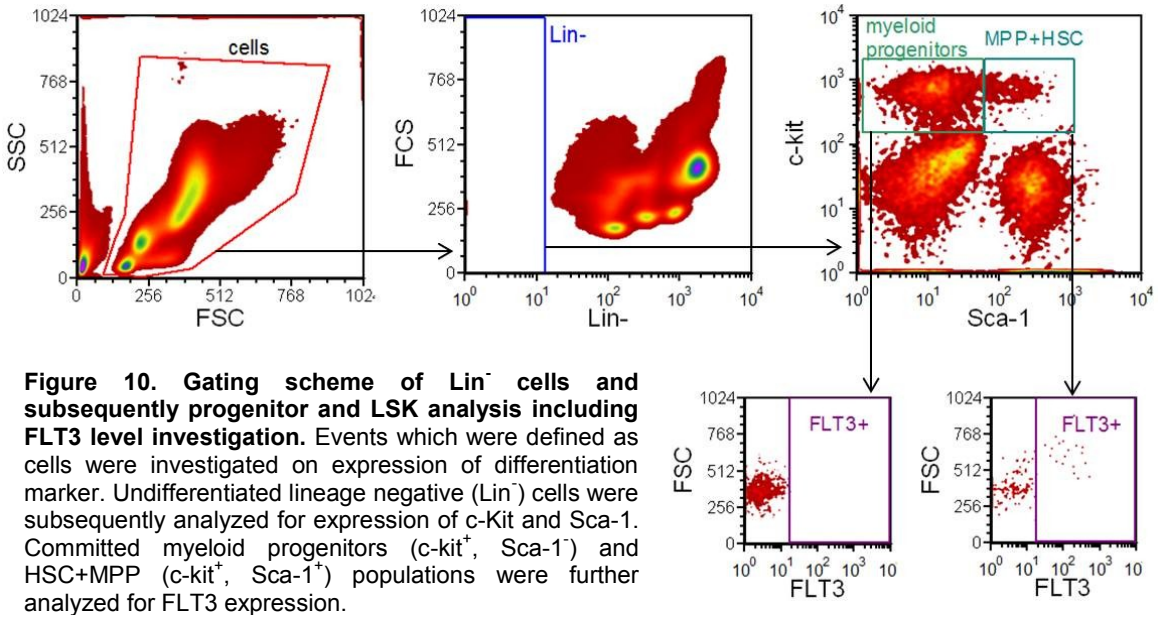

Figure 10. Gating scheme of Lin^- cells and subsequently progenitor and LSK analysis including FLT3 level investigation. Events which were defined as cells were investigated on expression of differentiation marker. Undifferentiated lineage negative (Lin^-) cells were subsequently analyzed for expression of c-Kit and Sca-1. Committed myeloid progenitors (c-kit^+, Sca-1^-) and HSC+MPP (c-kit^+, Sca-1^+) populations were further analyzed for FLT3 expression.

All flow cytometric analyses were performed on BD FACS Canto II (BD Bioscience, Heidelberg, Germany).

4.7 Cell lysis

Equivalent amount of transduced 32D cell lines were harvested into a 1.5 ml reaction tube and centrifuged (500 g, 5 min). Primary mouse cells were harvested as described in 4.10.2 and cells pelleted by centrifugation. Per 1 x 10^6 cells 30 µl RIPA buffer were added and cell lysis performed by up-and-down pipetting and vortexing of the cells. After

10 min incubation on ice the samples were centrifuged (5000 g, 5 min). Supernatant was transferred into a fresh tube, mixed with 5 x Laemmli sample buffer and boiled at 95 °C for 5 min.

4.8 SDS-PAGE and Western blotting

Separation and visualization of proteins in cell lysates were performed by immunoblotting. First SDS polyacrylamide gel electrophoresis (SDS-PAGE) was performed to separate the different proteins according to their molecular weight. A reference Page Ruler was used as molecular size marker. A 10 % separation gel and a 4 % collecting gel were casted for SDS-PAGE.

Separating gel (10 %)		**Stacking gel (4 %)**	
30 % Acrylamide	5 ml	30 % Acrylamide	1 ml
Separation Gel buffer	2.85 ml	Stacking Gel buffer	1.88 ml
20 % SDS	75 µl	20 % SDS	37.5 µl
ddH_2O	7.2 ml	ddH_2O	4.65 ml
20 % APS	60 µl	20 % APS	45 µl
TEMED	12 µl	TEMED	6 µl

Gels were run in 1 x electrophoresis buffer and 0.7 mA constantly per cm^2 gel with Mini Vertical Electrophoresis System (Hoefer, Holliston, USA). Afterwards, proteins were transferred from the gel onto 0.45 µm pore size PVDF membrane (Ammersham) using Wet Blot Immunoblotting (Biorad, Callifornia, USA). Prior to submersion to blotting buffer membrane was pre-wetted with methanol. The gel was equilibrated in blotting buffer and then placed in the “transfer sandwich”. Wet Blot was performed in transfer buffer overnight at 10 V constantly. Following Wet Blot the membrane was incubated in 1 % BSA in TBS-T for 30 min and incubated with primary antibody overnight. The membrane was washed 3 times for 10 min with TBS-T prior to incubation with horseradish peroxidase (HRP)-conjugated secondary antibody (solved in 1 % BSA in TBS-T, ratio 1:10 000; see Table 8) at room temperature for 30 min and 3 times washed in TBS-T for 10 min. Development was done by using enhanced chemoluminescence (Western Lightning ECL) and LAS 4000 imaging device (Fujifilm, Düsseldorf, Germany) and quantified with MultiGaugeV3.0 software (Fujifilm, Düsseldorf, Germany). After exposure, membranes were stripped with stripping buffer (55 °C, 30 min), incubated with 1 % BSA in TBS-T at room temperature for 30 min and re-probed with the desired primary and secondary antibody. Quantified site-specific phosphorylation divided through quantified pan phosphorylation of respective target was calculated to obtain specific phosphorylation of the protein.

4.9 Viability and Proliferation Assays

4.9.1 Colony forming unit (CFU) assay

32D muFLT3 ITD and 32D muFLT3 ITD PTP ko cells were harvested, counted and seeded in a density of 375 cells / well in 230 µl methylcellulose (R&D Systems) supplemented with 10 % hiFBS, 1 % Penicillin / Streptomycin solution and 220 µl IMDM media in a 24 well plate. After 6 days incubation at 37 °C 50 µl of Iodonitrotetrazoliumchloride (0.4 mg / ml) were added to stain the colonies overnight. To investigate the CFU forming capacity plates were scanned and colonies were counted manually.

Purified lineage negative precursors from BM and spleen were plated at a concentration of 250 cells per well in a 24 well plate in M3434 methylcellulose, containing mouse stem cell factor (SCF), mouse interleukin 3 (IL-3), human interleukin 6 (IL-6) and human erythropoietin (EPO) (StemCell Technologies,Vancouver, BC). Total colony counts and colony counts of burst-forming unit (erythroid precursor, BFU-E), granulocyte / macrophage (GM) and granulocyte / erythroide / megakaryocyte / monocyte (GEMM) precursors were obtained after 10 days at 37 °C and 5 % CO_2. Classification of colonies was done by cell and colony form and size. BFU-E colony clusters consisted of tiny cells with irregular shape, which were difficult to distinguish and appeared fused together. Colonies classified as CFU GM contained multiple cell clusters with dense core. Large monocytic cells had an oval to round shape. Granulocytic lineage cells were round and bright, and were much smaller with a more uniform size. CFU GEMM produced large colonies with a highly dense core and indistinct borders between core and peripheral cells. Monocytic and granulocytic cells were visible as well as cluster of large megakaryocytic cells. Afterwards, cells were harvested and used for replating, cytospin preparation and immunophenotypic characterization.

4.9.2 The Cell Titer-Blue® Assay (IC_{50})

To investigate the IC_{50} value of tyrosine kinase inhibitors in 32D muFLT3 ITD cell line and 32D muFLT3 ITD PTP ko cell lines, cells were seeded into a 96 well plate (Greiner; F-bottom, black) in a density of 2000 cells / well in normal cultivation media. Cells were treated with 11 different concentrations of AC220, PKC412 or DMSO as control for three days. After 3 days of incubation in a humid chamber at 37 °C, cells were treated with cell titer blue (Promega) for three hours. Thereby, viable cells were able to reduce the indicator dye resazurin to resorufin and generate a fluorescent signal. Nonviable cells have lost metabolic capacity and do not generate a fluorescent signal. Fluorescence was measured at TECAN Reader (Tecan, Salzburg, Austria) with excitation wavelength

540 nm and emission wavelength 610 nm. For each TKI concentration eightfold measurement was performed. IC_{50} values were calculated using non-linear best-fit regression analysis Sigma Plot V13.0 software.

4.10 Mouse work

4.10.1 Genotyping

To detect the knockout of Ptprj or Ptprc, respectively and presence of FLT3 ITD mutations in mice, the chromosomal DNA was extracted out of tail biopsies using the mouse direct PCR Kit (Bimake, München, Germany) following the manufacturers protocol. To amplify the isolated DNA PCR was performed using the primers listed in table 17. For validation of amplified DNA fragments agarose gel electrophoresis was used. Expected size of respective DNA fragments is shown in table 18.

Table 17. Primer used for Genotyping

Name	Sequence 5'-3'
Ptprj FWD	AGCTGTCGTCAGCCCAACTAGTGTG
Ptprj REV	GGAGAATGTATACGAAGTGCCTGGG
Ptprj Neo FWD	GGGCCAGCTCATTCCTCCCACTCAT
Ptprc WT FWD	CGATGATGATTGTACTAATTTCCTTTTTTT
Ptprc WT REV	GCTGGAGCACATGAGTCATTAGACAC
Ptprc ko FWD	GTAATCAGACTTTTAAGGCAGACCTC
Ptprc ko REV	TTGGCTACCCGTGATATTGCTG
FLT3 ITD FWD	AGGTACGAGAGTCAGCTGCAGAT
FLT3 ITD REV	TGTAAAGATGGAGTAAGTGCGGG

Table 18. Size of amplified PCR product

gene + mutation	size of PCR product (bp)
Ptprj WT	168
Ptprj ko	326
FLT3 WT	200
FLT3 ITD	224
Ptprc WT	250
Ptprc ko	300

4.10.2 Isolation and characterization of mouse organs

Mice were anesthetized with Isoflurane and terminated by cervical dislocation. The abdomen was opened to remove liver, kidneys and spleen for investigation of organ weight. The bones of the hind limbs were dissected and tissue and filaments completely removed. For preparation of bone marrow both ends of the bones were cut off and bone marrow was washed out with MACS Rinsing Solution (Milthenyi Biotech, Bergisch Gladbach, Germany) through a 0.4 µm sized mesh. Primary spleen cells were obtained

by pressing the spleen with PBS and a pistil through a cell strainer (0.7 µm). Cell solutions were centrifuged and erythrocyte-lysed at room temperature for 5 min with 1 x Erythrocyte lysis buffer. Afterwards cells were suspended in MACS Rinsing Solution (Milthenyi Biotech) and counted with a Neubauer counting chamber.

4.10.3 Blood analysis

Mice were anesthetized with Isoflurane and retro-orbital blood was collected with heparin-coated capillary tubes (Hirschmann Laborgeräte, Eberstadt, Germany). To determine the blood cell count 20 µl of blood were measured using a BC5300Vet Hematology system (Mindray, Darmstadt, Germany, kindly provided by Ilse Jacobsen group, Microbial Immunology, Leibniz Institute for Natural Product Research and Infection Biology, Hans Knöll Institute, Jena, Germany). To analyze the blood leukocytes and to obtain blood serum the mice were anesthetized and terminated by Isoflurane overdose (5 %) and final hearth puncture was performed with EDTA-coated syringes (EDTA concentration 1.6 mg/ml blood). The blood was centrifuged with 2000 g. The serum was aspirated and stored in 50 µl aliquots at -80 °C. Erythrocytes were lysed and the remaining blood cells were suspended in PBS + 2 % hiFBS and analyzed by flow cytometry. Furthermore, blood smears were prepared on poly-L-lysine-coated microscope slide (Thermo Scientific) for further cytological characterization.

4.10.4 Cytospin preparation

Primary cells of murine spleen and bone marrow, unpurified or Lin^- purified cells were processed as described before (4.10.2) and 150 000 cells were solved in 200 µl MACS Rinsing Buffer. Cell solution was transferred into a funnel, which was fixed on top of a filter card and poly-L-lysine coated object slide. The samples were centrifuged at 600 rpm for 5 min. The funnel and filtercard were carefully removed and the object slide was air-dried for 1 h and used for Pappenheim staining following the manufacturer's protocol (Morphisto; Pappenheim staining Kit). Cytospin analyses were used to investigate composition of harvested CFU and to further specify the lineage of cells which form the CFU.

4.10.5 MACS purification of lineage negative (Lin^-) cells

Purification of Lin^- cells from bone marrow and spleen cells of mice was performed by using MACS-based cell separation system and the Direct Lineage Cell Depletion Kit (Milthenyi, Bergisch Gladbach, Germany) following the manufacturer's protocol. In case of Ptprc knockout mice and FLT3 ITD knockin Ptprc knockout mice additional 5 µl of CD19 labeled MicroBeads were added per 2 x 10^7 cells and incubated at 4 °C for

10 min. Lin^- cells were collected, counted with a Neubauer counting chamber and used for the experiments.

4.10.6 Perfusion and Organ and Bone slice preparation

Mice were anesthetized with an Isoflurane overdose (5 %, > 10 min) prior to cardiac perfusion. Upon heart beat rate under 30 bpm (irreversible cardiovascular dysfunction) the abdomen and thorax were opened and perfusion with PBS was started by cardiac puncture via the left ventricle. The right atrium was punctured to enable the blood and PBS to left the mouse after circulation through the whole body. The flow rate of the perfusion solution was adapted to 3 ml / min. Until no more blood was washed out of the mouse, perfusion solution was changed from PBS to 4 % paraformaldehyde (PFA) and was run for 10 min. The organs (liver, kidney, spleen) and bones (tibia and femur) were carefully removed after fixation and post-fixed for 24 h in 4 % PFA. Organs were cut to size and rinsed with water for 2 h, followed by waxing using Microm STP 120 (Thermo Scientific). The waxing was performed in the following steps: 2 x 1 h 70 % ethanol, 1 h 96 % ethanol, 2 x 2 h 96 % ethanol, 2 x 2 h 99 % ethanol, 1 h 1/3 xylene and 2/3 ethanol; 1 h 2/3 xylene and 1/3 ethanol, 1 h xylene, 2 h xylene and finally 3 h paraffin. Afterwards, tissue samples were embedded in paraffin and cutted into 4 µm slices. Bones were decalcified prior to waxing. Therefore, femur and tibia were stored in decalcifier (Roth) for 5 days, replacing decalcifier each day.

4.10.7 µCT measurements

To characterize the bone structure and density dead mice were scanned with an *in vivo* micro-CT scanner TomoScope® Synergy Twin imaging system using a standard protocol with 65 kV. Three-dimensional anatomical pictures were gained using Imalytics software. ImpactView software (CT Imaging GmbH) was used to generate image slices and for region of interest measurement. Average bone density was calculated in hind limb bones. The cortical thickness index (CTI) which was defined as $CTI = \frac{r_{out} - r_{in}}{r_{out}}$ (r_{out} and r_{in} are the outer and inner radius of the cortical bone, respectively). The CTI is measured as the average value between 1.4 and 1.6 mm from the knee joint as the signal was reasonably stable for all mouse types in this range. The computations involved local orthogonalization of bone slices as previously described (Svensson et al. 2017). Furthermore, the roughness of the bone surface of hind legs was computed, using intensity threshold 78 for surface reconstruction of all CT images and roughness radius r=3 as previously described (Hoffmann et al. 2017). Analysis of CT data was performed by group of M. T. Figge (Applied Systems Biology, Leibniz Institute for Natural Product Research and Infection Biology, Hans Knöll Institute, Jena, Germany).

4.11 Staining of organ slices

4.11.1 Immunohistochemistry

Organ slices were dewaxed prior to staining. Therefore, slices were incubated three times in xylene for 5 min, washed in ethanol solution with decreasing ethanol concentration (99 % - 96 % - 96 % - 70 % - 50 %) 5 min each and rinsed in distilled water. Then antigen retrieval was performed by boiling the slices in 0.01 M citrate buffer (pH 6.0) at 630 W for 11 min. Samples were cooled down to room temperature, washed two times with PBS for 8 min and one times with PBS-T for 5 min followed by incubating the organ slices in blocking solution at 37 °C for 20 min. Organ slices were washed two times with PBS-T and incubated with primary antibody (diluted in blocking solution see table 10) at 4 °C overnight. Three times washing with PBS-T was performed prior to 2 h incubation with secondary AF488 goat anti-rabbit antibody diluted in blocking solution 1:250. After two times washing with PBS-T co-staining with DAPI was performed (20 min, diluted 1:200 in PBS), followed by 4 times washing with PBS for 8 min each. The organ slices were coverslipped in Fluoromount G and representative images were acquired using a Nikon eclipse Ti-E invert microscope system.

4.11.2 H & E staining

Organ slices were dewaxed prior to staining with hematoxilin and eosin as described in 4.10.6. Hematoxilin staining was performed for 24 min then slices were washed two times with ddH_2O and rinsed with tap water for 10 min until the slices appeared black / dark blue. For eosin staining the slices were incubated in eosin staining solution for 3 min and washed 2 times with ddH_2O. Afterwards the organ slices were dewatered by incubating them in ethanol solutions with increasing concentrations (50 % - 70 % - 96 % - 96 % - 99 %) 1 min respectively followed by three times xylene incubation for 5 min. The stained slices were coverslipped in Neomount (Merck) and representative images of H & E-stained sections were acquired using a Nikon eclipse Ti-E invert microscope system.

4.11.3 Myeloperoxidase (MPO) staining

Organ sliced were prepared as described in 4.11.1 until the washing steps before first blocking step. Then the endogen peroxidases were blocked by incubating slices in 3 % H_2O_2 diluted in 50 % Isopropanol for 20 min at room temperature followed by 10 min washing in ddH_2O. By incubating the slides in 50 mg $NaBH_4$ solved in 100 ml ddH_2O for 20 min the aldehyde groups were also blocked, again followed by 10 min washing in ddH_2O. The samples were washed in PBS and PBS-T for 5 min each prior to serum

blockage and incubation with primary and secondary antibody as described in 4.11.1. A biotinylated donkey anti-rabbit antibody was used as secondary antibody. After 2 times washing in PBS-T for 5 min the samples were incubated with vectostain ABC kit (Biozol, Echingen, Germany) according to the manufacturer's protocol. After washing once with PBS-T, 2 times with PBS and once with ddH_2O the samples were incubated with 3, 3` diaminobenzidine (DAB) (Sigmafast D4293) for 10 min followed by 4 times washing with ddH_2O. Counterstaining was performed with sour hemalum solution according to Mayer for 5 min followed by 15 min rinsing under tab water. Dewatering was performed as described in H & E staining part prior to cover slipping in Neomount. Specification of the MPO-antibody was validated by incubating organ sections with secondary antibody only (negative control) and detecting no positive signal.

4.12 Statistical analysis

Results and data obtained from experiments were reported in mean ± standard error of the mean (SEM). Comparisons between groups were made with one way Anova followed by Bonferroni post-test if appropriate. Significance of survival was tested with Log rank test using Graph Pad 5 software. Calculations were done with SigmaPlot V13.0 software and Graph Pad 5. Differences were considered significant if *p <0.05, **p <0.01 and ***p <0.001 compared to WT and #p <0.05, ##p <0.01 and ###p <0.001 compared to $FLT3^{ITD/ITD}$ as indicated in the figure legends.

5. Results

5.1 Effects of CRISPR/Cas9 mediated Ptprj and Ptprc ko in 32D muFLT3 ITD cells

Regulatory role of Ptprj and Ptprc on FLT3 WT activity was demonstrated in 32D muFLT3 WT cells (Arora et al. 2011). Further studies revealed that upon reactivation of Ptprj by quenching of cellular ROS, Ptprj controls the activity of FLT3 ITD in 32D muFLT3 ITD, MV4-11 and human primary AML cells on basis of shRNA mediated Ptprj knockdown (Godfrey et al. 2012). In order to better elucidate how Ptprj and Ptprc affects FLT3 ITD activity and to investigate potential overlapping functions of Ptprj and Ptprc CRISPR/Cas9 mediated knockout of both was performed in 32D muFLT3 ITD cells.

5.1.1 Generation of CRISPR/Cas9 mediated knockout of Ptprj and Ptprc

In order to inactivate Ptprj and/or Ptprc lentiviral transduction of 32D muFLT3 ITD cells with gRNA encoding lentiCRISPRv2 (Sanjana et al. 2014) targeting either Ptprj or Ptprc, was performed. Post transduction resistant cells were selected by Puromycin and clonally amplified. Knockout of Ptprj and Ptprc was verified by immunoblot (Figure 11). and flow cytometric analysis. In addition, inactivation was confirmed by sequencing of both gene internal target region alleles (data not shown). To study the previously demonstrated redundant role of Ptprj and Ptprc (Zhu et al. 2008) double knockout (ko) cells were generated. One clone carrying Ptprj ko (in the following named 32D muFLT3 ITD Ptprj ko), two clones carrying Ptprc ko (in the following named 32D muFLT3 ITD Ptprc ko I and ko II) and two clones carrying double PTP ko (in the following named 32D muFLT3 ITD Ptprj/Ptprc ko I and ko II) were selected from 32D muFLT3 ITD cells (Figure 11). The obtained cell clones were viable and did proliferate.

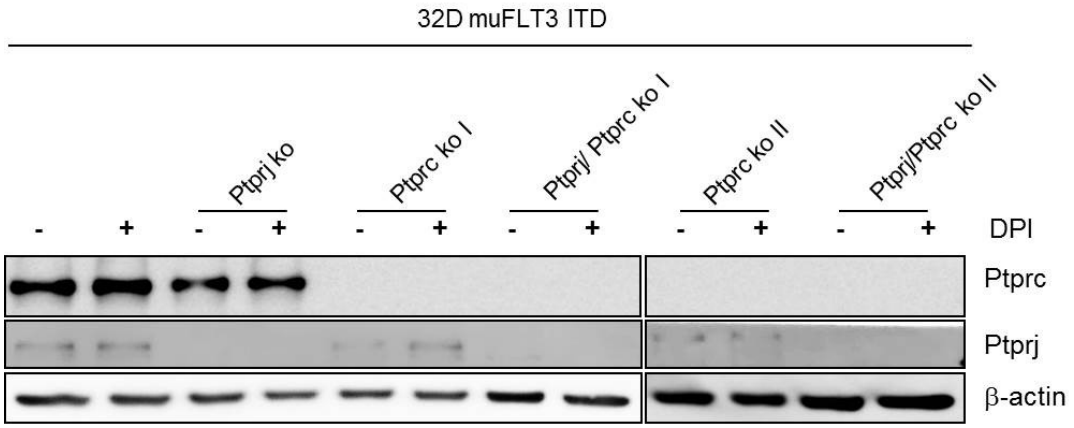

Figure 11. CRISPR/Cas9-mediated inactivation of Ptprj and Ptprc in 32D muFLT3 ITD cells. 32D muFLT3 ITD (control transduced), 32D muFLT3 ITD Ptprj ko, 32D muFLT3 ITD Ptprc ko I and II and 32D muFLT3 ITD Ptprj/Ptprc ko I and II cell lines were starved for 4 h in serum-free medium. DPI was added during starvation in a final concentration of 0.5 µM, untreated cells were incubated with respective amount of DMSO. Cells were lysed in RIPA buffer and equivalent amounts of protein were separated by SDS-PAGE and processed for immunodetection using antibody recognizing Ptprj. Blot was re-probed for Ptprc antibody and β-actin as control.

5.1.2 FLT3 ITD activity in 32D muFLT3 ITD cells lacking Ptprj and/or Ptprc

In order to study the effect of the loss of Ptprj or Ptprc on FLT3 ITD signaling, specific phosphorylation of FLT3 ITD and known downstream targets were analyzed using immunoblotting in 32D muFLT3 ITD cells inactivated for Ptprj and/or Ptprc (Figure 12A, B).

Specific FLT3 Y589 phosphorylation showed no significant changes in all PTP ko cell lines compared to 32D muFLT3 ITD cell line. Interestingly, STAT5 Y694 phosphorylation was significantly reduced in 32D muFLT3 ITD Ptprj ko and 32D muFLT3 ITD Ptprj/Ptprc ko I and II compared to 32D muFLT3 ITD cells. 32D muFLT3 ITD Ptprc ko I and II demonstrated reduced specific STAT5 phosphorylation, but without significance. In all PTP ko cell lines, except 32D muFLT3 ITD Ptprc ko II, specific AKT S473 phosphorylation was significantly reduced. In addition, specific Src Y416 phosphorylation was strongly reduced compared to 32D muFLT3 ITD cell line. Reduced Src Y416 phosphorylation indicates decreased Src activity. Insignificant effects on T202/Y204 ERK1/2 phosphorylation were observed in PTP ko cell lines compared to 32D muFLT3 ITD cells. Furthermore, the two clones of 32D muFLT3 ITD Ptprc ko cells reacted partially different. Because of clonal amplification after CRISPR/Cas9 transduced cells clonal effects cannot be excluded.

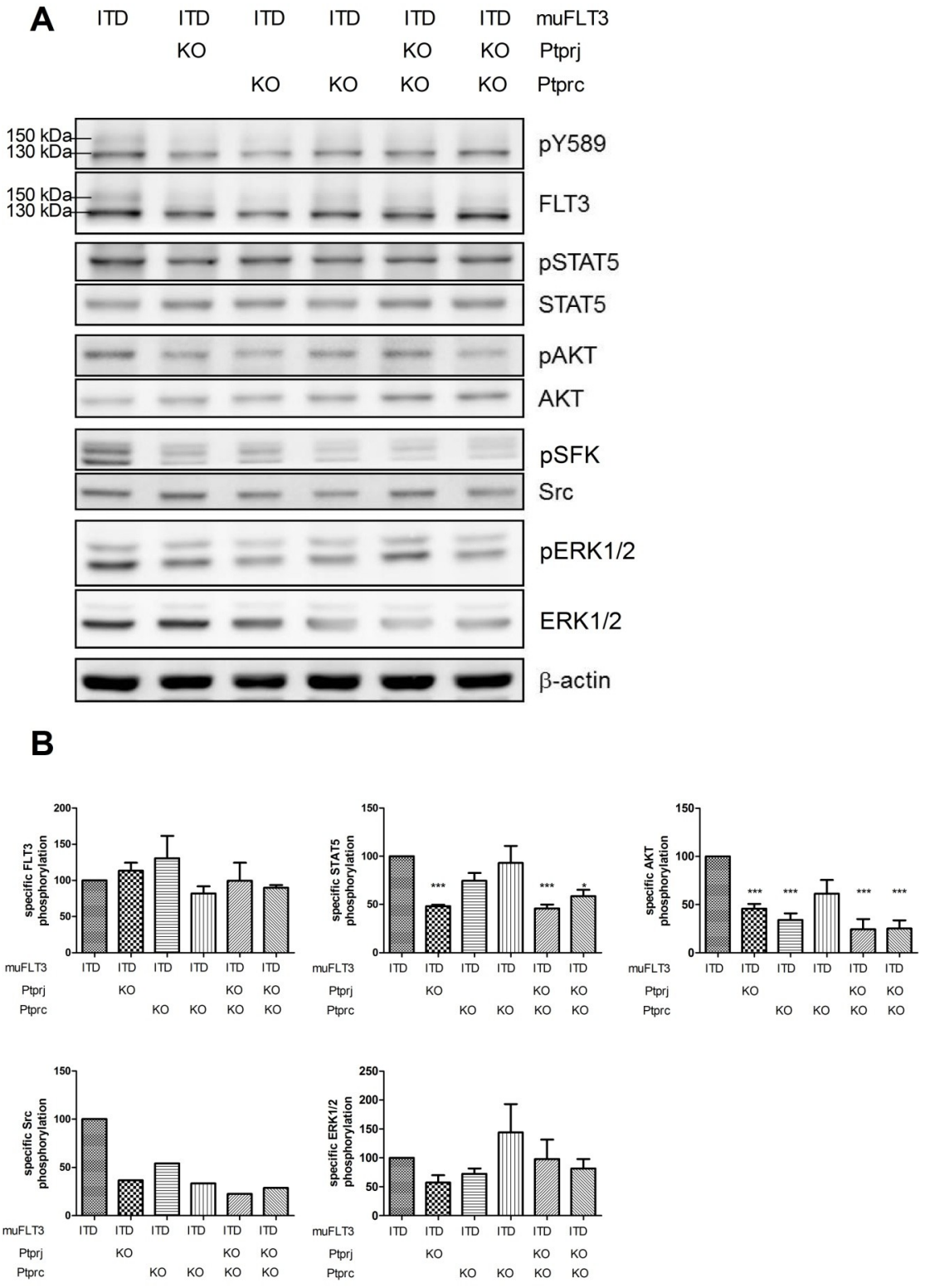

Figure 12. Signaling analysis in 32D muFLT3 ITD parental and indicated 32D muFLT3 ITD PTP ko cells. 32D muFLT3 ITD (control transduced), 32D muFLT3 ITD Ptprj ko, 32D muFLT3 ITD Ptprc ko and 32D muFLT3 ITD Ptprj/Ptprc ko cell line cells were starved for 4 h in serum free medium, lysed in RIPA buffer. Equivalent amounts of protein samples were separated by SDS-PAGE and processed for immunodetection using phosphosite specific antibodies recognizing FLT3 (pY589), pSTAT5 (Y694), pAKT (S473), pSFK (Y416) and pERK1/2 (T202/Y204). Blot was re-probed for total FLT3, STAT5, AKT, Src, ERK antibodies and β-actin as control. (A) Representative immunoblot; (B) Quantification of specific phosphorylation of FLT3, STAT5, AKT, Src and ERK1/2 in relation to total protein level of indicated proteins, values are given in mean ± SEM, n =4, expect Src probing n =1; ***p <0.001 compared to 32D muFLT3 ITD

5.1.3 Effect of ROS on Ptprj and Ptprc controlled signaling on FLT3 ITD downstream targets

Due to NOX4-driven ROS formation in FLT3 ITD cells reversible oxidation of the catalytic cysteine of the PTP domain led to reduction of Ptprj activity. This effect was demonstrated in HEK293, MV4-11 and MOLM13 cells and in primary AML blasts (Godfrey et al. 2012, Jayavelu et al. 2016). Treatment of PTP ko cells with ROS quenching agent DPI should give information about oxidation susceptibility of Ptprj and Ptprc. Therefore, FLT3 phosphorylation and downstream signaling was investigated in PTP ko cells after DPI treatment.

As previously published (Godfrey et al. 2012) 32D muFLT3 ITD cells showed reduction of specific FLT3 phosphorylation after DPI treatment. In all 32D muFLT3 ITD PTP ko cell lines specific FLT3 phosphorylation was downregulated upon DPI treatment (Figure 13A, B). Since this downregulation was still observed after DPI treatment in 32D muFLT3 ITD Ptprj/Ptprc ko cells, it can be speculated that further PTP or other mechanisms are involved in phosphorylation regulation of FLT3 ITD. Reduction of STAT5 Y694 phosphorylation after DPI treatment was revealed in both 32D muFLT3 ITD Ptprc ko I and II cell lines and in 32D muFLT3 ITD cells. Untreated 32D muFLT3 ITD Ptprj ko cells demonstrated strongly decreased STAT5 phosphorylation compared to parental cells, which was not further reduced after DPI treatment. Y694 STAT5 phosphorylation was strongly decreased in 32D muFLT3 ITD Ptprj/Ptprc ko cells. Upon DPI treatment just minor effects on specific STAT5 phosphorylation were observed. In 32D muFLT3 ITD cells specific AKT phosphorylation was 2-fold increased due to DPI treatment. In 32D muFLT3 ITD Ptprj ko cells no effect of DPI-treatment was observed. In contrast, both 32D muFLT3 ITD Ptprc ko cell lines as well as both 32D muFLT3 ITD Ptprj/Ptprc ko cell lines revealed slight up regulation of S473 AKT phosphorylation after DPI treatment. As already demonstrated above (Figure 12) phosphorylation of activating Src Y416 is strongly decreased in all investigated 32D muFLT3 ITD PTP ko cell lines. In 32D muFLT3 ITD Ptprj ko cells Y416 Src activity was further decreased upon DPI treatment whereas it did not alter in response to DPI treatment in 32D muFLT3 ITD Ptprc ko I and II and both 32D muFLT3 ITD Ptprj/Ptprc ko I and II. Most striking effects were observed on specific ERK1/2 phosphorylation upon DPI treatment in PTP ko cell lines. T202/Y204 ERK1/2 phosphorylation level were drastically reduced compared to untreated PTP ko cells and 32D muFLT3 ITD parental cells. In 32D muFLT3 ITD cells only slightly reduced ERK1/2 phosphorylation was obtained upon DPI treatment.

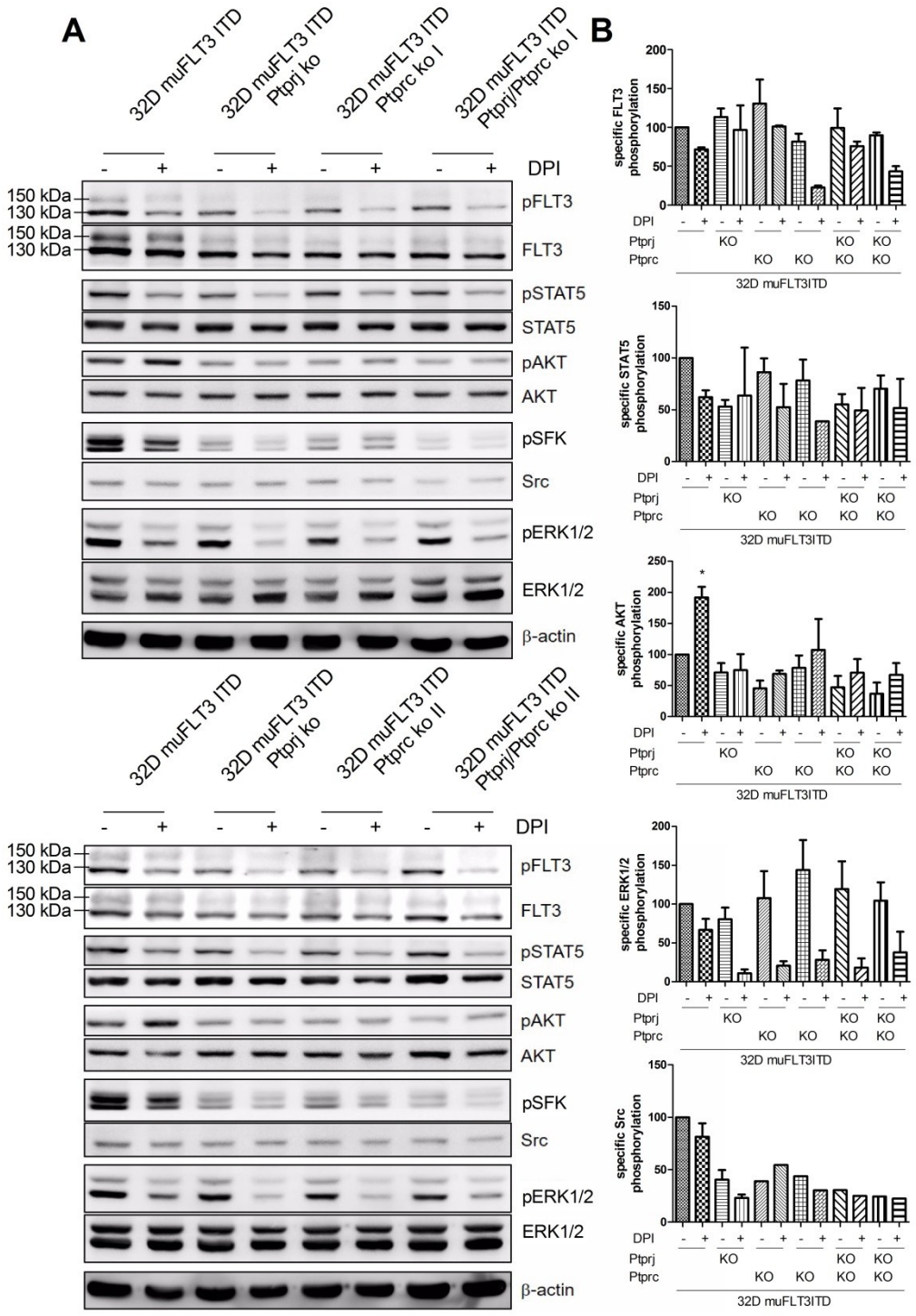

Figure 13. Signaling analysis in DPI treated 32D muFLT3 ITD cells and indicated 32D muFLT3 ITD PTP ko cell lines. 32D muFLT3 ITD (control transduced) and 32D muFLT3 ITD Ptprj ko, 32D muFLT3 ITD Ptprc ko and 32D muFLT3 ITD Ptprj/Ptprc ko cell lines were starved for 4 h and in parallel incubated with DPI (0.5 µM). Untreated cells were incubated with respective amount of DMSO for 4 h. Afterwards, cells were lysed in RIPA buffer, equivalent amounts of protein samples were separated by SDS-PAGE and processed for immunodetection using phosphosite specific antibodies recognizing FLT3 (pY589), pSTAT5 (Y694), pAKT (S473), pSrc (Y416) and pERK 1/2 (T202/Y204). Blot was re-probed for total FLT3, STAT5, AKT, Src, ERK1/2 antibodies and β-actin as control. (A) Representative immunoblots; (B) Quantification of specific phosphorylation of FLT3, STAT5, AKT, Src and ERK in relation to total protein level of indicated proteins, values are given in mean ± SEM, n=4, expect Src probing n=1; *p <0.001 compared to 32D muFLT3 ITD.

5.1.4 Lack of PTP affect total tyrosine phosphorylation

To investigate whether DPI treatment would influence Ptprj and Ptprc activity and whether further phosphatases except the both PTP analyzed would affect FLT3 ITD-mediated signaling events total tyrosine phosphorylation was checked in 32D muFLT3 ITD PTP ko cells (Figure 14A). Upon DPI treatment total tyrosine phosphorylation was about 30 % decreased in 32D muFLT3 ITD cells. In 32D muFLT3 ITD Ptprj ko and 32D muFLT3 ITD Ptprc ko I cells tyrosine phosphorylation was reduced to 65 % compared to 32D muFLT3 ITD cells (Figure 14B). Total tyrosine phosphorylation in untreated Ptprj or Ptprc ko cells was comparable to DPI treated 32D muFLT3 ITD cells. DPI treatment further decreased tyrosine phosphorylation in Ptprj ko or Ptprc ko cells. In cells lacking both PTP the overall tyrosine phosphorylation was 2-fold reduced compared to untreated 32D muFLT3 ITD cells. DPI treatment did not further decrease overall tyrosine phosphorylation in 32D muFLT3 ITD cells lacking both PTP (Figure 14B). Thus, it can be speculated that Ptprj and Ptprc mediate tyrosine phosphorylation in 32D muFLT3 ITD cells via Src. Furthermore, it may be concluded that these both PTP are the main regulators in 32D muFLT3 ITD cells.

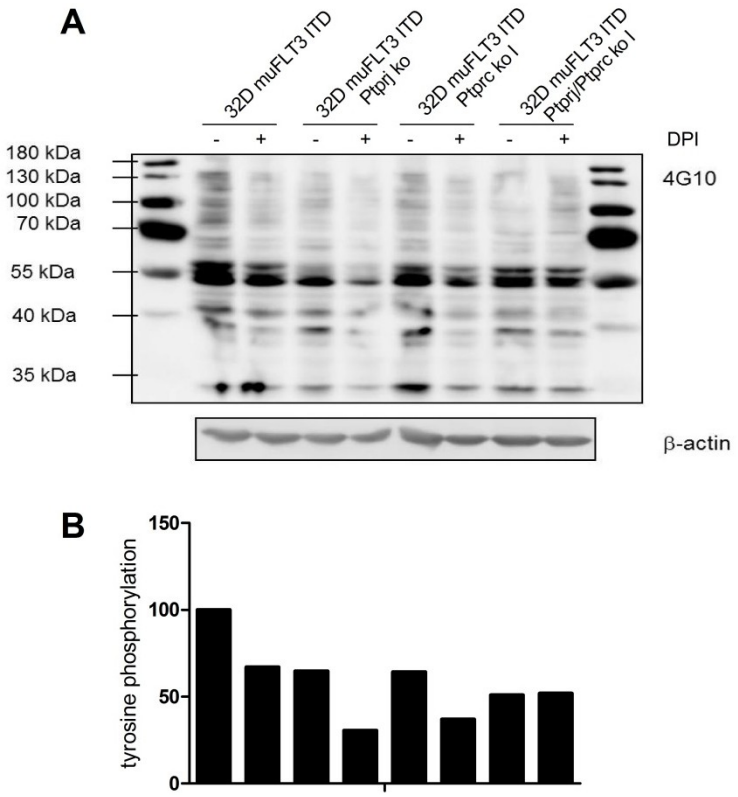

Figure 14. Total tyrosine phosphorylation pattern in 32D muFLT3 ITD and indicated 32D muFLT3 ITD PTP ko cell lines after DPI treatment. (A) 32D muFLT3 ITD (control transduced) and 32D muFLT3 ITD Ptprj ko, 32D muFLT3 ITD Ptprc ko I and 32D muFLT3 ITD Ptprj/Ptprc ko I cell lines were starved for 4 h and in parallel incubated with DPI (0.5 µM). Untreated cells were incubated with respective amount of DMSO for 4 h. Afterwards, cells were lysed in RIPA buffer, equivalent amounts of protein samples were separated by SDS-PAGE and processed for immunodetection. Total tyrosine phosphorylation was detected by 4G10 antibody. Blot was re-probed with β-actin as control. (B) Quantification of overall tyrosine phosphorylation normalized to β-actin expression, n=1.

5.1.5 Inactivation of Ptprj and Ptprc increase the IC_{50} of TKI

Elevated kinase activity of FLT3 is known to shift the dose-response curve for TKI towards somewhat lower sensitivity (Tse et al. 2002). To investigate if inactivation Ptprj and Ptprc affect the activity of FLT3 ITD in 32D muFLT3 ITD cells IC_{50} assay was performed in 32D mu FLT3 ITD PTP ko cells. AC220 and PKC412, FLT3 ITD inhibitors, used for AML treatment in clinical trials, were analyzed for their respective IC_{50} value in PTP ko cells. Interestingly, 32D muFLT3 ITD Ptprj ko and 32D muFLT3 ITD Ptprj/Ptprc ko II cells revealed decreased AC220 sensitivity, demonstrated by significantly increased IC_{50} value. 32D muFLT3 ITD Ptprc ko cells also showed increased IC_{50} value of AC220 but without significance (Figure 15A). In line with the results obtained with AC220 the susceptibility of PKC412 in 32D muFLT3 ITD PTP ko cells was decreased compared to parental 32D muFLT3 ITD cells depicted by a striking increase of PKC412 IC_{50} value (Figure 15B).

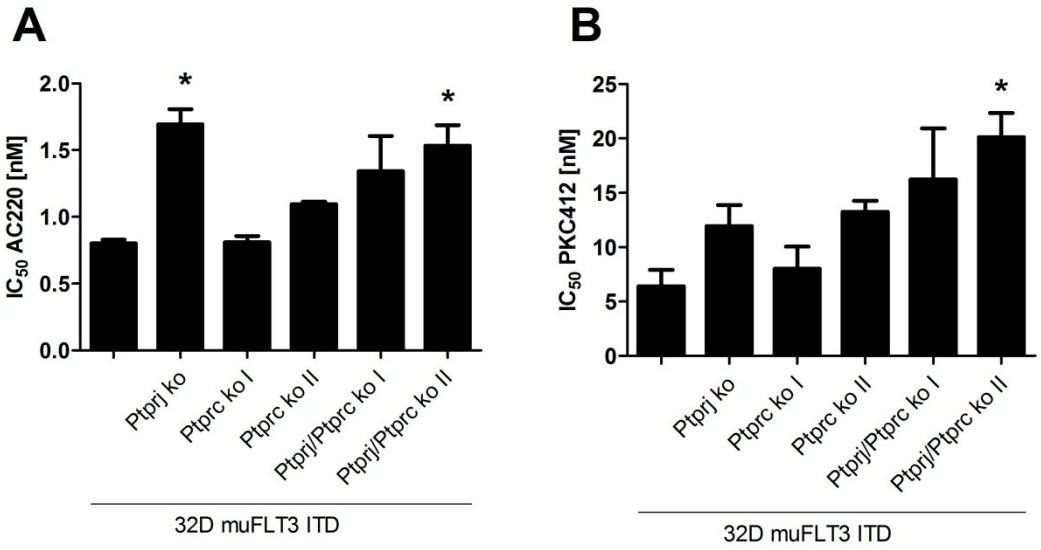

Figure 15. Knockout of RPTP increased IC50 value of FLT3 inhibitors. 32D muFLT3 ITD (control transduced), 32D muFLT3 ITD Ptprj ko, 32D muFLT3 ITD Ptprc ko I and II and 32D muFLT3 ITD Ptprj/Ptprc ko I and II cells were analyzed for IC_{50} value of TKI AC220 and PKC412 using cell titer blue viability assay. Values are given as mean ± SEM, n=3, *p <0.05 compared to 32D muFLT3 ITD.

5.1.6 Clonal growth of 32D muFLT3 ITD PTP ko cells

Increased FLT3 ITD activity drives cell transforming capacity and uncontrolled proliferation. If Ptprj and Ptprc negatively regulate FLT3 ITD-driven transforming capacity, 32D muFLT3 ITD cells with genetic inactivation of either Ptprj or Ptprc or both should demonstrate increase clonogenic growth. 32D muFLT3 ITD Ptprj ko and 32D muFLT3 ITD Ptprc ko I and II showed no altered CFU numbers compared to 32D muFLT3 ITD cells (Figure 16). In contrast, combinatory knockout of Ptprj and Ptprc in 32D muFLT3 ITD cells revealed increased CFU numbers compared to 32D muFLT3 ITD

cells but without reaching statistical significance. In line with signaling results it can be concluded, that lack of Ptprj and Ptprc did not alter FLT3 ITD activity significantly.

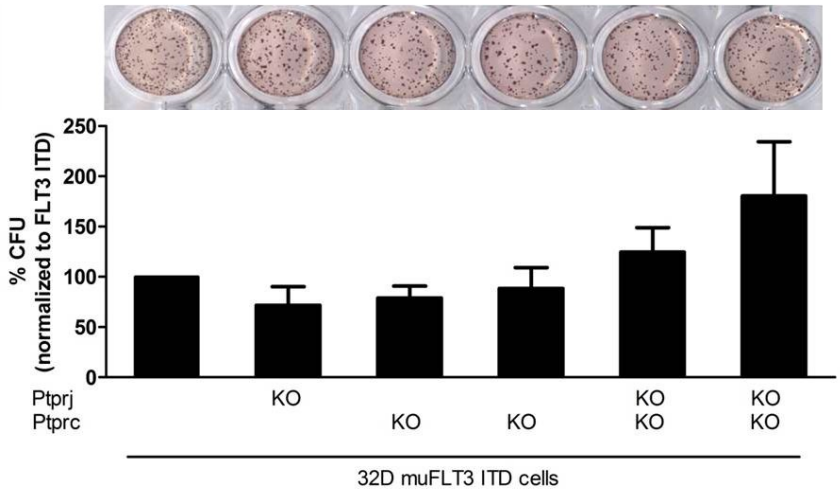

Figure 16. Colony formation of 32D muFLT3 ITD and indicated 32D muFLT3 ITD PTP ko cell lines. 32D muFLT3 ITD (control transduced), 32D muFLT3 ITD Ptprj ko, 32D muFLT3 ITD Ptprc ko I and 32D muFLT3 ITD Ptprj/Ptprc ko I cells were plated in a density of 375 cells / well on methylcellulose medium. n=3, each experiment performed in duplicates; values are given as mean % normalized to 32D muFLT3 ITD ± SEM

5.2 Effects of inactivation of Ptprj and Ptprc on hematopoiesis in FLT3$^{ITD/ITD}$ mice

FLT3 plays a pivotal role in hematopoiesis. Mutations of FLT3 have been linked to hematopoietic malignancies. In about 30 % of AML FLT3 ITD has been observed, causing constitutive kinase activity and transforming potential (Griffith et al. 2004). RPTP Ptprj and Ptprc are also expressed in the hematopoietic compartment. Several approaches have been used to unravel the potential regulatory role of Ptprj and Ptprc on mutated FLT3 ITD kinase at the cellular level (Arora et al. 2011, Godfrey et al. 2012). In order to study whether Ptprj and Ptprc affect FLT3 ITD activity *in vivo*, FLT3$^{ITD/ITD}$ mice (Lee et al. 2007) were crossed with Ptprj$^{-/-}$ or Ptprc$^{-/-}$ mice and phenotypically characterized.

5.2.1 Lack of Ptprj promotes myeloproliferative disease in FLT3$^{ITD/ITD}$ mice

5.2.1.1 Weight development and survival

To investigate whether single or combinatorial mutation of FLT3 ITD and Ptprj impair normal mice developmental, body weight analyses were performed. Neither male nor female FLT3$^{ITD/ITD}$ Ptprj$^{-/-}$ mice did show aberrant total body weight compared to WT and mice with single mutation (Figure 17).

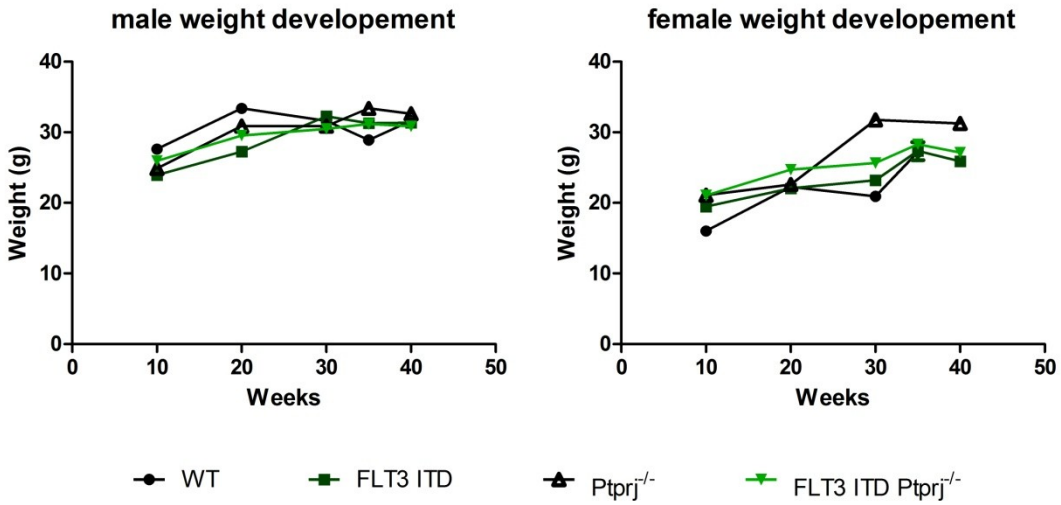

Figure 17. Age dependent weight development of WT, FLT3$^{ITD/ITD}$, Ptprj$^{-/-}$ and FLT3$^{ITD/ITD}$ Ptprj$^{-/-}$ mice. WT (black circle), FLT3$^{ITD/ITD}$ (dark green square), Ptprj$^{-/-}$ (white triangle) and FLT3$^{ITD/ITD}$ Ptprj$^{-/-}$ (light green triangle) male (left panel) and female (right panel) mice were analyzed for their total body weight (g) at the age of 10 to 40 weeks; values are given as mean, n=3

Survival studies of WT, FLT3$^{ITD/ITD}$, Ptprj$^{-/-}$ and FLT3$^{ITD/ITD}$ Ptprj$^{-/-}$ mice revealed mutation-induced shortening of life expectancy. WT and Ptprj$^{-/-}$ mice did not show decreased life expectancy within 300 days. FLT3$^{ITD/ITD}$ mice showed a mean life expectancy of about 250 days (35 weeks) whereas in FLT3$^{ITD/ITD}$ Ptprj$^{-/-}$ mice the life expectancy was only 200 days (28 weeks), although with the number of mice analyzed so far, this difference was not yet statistically significant. The mean survival of FLT3$^{ITD/ITD}$ Ptprj$^{-/-}$ mice was significantly reduced compared to WT and Ptprj$^{-/-}$ littermates. Early onset of more progressive disease was observed in FLT3$^{ITD/ITD}$ Ptprj$^{-/-}$ mice compared to FLT3$^{ITD/ITD}$ mice (Figure 18). Due to the shortened life expectancy all subsequent experiments of this study were carried out with mice at the age of 30 - 35 weeks.

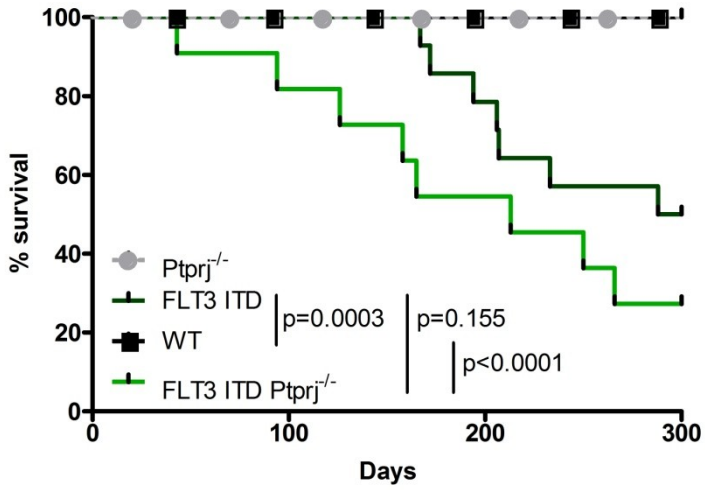

Figure 18. Kaplan Meier Plot of WT, FLT3$^{ITD/ITD}$, Ptprj$^{-/-}$ and FLT3$^{ITD/ITD}$ Ptprj$^{-/-}$ mice. WT (black, n=20) FLT3$^{ITD/ITD}$ (dark green, n=14) Ptprj$^{-/-}$ (grey, n=18) and FLT3$^{ITD/ITD}$ Ptprj$^{-/-}$ (light green, n=11) mice were analyzed for life expectancy. Significance was tested using log rank and indicated in the figure.

5.2.1.2 Organ weight and histological structure

Next, we addressed the question of organ weight and structure. Ptprj$^{-/-}$ mice did not show aberrant organ weight compared to WT mice. A progressive development of splenomegaly was observed in FLT3$^{ITD/ITD}$ mice (Lee et al. 2007), which was not further pronounced in FLT3$^{ITD/ITD}$ Ptprj$^{-/-}$ mice (Figure 19). FLT3$^{ITD/ITD}$ mice the liver weight was slightly increased compared to WT mice. In contrast, the liver weight of FLT3$^{ITD/ITD}$ Ptprj$^{-/-}$ mice was significantly increased compared to WT littermates, indicating hepatomegaly. In FLT3$^{ITD/ITD}$ mice kidneys showed the tendency of increased weight compared to WT littermates, which was more pronounced in FLT3$^{ITD/ITD}$ Ptprj$^{-/-}$ mice.

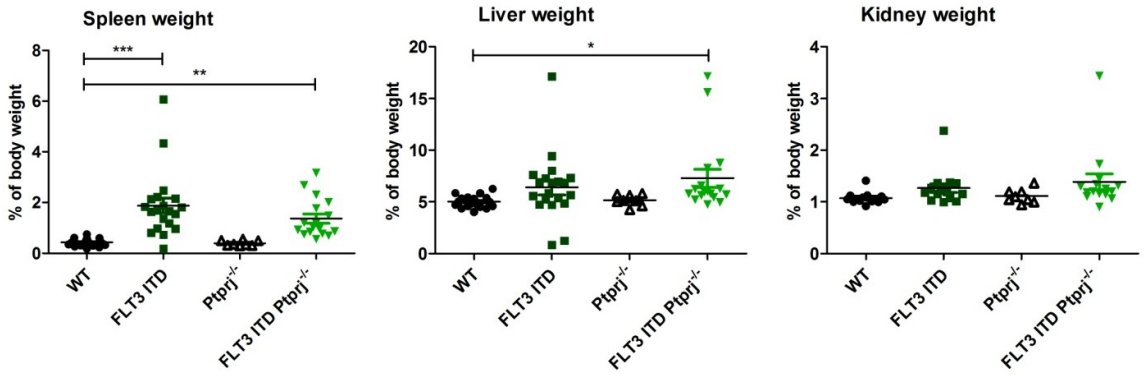

Figure 19. Inactivation of Ptprj in FLT3$^{ITD/ITD}$ mice results splenohepatomegaly. Spleen (left panel), liver (middle panel) and kidney (right panel) weight (% of total body weight) of 30 - 35 weeks old WT(black circle, n=24), FLT3$^{ITD/ITD}$ (dark green square, n=20), Ptprj$^{-/-}$ (white triangle, n=8) and FLT3$^{ITD/ITD}$ Ptprj$^{-/-}$ (light green triangle, n=17) mice were analyzed. *p <0.05, **p <0.01, ***p <0.001 compared to WT mice.

Since splenohepatomegaly was not further increased in response to depletion of Ptprj in FLT3$^{ITD/ITD}$ mice, we next addressed the question, if the tissue structures as well as the nature and amount of possible infiltrated cells would provide explanations of the shortened life span of the FLT3$^{ITD/ITD}$ Ptprj$^{-/-}$ mice. Tissue sections stained with H & E displayed no abundant alteration of spleen and liver structure of Ptprj$^{-/-}$ mice compared to WT controls. In contrast, FLT3$^{ITD/ITD}$ mice exhibited loss of spleen separation in white and red pulp and demonstrated expansion of red splenic pulp. This effect was even more prominent in FLT3$^{ITD/ITD}$ Ptprj$^{-/-}$ mice (Figure 20). Histopathology of liver sections demonstrated infiltration of leukemic cells in FLT3$^{ITD/ITD}$ mice and more progressive in FLT3$^{ITD/ITD}$ Ptprj$^{-/-}$ mice. Infiltrations occurred predominantly around liver sinusoids, but were also spread throughout the organ. While histopathology of kidneys derived from FLT3$^{ITD/ITD}$ or Ptprj$^{-/-}$ mice revealed similar histological structures as WT organs, FLT3$^{ITD/ITD}$ Ptprj$^{-/-}$ kidneys showed a massive infiltration of leukemic cells in the renal medulla resulting in an obvious reduction of the Bowman's space around the glomerula capsule (Figure 20 arrow head, indicated as GC). Similar to liver sinusoids accumulation of these cells appeared to be linked to arteries.

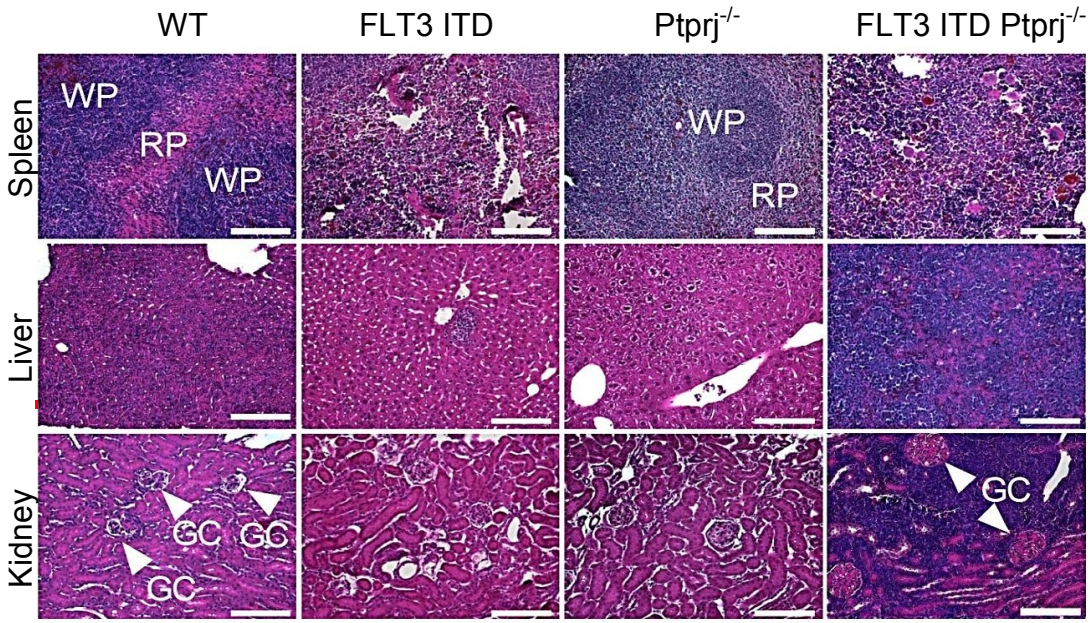

Figure 20. Infiltration of leukemic cells in peripheral organs due to inactivation of Ptprj in FLT3$^{ITD/ITD}$ mice. Representative H & E histopathology showing spleen (top), liver (middle) and kidney (bottom) architecture from 30 - 35 weeks old WT, FLT3$^{ITD/ITD}$, Ptprj$^{-/-}$ and FLT3$^{ITD/ITD}$ Ptprj$^{-/-}$ mice (WP= white pulp, RP= red pulp; GC, glomerulus capsule with arrows), scale bar: 100 µm.

To identify the nature of infiltrated cells immunohistochemistry of paraffin-embedded spleen, liver and kidney sections was carried out. Myeloperoxidase (MPO) is a hallmark enzyme of the myeloid lineage (Kim et al. 2012). Analysis of Ptprj$^{-/-}$ mice showed no abnormalities compared to WT mice. MPO staining of spleen sections could demonstrate the expansion of red pulp (MPO-positive cells) in FLT3$^{ITD/ITD}$ mice but more pronounced in FLT3$^{ITD/ITD}$ Ptprj$^{-/-}$ mice. This was accompanied by impaired separation of white and red pulp of spleen in FLT3$^{ITD/ITD}$ mice and more pronounced in FLT3$^{ITD/ITD}$ Ptprj$^{-/-}$ mice. Staining of organs from FLT3$^{ITD/ITD}$ Ptprj$^{-/-}$ mice demonstrated infiltration of MPO-positive cells in liver and kidney. MPO-positive cell infiltration was not observed in age-matched WT littermates (Figure 21).

Splenomegaly was less prominent in FLT3$^{ITD/ITD}$ Ptprj$^{-/-}$ mice than in FLT3$^{ITD/ITD}$ mice (Figure 19). However, analysis of organ structure revealed a more progressive infiltration of MPO-positive cells in FLT3$^{ITD/ITD}$ Ptprj$^{-/-}$ mice compared to mice with single mutation and WT mice (Figure 21). The severe destruction of organ architecture probably led to impaired organ function.

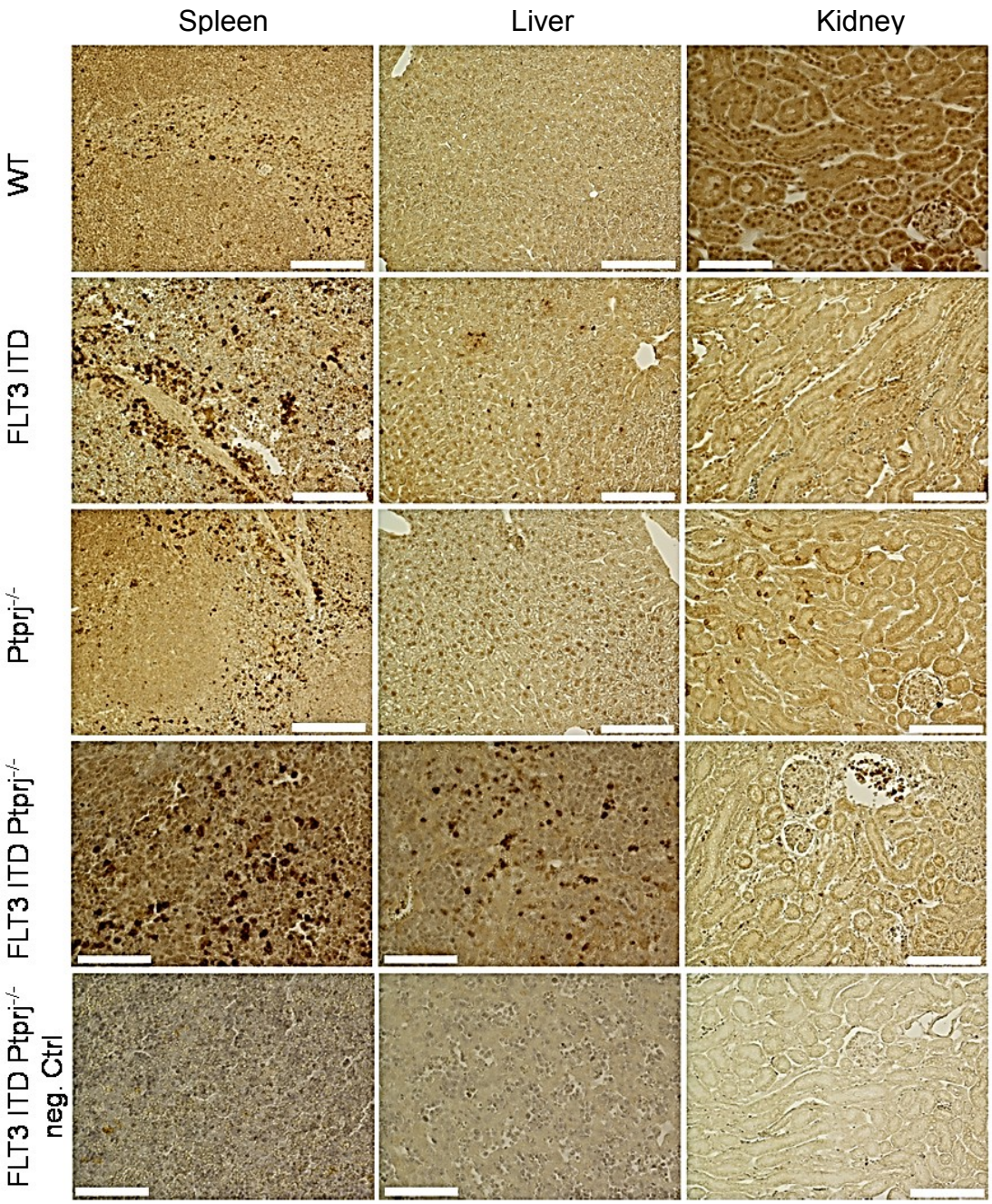

Figure 21. Accumulation of MPO positive cells in organs of FLT3$^{ITD/ITD}$ Ptprj$^{-/-}$ mice. Representative images of MPO stained spleen, liver and kidney sections from WT, FLT3$^{ITD/ITD}$, Ptprj$^{-/-}$ and FLT3$^{ITD/ITD}$ Ptprj$^{-/-}$ mice. Sections from FLT3$^{ITD/ITD}$ Ptprj$^{-/-}$ mice incubated without primary antibody were used as negative control. Scale bar indicates 100 µm.

5.2.1.3 Peripheral blood analysis

In order to analyze the myeloproliferative phenotype the composition of the peripheral blood was characterized. The peripheral blood composition of Ptprj$^{-/-}$ mice did not show an aberrant phenotype compared to WT littermates. Consistent with earlier findings in FLT3$^{ITD/ITD}$ mice (Lee et al. 2007, Li et al. 2008), 3- and 6- fold increased numbers of neutrophils and monocytes were observed in 30 - 35 weeks old mice. Inactivation of Ptprj in FLT3$^{ITD/ITD}$ mice further pronounced this effect. Elevated white blood cell count (WBC, Figure 22A) and WBC differentials (Figure 22E) confirmed the expansion of monocytec / granulocytic population in FLT3$^{ITD/ITD}$ Ptprj$^{-/-}$ mice indicating a more progressive myeloproliferative disease. Moreover, a decrease of the lymphocytic population was observed in FLT3$^{ITD/ITD}$ animals, which was more pronounced in FLT3$^{ITD/ITD}$ Ptprj$^{-/-}$ mice pointing to an impaired lymphocyte development or displacement of lymphocytes. Red blood cell count (RBC, Figure 22B), number of platelets (Figure 22C) and hemoglobin (HGB, Figure 22D) of FLT3$^{ITD/ITD}$ animals were significantly reduced compared to age-matched WT littermates. Knockout of Ptprj in FLT3$^{ITD/ITD}$ mice did not further elevate this effect.

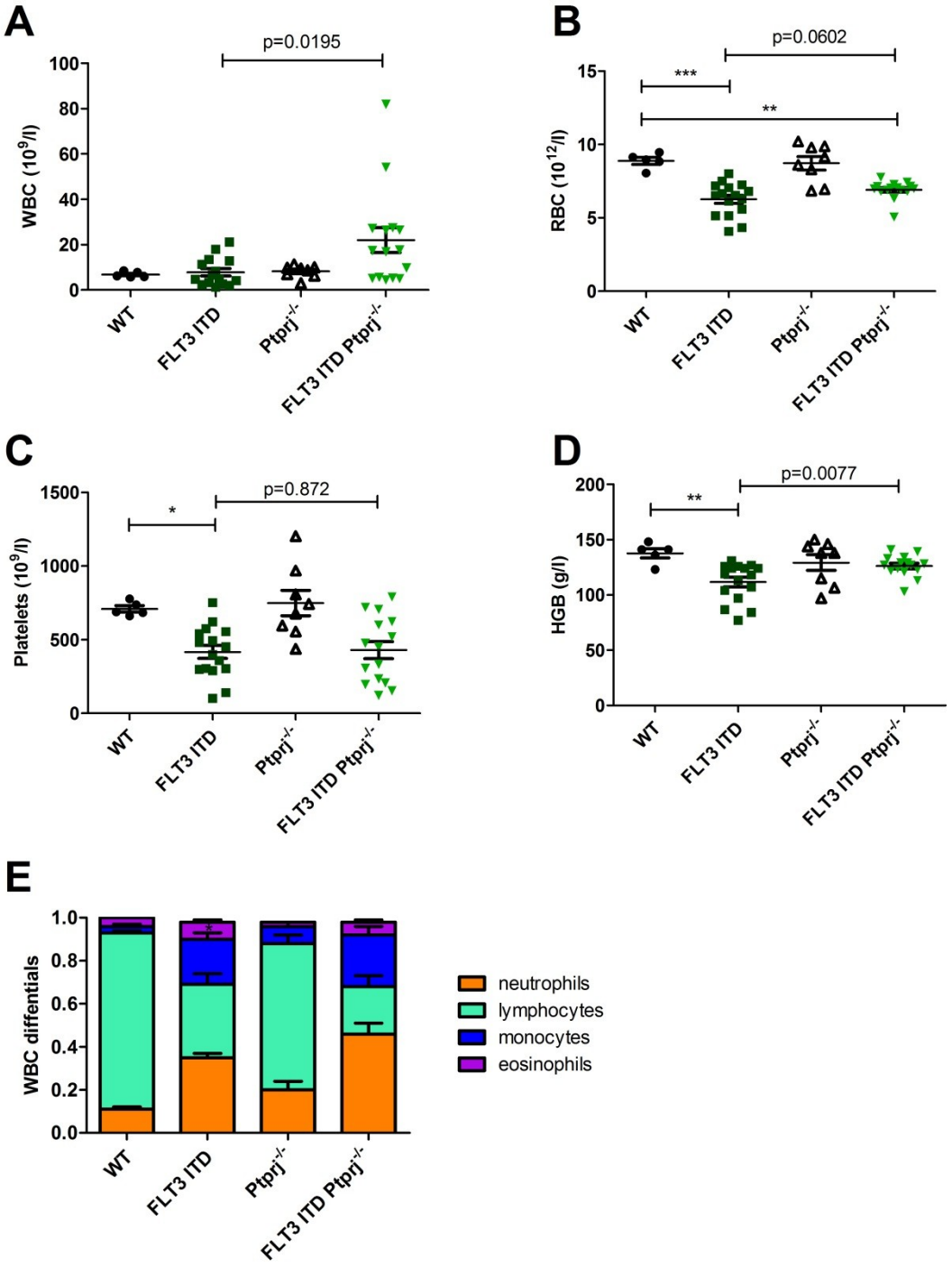

Figure 22. FIT3$^{ITD/ITD}$ Ptprj$^{-/-}$ mice develop myeloproliferative neoplasm. White blood cell count (WBC; A), red blood cell count (RBC, B), number of platelets (C) and hemoglobin (HGB, D) are presented for WT, FLT3$^{ITD/ITD}$, Ptprj$^{-/-}$ FLT3$^{ITD/ITD}$ Ptprj$^{-/-}$ mice at the age of 30 – 35 weeks. WBC differentials (E) normalized to total amount of leukocytes are demonstrated. Samples of peripheral blood were analyzed using a Mindray BC5300Vet Hematology system. Bar (A-D) indicates mean ± SEM. White blood cell count differentials are shown in means ± SEM indicating. *p <0.05, **p <0.01, ***p <0.001 compared to WT. #p <0.05 compared to FLT3$^{ITD/ITD}$.

5.2.1.4 Impaired lymphopoiesis and extramedullary hematopoiesis

Myeloid expansion was analyzed by flow cytometric analyses. In BM no changes of the myeloid population compared to WT littermates were observed in none of the mutated mice investigated (Figure 23A). Splenic cells from $FLT3^{ITD/ITD}$ mice demonstrated a slight increase of CD11b / Gr-1 positive population which was significantly increased in $FLT3^{ITD/ITD}$ $Ptprj^{-/-}$ mice (Figure 23B). Strongly reduced amount of $CD19^{+}$ B lymphoid cells out of myeloid undifferentiated ($Gr\text{-}1^{-}$ / $CD11b^{-}$) population was observed in both BM and spleen of $FLT3^{ITD/ITD}$ animals compared to WT mice. In $FLT3^{ITD/ITD}$ $Ptprj^{-/-}$ mice the reduction of $CD19^{+}$ B cells was further increased compared to WT mice. $CD19^{+}$ splenic B cells were about 2-fold down regulated in $FLT3^{ITD/ITD}$ $Ptprj^{-/-}$ mice compared to $FLT3^{ITD/ITD}$ mice (Figure 23B). $CD3\varepsilon^{+}$ T cell population did not show any changes in spleen and BM of mice with single mutation and $FLT3^{ITD/ITD}$ $Ptprj^{-/-}$ mice compared to WT controls.

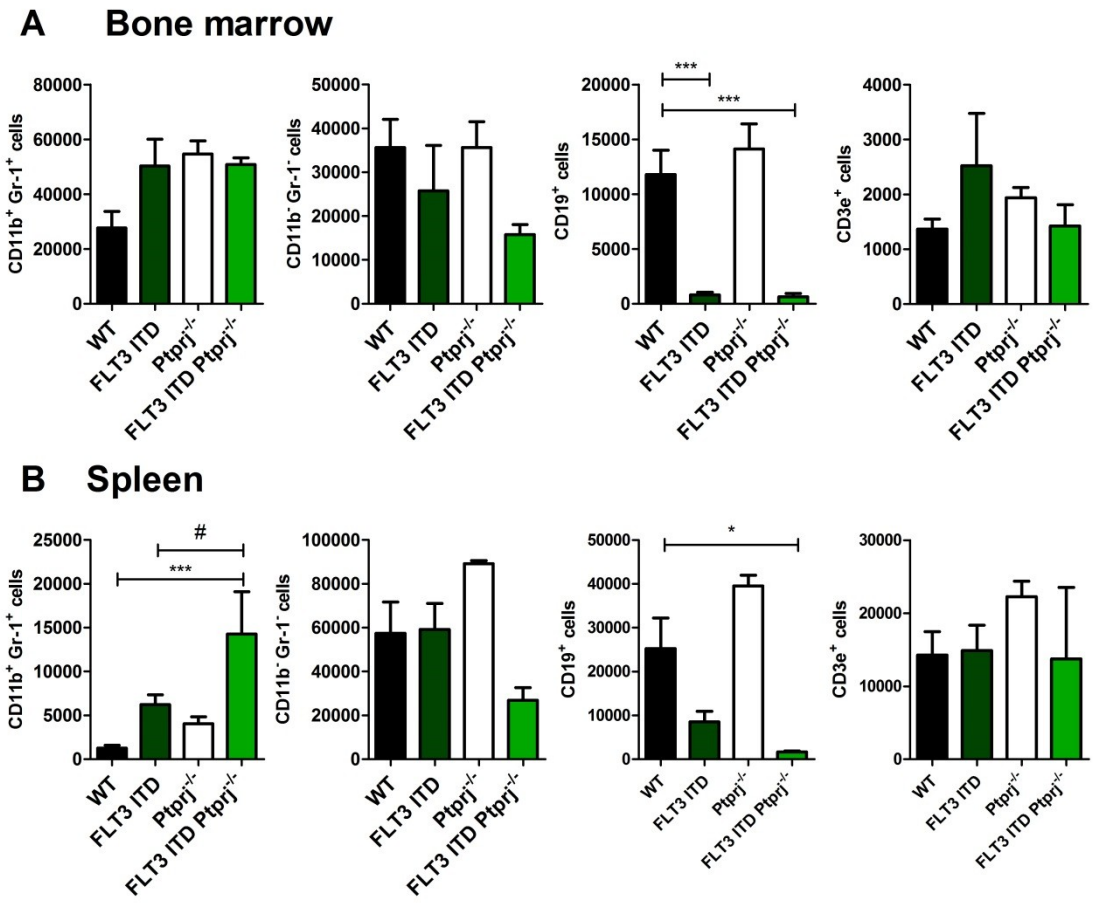

Figure 23. Mutant $FLT3^{ITD/ITD}$ $Ptprj^{-/-}$ mice show B cell lymphocytopenia. Immunophenotype of BM and spleen cells from 30 - 35 weeks old WT, $FLT3^{ITD/ITD}$, $Ptprj^{-/-}$ and $FLT3^{ITD/ITD}$ $Ptprj^{-/-}$ mice were analyzed concerning CD11b, Gr-1, CD19 and CD3ε expression. Graphical presentation of CD11b / Gr-1 expression and CD19 as well as CD3ε expression in $CD11b^{-}$ / $Gr\text{-}1^{-}$ population in BM (A) and spleen (B) were demonstrated as absolute cell number. Values are given as mean ± SEM out of $1x10^{5}$ cells analyzed; *p <0.05,***p <0.001 compared to WT; # p <0.05 compared to $FLT3^{ITD/ITD}$; n=5 per genotype.

Next, we addressed the question whether the stem cell population was changed in BM or spleen of mice harboring a single or double mutation to investigate possible extramedullary hematopoiesis. Interestingly, splenic lineage negative (Lin^-) cells of $Ptprj^{-/-}$ mice were 50 % reduced compared to WT mice (Figure 24A). Lin^- BM cells, myeloid progenitor and LSK population of $Ptprj^{-/-}$ mice did not show any alterations compared to WT littermates. Flow cytometric characterization revealed a 2.5-fold elevation of Lin^-cells in BM of $FLT3^{ITD/ITD}$ $Ptprj^{-/-}$ mice compared to $FLT3^{ITD/ITD}$ mice In BM the amount of Lin^- cells in $FLT3^{ITD/ITD}$ mice did not change significantly by contrast with WT littermates. The Lin^- population in spleen (Figure 24B) was changed marginally in $FLT3^{ITD/ITD}$ and $FLT3^{ITD/ITD}$ $Ptprj^{-/-}$ mice. According to Li and co-workers the number of Lin^- $Sca\text{-}1^-$ $c\text{-}Kit^+$ (committed myeloid progenitors) cells in spleen was severely enhanced in $FLT3^{ITD/ITD}$ mice (Li et al. 2008, Li et al. 2011). A similar increase was also observed in our experiments with $FLT3^{ITD/ITD}$ mice which was further pronounced in $FLT3^{ITD/ITD}$ $Ptprj^{-/-}$ mice in BM and spleen. Similarly, the numbers of Lin^- $Sca\text{-}1^+$ $c\text{-}kit^+$ (LSK) cells, which were already several-fold enriched in $FLT3^{ITD/ITD}$ spleens compared with WT mice, were significantly further enhanced in $FLT3^{ITD/ITD}$ $Ptprj^{-/-}$ mice. In BM only small differences of these cell populations were observed. Taken together, these data demonstrate that inactivation of Ptprj in $FLT3^{ITD/ITD}$ mice results in an increase of Lin^-, myeloid progenitors and LSK cells showing a pronounced accumulation in spleen and indicating extramedullary hematopoiesis.

In murine hematopoiesis, WT FLT3 expression was demonstrated in all progenitors of granulocytes/macrophages including GMP and CMP (Kikushige et al. 2008). Here FLT3 expression was analyzed in myeloid progenitors and LSK cells of BM and spleen. Ptprj knockout did not change the amount of FLT3-positive myeloid progenitors in BM and spleen compared to WT mice. Interestingly, in $Ptprj^{-/-}$ mice the number of FLT3-positive LSK was increased in BM whereas in spleen no alteration was observed compared to WT littermates. In myeloid progenitors, FLT3 ITD mutation resulted in 5- or 39-fold elevation of FLT3-positive cells in BM and spleen, respectively compared to WT littermates (Figure 24C, D). There was a trend of further enhanced numbers of FLT3-positive progenitors in $FLT3^{ITD/ITD}$ $Ptprj^{-/-}$ mice; however, the differences did not reach statistical significance. In $FLT3^{ITD/ITD}$ $Ptprj^{-/-}$ mice FLT3-positive LSK cells were enhanced in spleen only compared to WT mice indicating extramedullary hematopoiesis. In BM the number of FLT3-positive LSK cells was comparable to WT littermates and even lower than compared to $FLT3^{ITD/ITD}$ and $Ptprj^{-/-}$ mice.

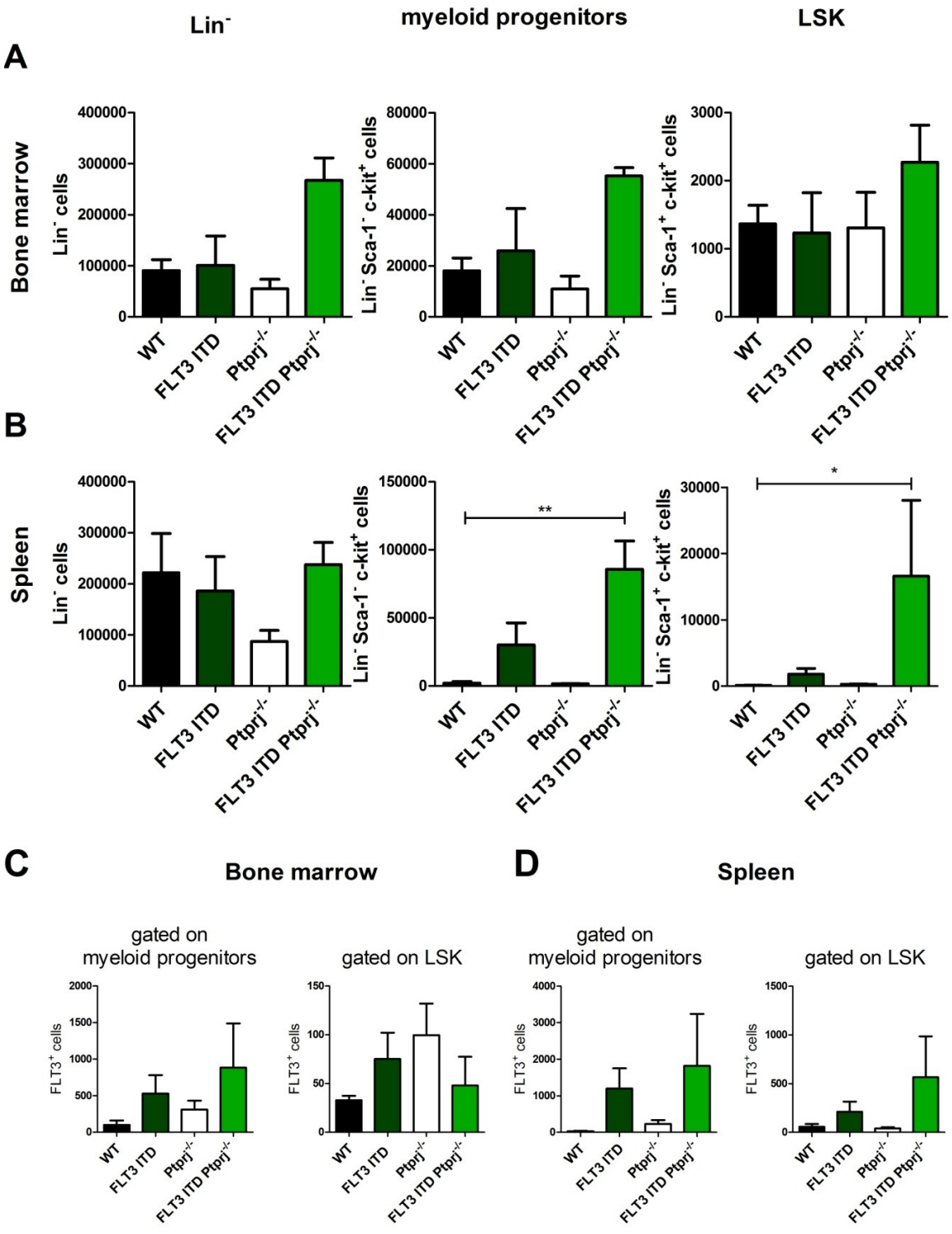

Figure 24. FLT3$^{ITD/ITD}$ Ptprj$^{-/-}$ animals show extramedullary hematopoiesis in spleen. Immunophenotype of BM and spleen cells derived from 30 – 35 weeks old WT, FLT3$^{ITD/ITD}$, Ptprj$^{-/-}$ and FLT3$^{ITD/ITD}$ Ptprj$^{-/-}$ mice were investigated. Total amount of Lin$^-$, Lin$^-$ c-kit$^+$ Sca-1$^-$ (committed myeloid progenitors) and Lin$^-$ c-kit$^+$ Sca-1$^+$ (LSK) cells in BM (A) and spleen (B) are demonstrated. Graphical presentation of FLT3$^+$ cells within these populations is shown for BM (C) and spleen (D). Values are given as mean ± SEM demonstrating cell number out of 1x10^6 cells analyzed; *p<0.05, **p<0.01 compared to WT. n=4 per genotype.

5.2.1.5 Clonogenic growth and transforming capacity

Repopulation capacity of progenitor cells was investigated to analyze the transforming capacity of Lin^- cells and to get information whether the phenotype describes a leukemic or proliferative disease. A leukemic phenotype is characterized by repopulation capacity of these cells. Increased clonogenic growth would indicate increased FLT3 ITD activity in response to Ptprj inactivation. Furthermore, the myeloproliferative phenotype could be assessed by the respective CFU units. Thus, progenitor cells of BM and spleen were MACS sorted for Lin^- immunophenotype and subsequently evaluated by *in vitro* clonogenic assay in M3434 methylcellulose.

While the number of colony forming units of BM granulocytes/macrophages (CFU GM) of WT, $FLT3^{ITD/ITD}$ or $Ptprj^{-/-}$ mice showed no significant change, the number of CFU GM from BM of $FLT3^{ITD/ITD}$ $Ptprj^{-/-}$ mice was significantly elevated compared with all other genotypes (Figure 25A). While Lin^- cells purified from spleen of $FLT3^{ITD/ITD}$ mice revealed only a slight increase of clonogenic growth, splenic Lin^- cells from $FLT3^{ITD/ITD}$ $Ptprj^{-/-}$ mice showed a significantly upregulated clonal growth, compared with Lin^- cells of WT mice (Figure 25B). The numbers of multipotential granulocyte, erythroid, macrophage, megakaryocyte progenitor cells (CFU GEMM) and erythroid progenitor cells (CFU BFU) showed no alterations within the genotypes. For assessment of the potential repopulation capacity cells from CFU GM were harvested and reseeded in M3434 methylcellulose. No subsequent colony formation was observed irrespective of the genotype indicating lack of repopulating capacity. Subsequent cytospin analyses confirmed myeloid lineage of cells (Figure 25C).

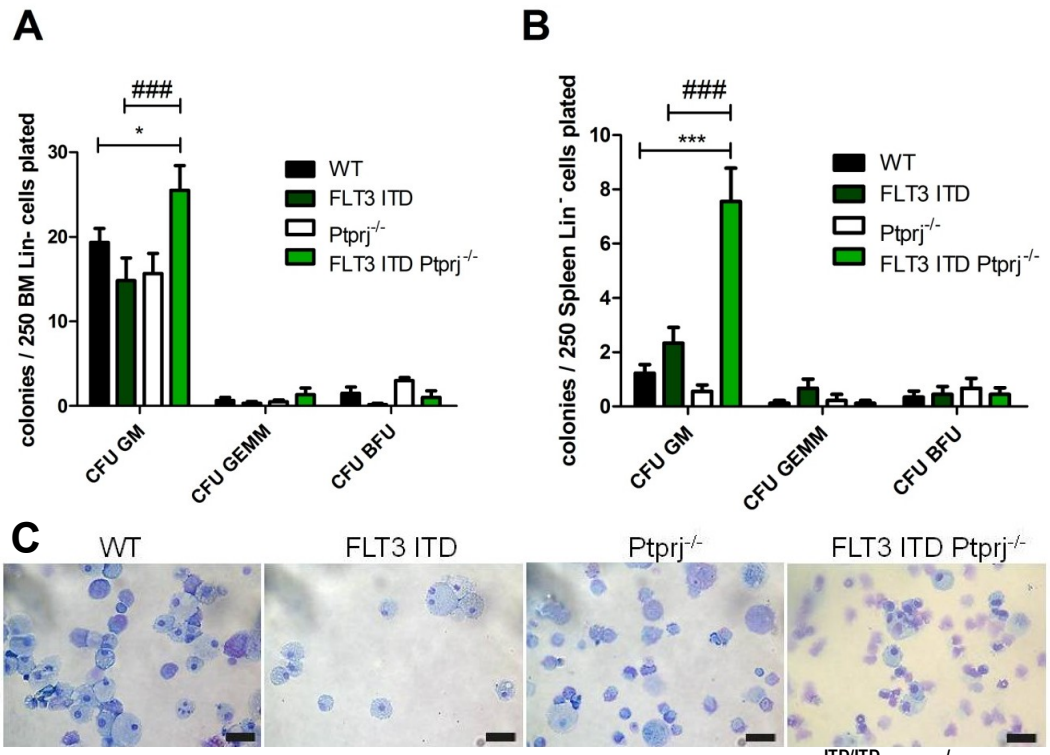

Figure 25. Promotion of clonogenic growth of splenic Lin- cells of FLT3$^{ITD/ITD}$ Ptprj$^{-/-}$ mice. Lin^{-} BM (A) and spleen (B) cells from 30 - 35 week old WT, FLT3$^{ITD/ITD}$, Ptprj$^{-/-}$ and FLT3$^{ITD/ITD}$ Ptprj$^{-/-}$ mice were plated on M3434 methylcellulose medium (containing SCF-1, IL-3, EPO) and scored for colony formation 7 days later, n=9. Values are given in mean ± SEM, BM colonies were harvested and analyzed by cytospin (C). Scale bar indicates 25 µm. *p <0.05, ***p <0.001 compared to WT; ###p <0.001 compared to FLT3$^{ITD/ITD}$.

5.2.1.6 Specific FLT3 activity

The ITD mutation of FLT3 results in retention of mutated receptor in intracellular membranes, indicating by impaired maturation, e.g. a prevalence of the incompletely glycosylated, high-mannose form of 130 kDa and aberrant signaling towards downstream targets (Schmidt-Arras et al. 2005, Schmidt-Arras et al. 2009, Choudhary et al. 2009). In order to assess FLT3 ITD kinase activity and maturation in response to inactivation of Ptprj, MACS-purified Lin^{-} cell from the BM of 30 week old mice were probed for activity-specific phosphorylation of the receptor. While in WT or Ptprj$^{-/-}$ cells the level of FLT3 expression was too low to be detected by immunoblotting, FLT3 ITD ligand-independent phosphorylation activity of Y591 and Y589 could be detected in FLT3$^{ITD/ITD}$. FLT3$^{ITD/ITD}$ Ptprj$^{-/-}$ mice showed a moderately but significantly increased FLT3 Y591 phosphorylation compared to FLT3$^{ITD/ITD}$ mice (Figure 26).

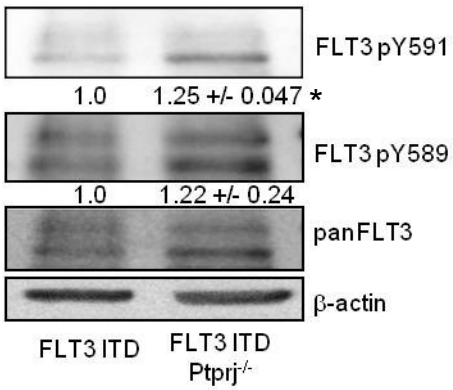

Figure 26. Increased specific FLT3 phosphorylation in FLT3$^{ITD/ITD}$ Ptprj$^{-/-}$ mice. Lin^{-} purified BM cells of 30 weeks old FLT3$^{ITD/ITD}$ and FLT3$^{ITD/ITD}$ Ptprj$^{-/-}$ mice were lysed in RIPA buffer and equivalent amounts of protein were separated by SDS-PAGE and processed for immunodetection using phosphosite specific antibodies recognizing pY591 and pY589 of FLT3 protein. Blot was re-probed for total FLT3 antibody and β-actin as control. Quantification of signal intensity normalized to FLT3 ITD is shown as mean ± SEM, n=3. *p<0.05 compared to FLT3$^{ITD/ITD}$ mice.

To further investigate the signaling activity of FLT3, splenic cells of 30 weeks old WT, FLT3$^{ITD/ITD}$, Ptprj$^{-/-}$ and FLT3$^{ITD/ITD}$ Ptprj$^{-/-}$ mice were probed for specific phosphorylation of FLT3 ITD downstream targets. Specific AKT S473 phosphorylation was significantly down regulated in FLT3$^{ITD/ITD}$, Ptprj$^{-/-}$ and FLT3$^{ITD/ITD}$ Ptprj$^{-/-}$ compared to WT mice (Figure 27A, B). Interestingly, in FLT3$^{ITD/ITD}$ Ptprj$^{-/-}$ mice specific Src Y416 phosphorylation was significantly increased compared with WT mice whereas mice harboring a single mutation showed no effects. ERK1/2 (T202/Y204) phosphorylation did not show any effect due to FLT3$^{ITD/ITD}$ mutation or Ptprj knockout. Immunoblot investigation of STAT5 failed due to highly unspecific antibody although several pSTAT5 antibodies were tested.

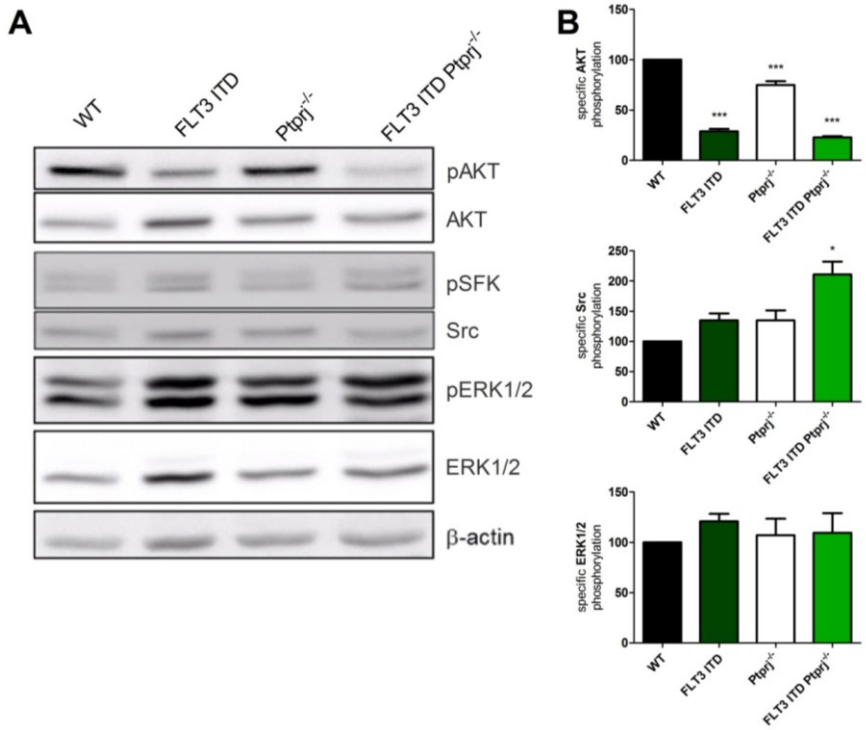

Figure 27. Signaling analysis of splenic FLT3$^{ITD/ITD}$ Ptprj$^{-/-}$ cells. Spleen cells of 30 - 35 weeks old WT, FLT3$^{ITD/ITD}$, Ptprj$^{-/-}$ and FLT3$^{ITD/ITD}$ Ptprj$^{-/-}$ mice were lysed in RIPA buffer and equivalent amounts of protein were separated by SDS-PAGE and processed for immunodetection using phosphosite specific antibodies recognizing AKT (S473), SFK (Y416) and ERK1/2 (T202/Y204). Blot was re-probed for total AKT, Src and ERK antibody and β-actin as control. (A) Representative immunoblot; (B) Quantification of specific phosphorylation of, AKT, Src and ERK in relation to total protein level of indicated proteins, values are given in mean ± SEM, n=3; *p<0.05, ***p <0.001 compared to WT mice.

5.2.2 Lack of Ptprc promotes MPN and bone aberrancies in FLT3$^{ITD/ITD}$ mice

5.2.2.1 Weight development and survival

To investigate whether mutation of FLT3 ITD or knockout of Ptprc or combinatory mutation resulted in impaired mice development mice weight was investigated. Comparative analysis of age-dependent weight development from WT, FLT3$^{ITD/ITD}$, Ptprc$^{-/-}$ and FLT3$^{ITD/ITD}$ Ptprc$^{-/-}$ mice showed no significant difference neither in male nor in female mice (Figure 28).

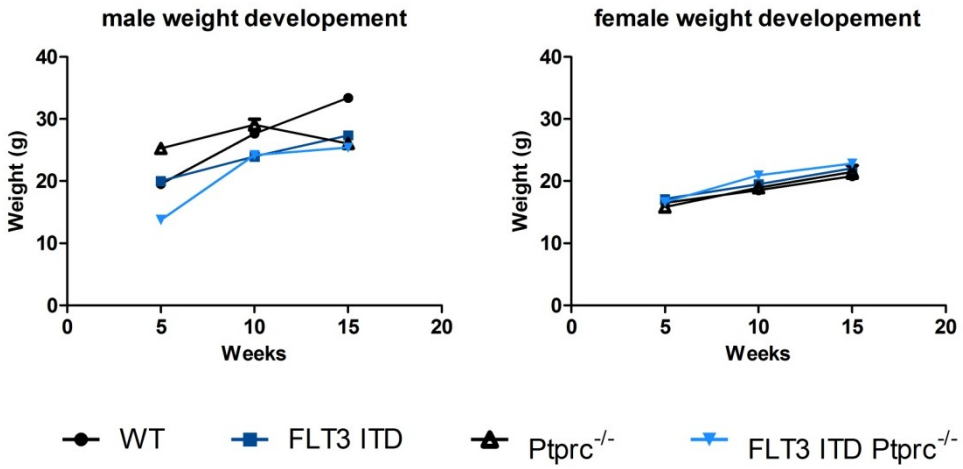

Figure 28. Age dependent weight development of WT, FLT3$^{ITD/ITD}$, Ptprc$^{-/-}$ and FLT3$^{ITD/ITD}$ Ptprc$^{-/-}$ mice. WT (black circle), FLT3$^{ITD/ITD}$ (dark blue square), Ptprc$^{-/-}$ (white triangle) and FLT3$^{ITD/ITD}$ Ptprc$^{-/-}$ (light blue triangle) male (left panel) and female (right panel) mice were analyzed for their total body weight (g) at the age of 5 to 15 weeks; values are given as mean, n =3.

Life span of mice was analyzed to address the question if FLT3$^{ITD/ITD}$ Ptprc$^{-/-}$ mice developed a more progressive phenotype than FLT3$^{ITD/ITD}$ mice. As seen in Figure 29, FLT3$^{ITD/ITD}$ mice had a shortened mean survival compared to WT littermates and started to die from day 170 (24 weeks). FLT3$^{ITD/ITD}$ mice showed a mean life expectancy of 250 days (35 weeks). Remarkably, the life span of FLT3$^{ITD/ITD}$ Ptprc$^{-/-}$ mice was drastically shortened. They started to die from day 37 already demonstrating a more progressive phenotype than FLT3$^{ITD/ITD}$ mice. The mean life expectancy of FLT3$^{ITD/ITD}$ Ptprc$^{-/-}$ mice (157 days/ 22 weeks) was significantly shortened compared to WT and Ptprc$^{-/-}$ littermates and even close to significantly decreased compared to FLT3$^{ITD/ITD}$ littermates ($p < 0.06$). Statistical analyses of animal survival within the first 150 days showed a significantly reduced survival of FLT3$^{ITD/ITD}$ Ptprc$^{-/-}$ mice compared with WT mice and mice harboring single mutations (log rank test $p=0.0014$). Shortened life span of FLT3$^{ITD/ITD}$ Ptprc$^{-/-}$ mice indicates increased aggressiveness of FLT3 ITD-driven disease. Due to the short life span of FLT3$^{ITD/ITD}$ Ptprc$^{-/-}$ mice all subsequent experiments were carried out with mice at the age of 12 - 17 weeks.

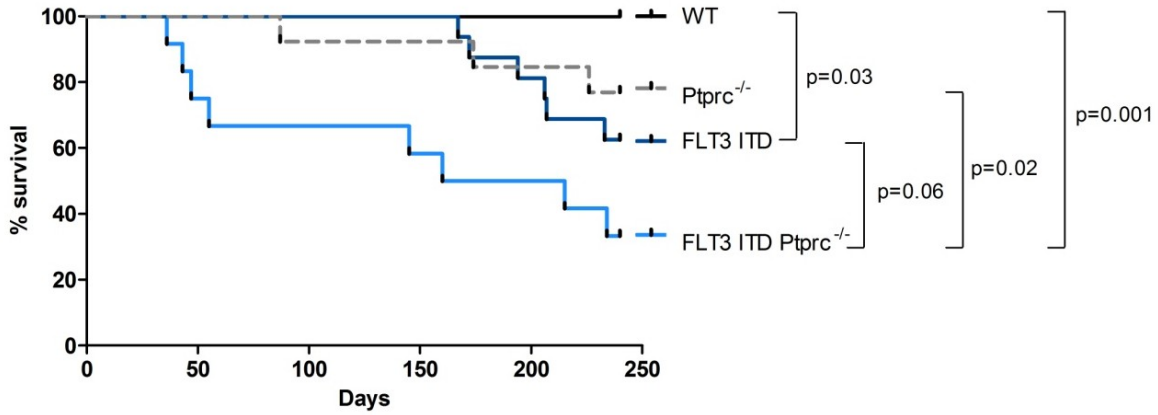

Figure 29. Kaplan Meier Plot of WT, FLT3$^{ITD/ITD}$, Ptprc$^{-/-}$ and FLT3$^{ITD/ITD}$ Ptprc$^{-/-}$ mice. WT (black, n=10) FLT3$^{ITD/ITD}$ (dark blue, n=15) Ptprc$^{-/-}$ (grey, n=10) and FLT3$^{ITD/ITD}$ Ptprc$^{-/-}$ (light blue, n=12) mice were analyzed for life expectancy; Statistical significance was validated by log rank test.

5.2.2.2 Organ weight and architecture

Comparative analysis of organ weight revealed no change in FLT3$^{ITD/ITD}$ and Ptprc$^{-/-}$ mice compared to WT littermates. In FLT3$^{ITD/ITD}$ Ptprc$^{-/-}$ mice significantly increased organ weights were observed compared to WT mice (Figure 30). Spleen weight of mice harboring both mutations was more than 3-fold increased, liver weight was doubled compared to mice with single mutation and WT littermates. Kidney weight was significantly increased compared to WT littermates. These results point to a severe disease in FLT3$^{ITD/ITD}$ Ptprc$^{-/-}$ mice probably affecting hematopoiesis.

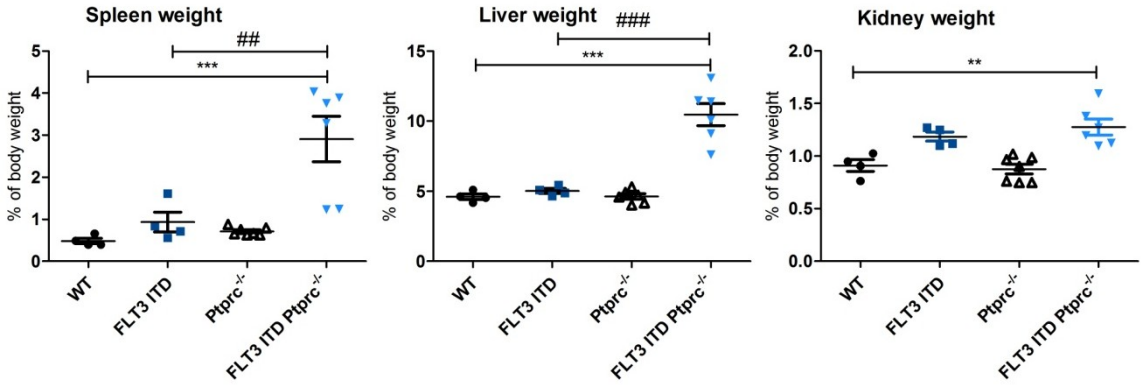

Figure 30. Inactivation of Ptprc in FLT3$^{ITD/ITD}$ mice results in severe splenohepatomegaly and nephromegaly. Spleen (left panel), liver (middle panel) and kidney (right panel) weight (% of total body weight) of 12 - 17 weeks old WT (black circle, n=4), FLT3$^{ITD/ITD}$ (dark blue square, n=4), Ptprc$^{-/-}$ (white triangle, n=7) and FLT3$^{ITD/ITD}$ Ptprc$^{-/-}$ (light blue triangle, n=6) mice were analyzed. **p <0.01, ***p <0.001 compared to WT mice. ##p <0.01 ###p <0.001 compared to FLT3$^{ITD/ITD}$ mice.

In order to elucidate the reason of decreased life span and splenohepatomegaly in FLT3$^{ITD/ITD}$ Ptprc$^{-/-}$ mice, histopathological analyses of the peripheral organs were performed. In Ptprc$^{-/-}$ mice, no aberrancies of organ architecture were discovered compared to WT controls. As outlined before, an infiltration of leukemic cells and disturbance of red and white pulp separation of the spleen compared to WT spleen was

already observed in FLT3$^{ITD/ITD}$ mice, but it was clearly more pronounced in FLT3$^{ITD/ITD}$ Ptprc$^{-/-}$ mice (Figure 31). Leukemic cell infiltration was observed in kidney of FLT3$^{ITD/ITD}$ Ptprc$^{-/-}$ mice, but none of the mice with single mutation displayed aberrancies compared to WT controls. In liver samples of FLT3$^{ITD/ITD}$ mice few infiltrated cells were observed predominantly at liver sinusoids. The infiltration was much stronger in FLT3$^{ITD/ITD}$ Ptprc$^{-/-}$ mice. Leukemic cells were observed close to liver sinusoid but also spread throughout the tissue. Disturbed tissue structures of peripheral organs might result in impaired organ function and in turn shortened life span of FLT3$^{ITD/ITD}$ Ptprc$^{-/-}$ mice.

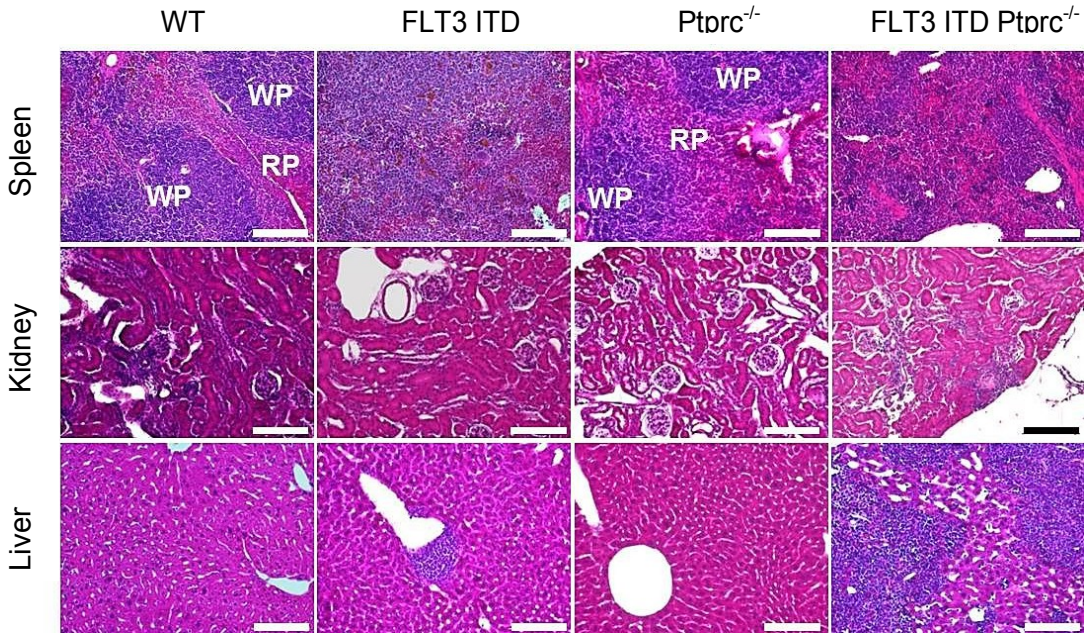

Figure 31. Infiltration of leukemic cells in peripheral organs due to Ptprc inactivation in FLT3$^{ITD/ITD}$ mice. Representative H & E histopathology showing spleen (top), kidney (middle) and liver (bottom) architecture from 12 - 17 weeks old WT, FLT3$^{ITD/ITD}$, Ptprc$^{-/-}$ and FLT3$^{ITD/ITD}$ Ptprc$^{-/-}$ mice (WP= white pulp, RP= red pulp). Scale bar indicates 100 µm.

To further elucidate the lineage origin of infiltrated cells the peripheral organs were checked for MPO-positive cells by immunohistochemistry. MPO is the hallmark enzyme of the myeloid lineage (Kim et al. 2012). Livers of FLT3$^{ITD/ITD}$ Ptprc$^{-/-}$ mice exhibited multiple accumulations of MPO-positive cells around the liver sinusoids but also spread throughout the tissue, which was observed in any of the controls (Figure 32A). In spleen, MPO-positive cells normally occur in areas of red pulp as it was found in mice with single mutation and WT controls (Figure 32B). However, in FLT3$^{ITD/ITD}$ mice clearly increased amount of MPO-positive cells was observed in spleen when compared to WT controls. A drastically increased quantity of MPO-positive cells, spread throughout the complete tissue, was observed in spleens of FLT3$^{ITD/ITD}$ Ptprc$^{-/-}$ mice, indicating the loss of segmentation of the spleen by propagation of red pulp and the infiltration of MPO-positive cells in spleen. Although the kidney weight was significantly increased and H & E staining indicated slight infiltration of leukemic cells no infiltration of MPO-positive cells

was detected in FLT3$^{ITD/ITD}$ Ptprc$^{-/-}$ mice (Figure 32C). Specification of the MPO-antibody was validated by negative controls (Figure 32D).

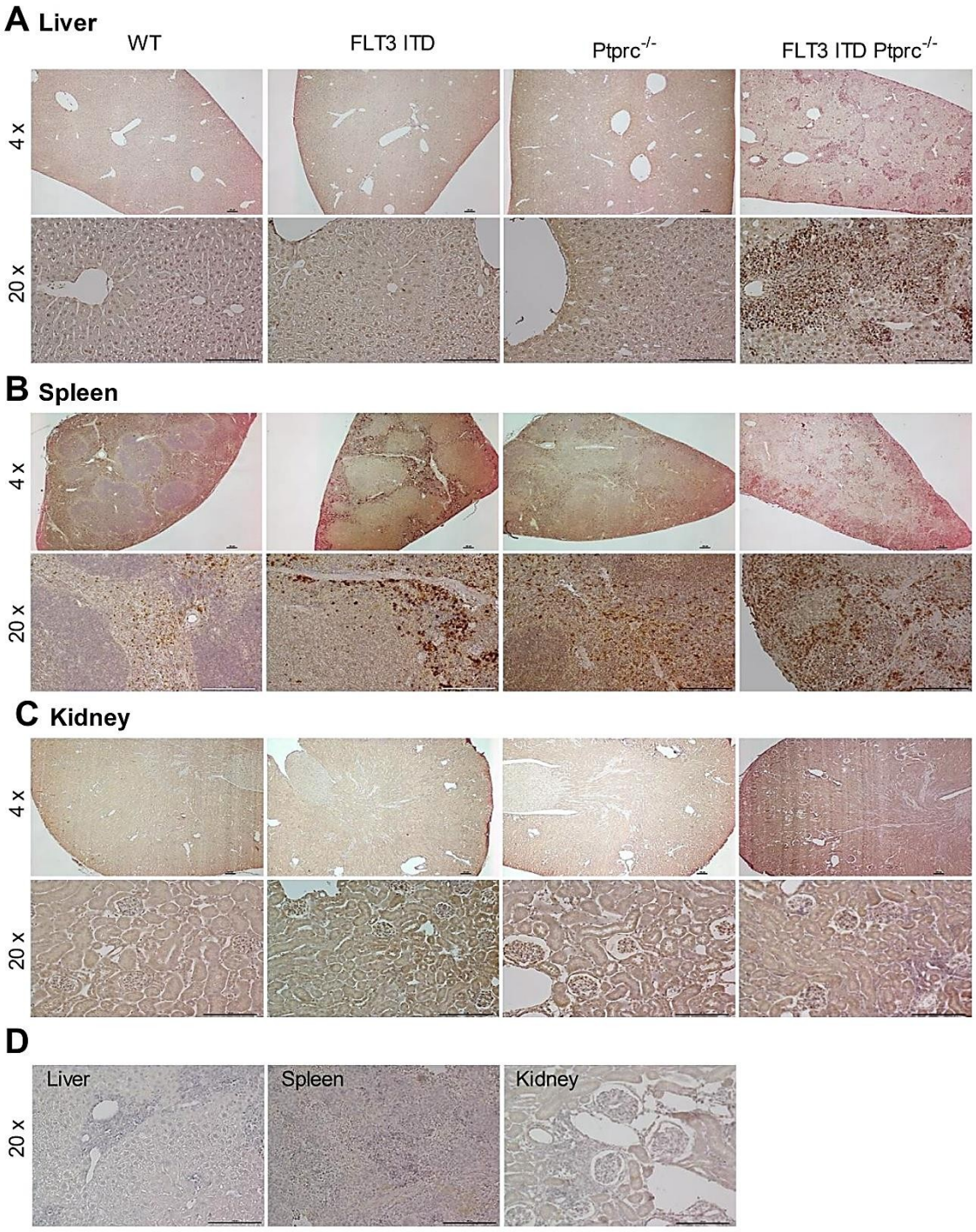

Figure 32. Infiltration of MPO-positive cells in organs of FLT3$^{ITD/ITD}$ Ptprc$^{-/-}$ mice. Representative images of MPO stained liver (A), spleen (B) and kidney (C) sections of WT, FLT3$^{ITD/ITD}$, Ptprc$^{-/-}$ and FLT3$^{ITD/ITD}$ Ptprc$^{-/-}$ mice at the age of 12 - 17 weeks as well as negative controls (D) of liver, spleen and kidney from FLT3$^{ITD/ITD}$ Ptprc$^{-/-}$ mice, which were incubated without primary antibody. Organs were co-stained with sour hemalaun according to Mayer, Magnification 4 x and 20 x as indicated. Scale bar indicates100 µM.

5.2.2.3 Analysis of peripheral blood

Next, the peripheral blood composition was investigated to address whether $FLT3^{ITD/ITD}$ $Ptprc^{-/-}$ mice developed a hematopoietic disease. $FLT3^{ITD/ITD}$ mice were reported to develop a myeloproliferative disease (Lee et al. 2007) or rather a leukemia-like disease (Li et al. 2008) characterized by an increased white blood cell count (WBC) and anemic features. 15 weeks old $FLT3^{ITD/ITD}$ mice showed no significant alterations of WBC, red blood cell count (RBC), platelets and hemoglobin (HGB) (Figure 33A - D). In contrast, $FLT3^{ITD/ITD}$ $Ptprc^{-/-}$ mice at the same age demonstrated a 22-fold significantly increased WBC compared to WT mice and $FLT3^{ITD/ITD}$ mice. Thus, the hematologic profile indicates a leukocytosis (Figure 33A). In addition to leukocytosis, RBC and HGB were significantly decreased compared to $FLT3^{ITD/ITD}$ mice revealing anemia and potentially an impaired erythropoiesis (Figure 33B, D). Furthermore, the amount of platelets was significantly diminished in $FLT3^{ITD/ITD}$ $Ptprc^{-/-}$ mice compared to $FLT3^{ITD/ITD}$ animals (Figure 33C). Analysis of WBC differentials unraveled an increase of granulocytic and monocytic leukocytes in $FLT3^{ITD/ITD}$ mice which was more pronounced in $FLT3^{ITD/ITD}$ $Ptprc^{-/-}$ mice and accompanied by an almost total loss of lymphocytes (Figure 33E). Moreover, the absolute cell number of myeloid cells was severely increased compared to mice with single mutation and WT littermates, pointing to a myeloproliferative disease (Figure 33F). Comparative analysis of stained peripheral blood smears demonstrated that $FLT3^{ITD/ITD}$ $Ptprc^{-/-}$ mutated mice were suffered by a severe monocytosis quite in contrast to $FLT3^{ITD/ITD}$ mice (Figure 33G). Interestingly, in $Ptprc^{-/-}$ mice significantly decreased RBC numbers were observed compared to WT mice.

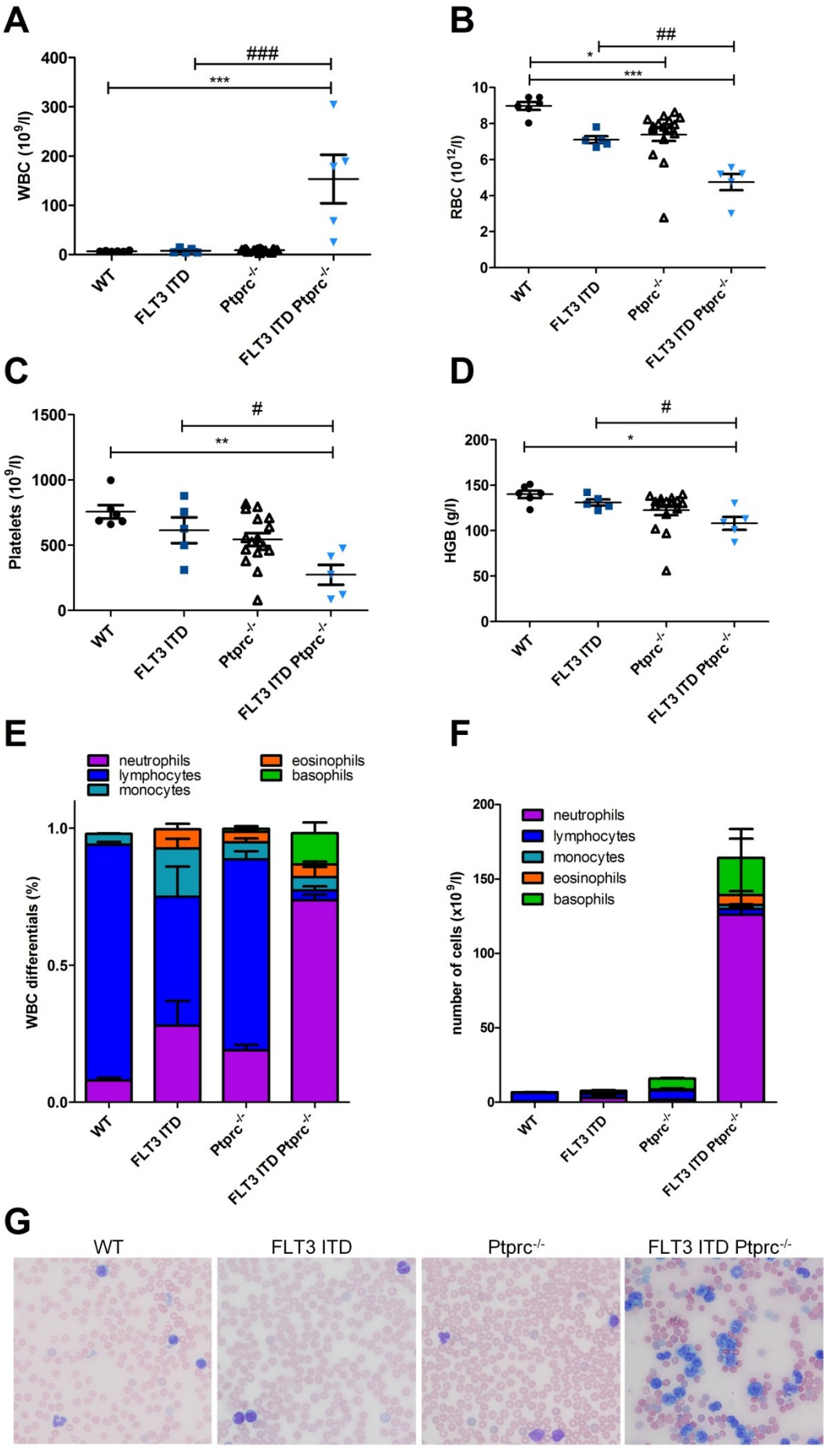
A
WBC (10^9/l)
400
300
200
100
0
###
***
WT
FLT3 ITD
Ptprc-/-
FLT3 ITD Ptprc-/-
B
RBC (10^12/l)
10
8
6
4
2
0
##
*
***
C
Platelets (10^9/l)
1500
1000
500
0
#
**
D
HGB (g/l)
200
150
100
50
0
E
neutrophils
lymphocytes
monocytes
eosinophils
basophils
WBC differentials (%)
1.0
0.5
0.0
F
number of cells (x10^9/l)
200
150
100
50
0
G
WT
FLT3 ITD
Ptprc-/-
FLT3 ITD Ptprc-/-

Figure 33. FLT3$^{ITD/ITD}$ Ptprc$^{-/-}$ mice develop severe monocytosis. Samples of peripheral blood were analyzed from 12 – 17 week old WT, FLT3$^{ITD/ITD}$, Ptprc$^{-/-}$ and FLT3$^{ITD/ITD}$ Ptprc$^{-/-}$ mice using a Mindray BC5300Vet Hematology system. White blood cells count (A), red blood cell count (RBC, B), platelets (C) and hemoglobin (HGB, D) are demonstrated. WBC differentials (E) and absolute amount of cells (F) are shown. Bar indicates mean ± SEM. *p <0.05, **p <0.01, ***p <0.001 compared to WT. #p <0.05 compared to FLT3$^{ITD/ITD}$. (G) Representative Images of peripheral blood smears of 12 – 17 week old WT, FLT3$^{ITD/ITD}$, Ptprc$^{-/-}$ and FLT3$^{ITD/ITD}$ Ptprc$^{-/-}$ mice stained with Pappenhain staining kit (Morphisto GmbH).

5.2.2.4 Block of lymphopoiesis and extramedullary hematopoiesis

To verify the expansion of myeloid cells and loss of lymphocytes flow cytometric analyses were performed. Analysis of the myeloid differentiation markers CD11b and Gr-1 demonstrated a 6-fold increase of CD11b / Gr-1 positive cells in spleen of FLT3$^{ITD/ITD}$ mice compared to WT mice, which was further increased 12-fold in spleen of FLT3$^{ITD/ITD}$ Ptprc$^{-/-}$ mice (Figure 34A, B). In contrast, in BM no aberrancies were observed in the CD11b^{+} / Gr-1^{+} cell population. The cell population, which was negative for CD11b and Gr-1, was significantly decreased in BM and spleen of FLT3$^{ITD/ITD}$ and FLT3$^{ITD/ITD}$ Ptprc$^{-/-}$ mice compared with WT mice. This was mainly due to a significantly decreased population of CD19-positive B cells. The latter effect was clearly seen in BM and spleen of FLT3$^{ITD/ITD}$ mice and was even more pronounced in the FLT3$^{ITD/ITD}$ Ptprc$^{-/-}$ mice. Compared to WT mice the amount of CD3ε^{+} T cells was significantly reduced in BM of Ptprc$^{-/-}$ mice. In BM of FLT3$^{ITD/ITD}$ and FLT3$^{ITD/ITD}$ Ptprc$^{-/-}$ mice no change compared to WT mice was observed. In spleen CD3ε positive T cells were significantly reduced in Ptprc$^{-/-}$ and FLT3$^{ITD/ITD}$ Ptprc$^{-/-}$ mice compared to WT mice. Taken together, these data indicate a myeloproliferative disease and lack of lymphocytes in FLT3$^{ITD/ITD}$ mice, a phenotype which was more pronounced in FLT3$^{ITD/ITD}$ Ptprc$^{-/-}$ mice.

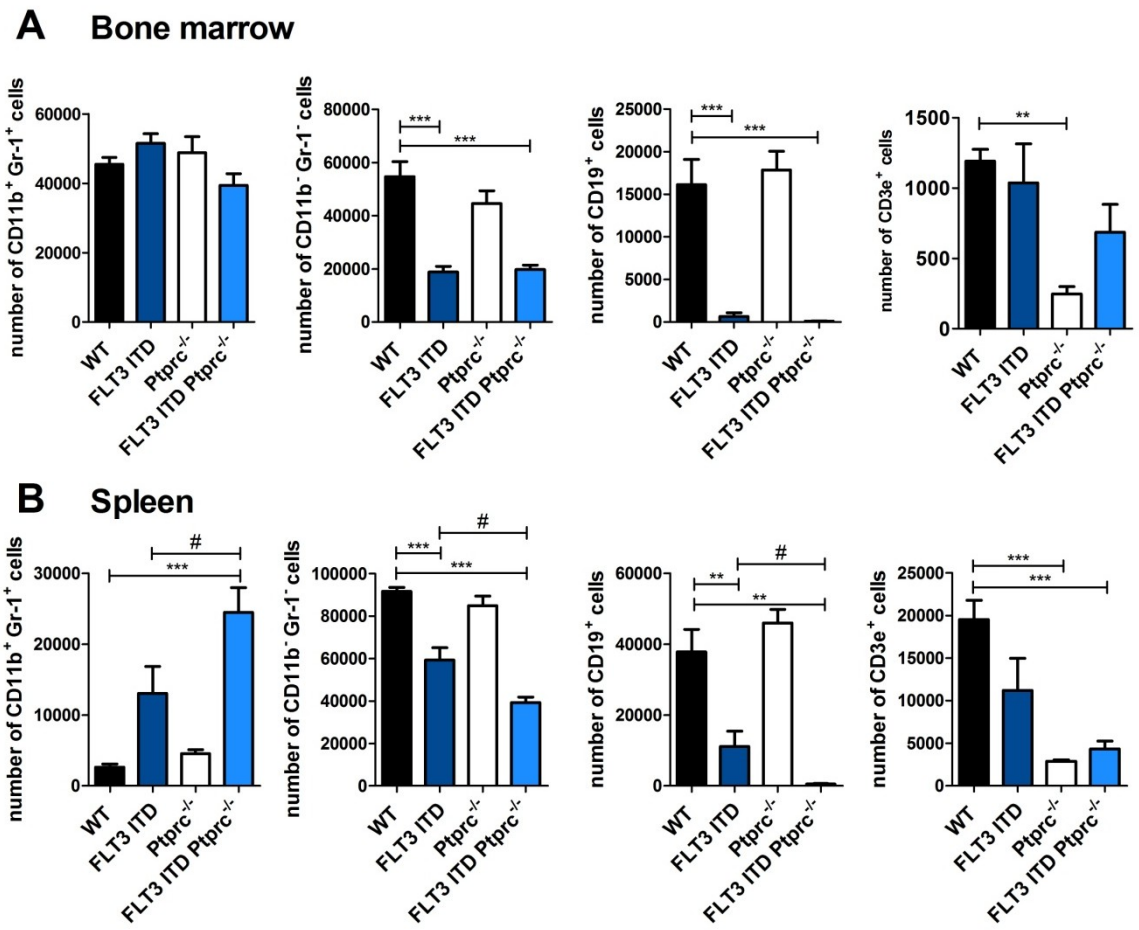

Figure 34. FLT3$^{ITD/ITD}$ Ptprc$^{-/-}$ mice show B cell lymphocytopenia. Immunophenotype of BM and spleen cells were analyzed for CD11b, Gr-1, CD19 and CD3ε expression. 12 - 17 weeks old WT, FLT3$^{ITD/ITD}$, Ptprc$^{-/-}$ and FLT3$^{ITD/ITD}$ Ptprc$^{-/-}$ mice were analyzed. Graphical presentation of CD11b/Gr-1 expression and CD19 as well as CD3ε expression in CD11b^{-} / Gr-1^{-} population in BM (A) and spleen (B) were demonstrated as absolute cell number. Values are given as mean ± SEM out of 1x10^{5} cells analyzed; *p <0.05, ***p <0.001 compared to WT; # p <0.05, ## p <0.01 compared to FLT3$^{ITD/ITD}$ mice. n=5 per genotype.

To further characterize the myeloproliferative phenotype in FLT3$^{ITD/ITD}$ Ptprc$^{-/-}$ mice, further flow cytometric analyses were performed to assess the composition of hematopoietic stem and precursor cells in BM and spleen. A slight elevation of Lin^{-} cells in FLT3$^{ITD/ITD}$, Ptprc$^{-/-}$ and in FLT3$^{ITD/ITD}$ Ptprc$^{-/-}$ mice was observed in BM and spleen compared to WT controls (Figure 35A, B). A several-fold increase of myeloid progenitor population was observed in BM and spleen of FLT3$^{ITD/ITD}$ mice, but this increase was more pronounced in FLT3$^{ITD/ITD}$ Ptprc$^{-/-}$ mice. Similar results were observed while analyzing LSK cell population. Specifically, the number of LSK cells in BM was more than 3-fold and in spleen more than 6-fold increased compared to FLT3$^{ITD/ITD}$ mice, indicating extramedullary hematopoiesis in FLT3$^{ITD/ITD}$ Ptprc$^{-/-}$ mice. Investigation of FLT3 level in myeloid progenitors and LSK cells revealed a significant increase in the BM of FLT3$^{ITD/ITD}$ Ptprc$^{-/-}$ mice. Remarkably, a 70-fold increased amount of FLT3 expressing LSK cells in FLT3$^{ITD/ITD}$ Ptprc$^{-/-}$ mice compared to FLT3$^{ITD/ITD}$ mice was observed. In contrast, mice harboring a single mutation did not show any alteration in FLT3 level of

BM LSK cells compared to WT littermates Figure 35C). In spleen the FLT3 level of LSK cells was already increased in FLT3$^{ITD/ITD}$ mice but 6-fold further increased in FLT3$^{ITD/ITD}$ Ptprc$^{-/-}$ mice when compared to FLT3$^{ITD/ITD}$ mice. These data affirm extramedullary hematopoiesis in FLT3$^{ITD/ITD}$ Ptprc$^{-/-}$ mice.

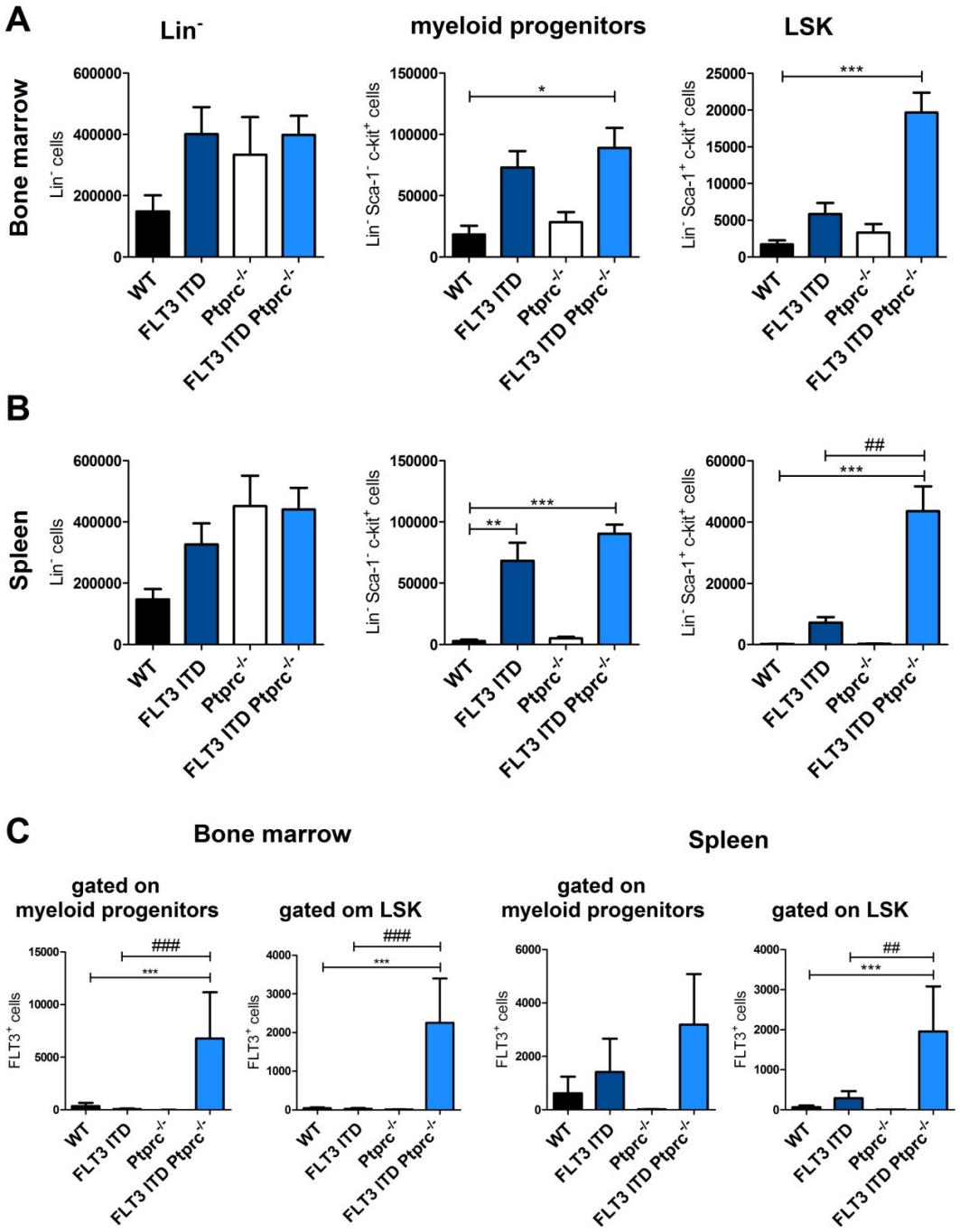

Figure 35. FLT3$^{ITD/ITD}$ Ptprc$^{-/-}$ mice show extramedullary hematopoiesis and increased FLT3 level. Immunophenotype of BM and spleen cells from FLT3$^{ITD/ITD}$ Ptprc$^{-/-}$ mice showed expansion in Lin$^-$ c-kit$^+$ Sca-1$^-$ (myeloid progenitors) and Lin$^-$ c-kit$^+$ Sca-1$^+$ (LSK) population and amount of FLT3$^+$ cells. Graphical presentation of lineage negative (Lin$^-$), myeloid progenitors, LSK cells in BM (A) and spleen (B) derived from 12 – 17 weeks old WT, FLT3$^{ITD/ITD}$, Ptprc$^{-/-}$ and FLT3$^{ITD/ITD}$ Ptprc$^{-/-}$ mice. (C) FLT3 expression level of myeloid progenitors and LSK cells analyzed in BM or spleen cells. Values are given as mean ± SEM out of 1x10^6 cells analyzed *p <0.05, **p <0.0, ***p <0.001 compared to WT. ##p <0.01, ###p <0.001 compared to FLT3$^{ITD/ITD}$ mice. n =4 per genotype.

During histological examinations large multinucleated cells were observed in spleens of FLT3$^{ITD/ITD}$ Ptprc$^{-/-}$ mice. Further immunohistochemical analysis (CD41 and DAPI staining) identified these cells as megakaryocytes. CD41-positive megakaryocytes normally occur in BM and not in spleen as demonstrated in WT and Ptprc$^{-/-}$ mice (Figure 36). In BM of FLT3$^{ITD/ITD}$ mice a reduced quantity of CD41-positive cells was observed and some megakaryocytes in spleen were detectable. Remarkably, only very low amounts of CD41-positive cells were observed in BM of FLT3$^{ITD/ITD}$ Ptprc$^{-/-}$ mice, but high amounts of CD41-positive cells in spleen, confirming extramedullary hematopoiesis.

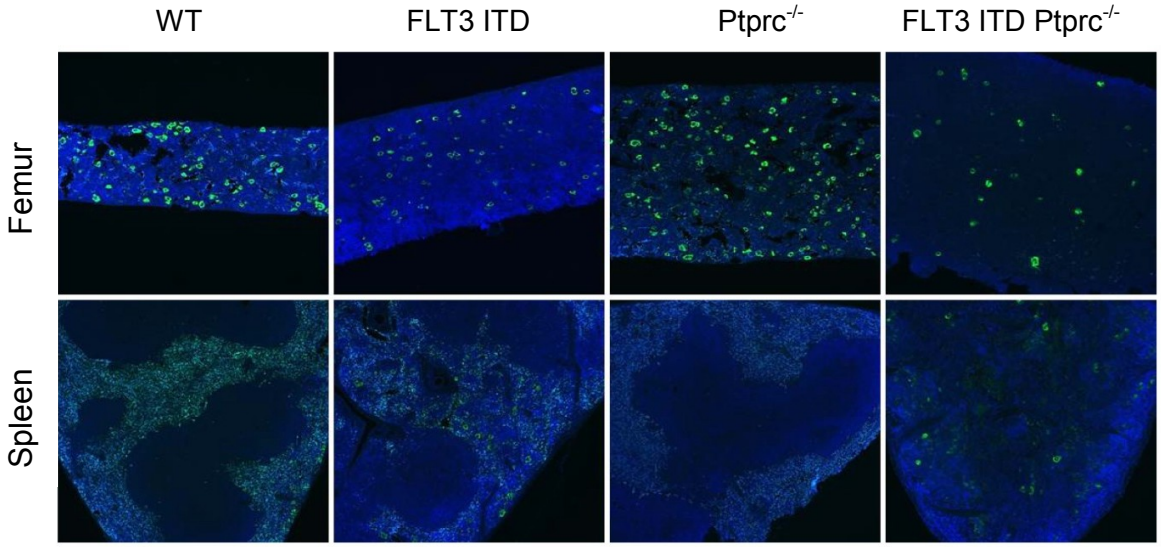

Figure 36. Detection of megakaryocytes in spleen. Immunohistochemistry of femur and spleen sections of indicated mouse genotypes were stained with megakaryocyte marker CD41 and DAPI. Representative images are demonstrated. Magnification 20x.

5.2.2.5 Clonogenic growth and transformation capacity

Next, we addressed the question if the repopulating capacity of extramedullary Lin$^-$ cells was altered in FLT3$^{ITD/ITD}$ Ptprc$^{-/-}$ mice. The repopulation capacity gives information about the transforming and proliferating capacity of Lin$^-$ cells to assess an either leukemic or myeloproliferative phenotype. Increased clonogenic growth would indicate increased FLT3 ITD activity in response to Ptprc inactivation. To this end, MACS purified Lin$^-$ BM and spleen cells were seeded in M3434 methylcellulose, containing (SCF, IL-3, IL-6 and EPO) and analyzed for their clonogenic growth. The number of CFU GM in BM was not altered in mice with single mutation and FLT3$^{ITD/ITD}$ Ptprc$^{-/-}$ mice compared to WT mice (Figure 37A). In contrast, the amount of CFU GM was significantly increased in splenic Lin$^-$ cells of FLT3$^{ITD/ITD}$ Ptprc$^{-/-}$ mice when compared to FLT3$^{ITD/ITD}$ and WT mice. Colonies of CFU GEMM and CFU BFU were hardly observed. Increased numbers of CFU GM and unchanged numbers of CFU GEMM and CFU BFU in spleen are typically observed in a MPN. Comparative cytospin analyses of harvested CFU verified the granulocytic/ macrophage phenotype of the cells (Figure 37B). To assess the re-

population capacity of GM CFU, cells were harvested and re-seeded. Since no colonies were observed it can be concluded that cells lacked re-population capacity indicating the development of a MPN rather than a leukemic disease.

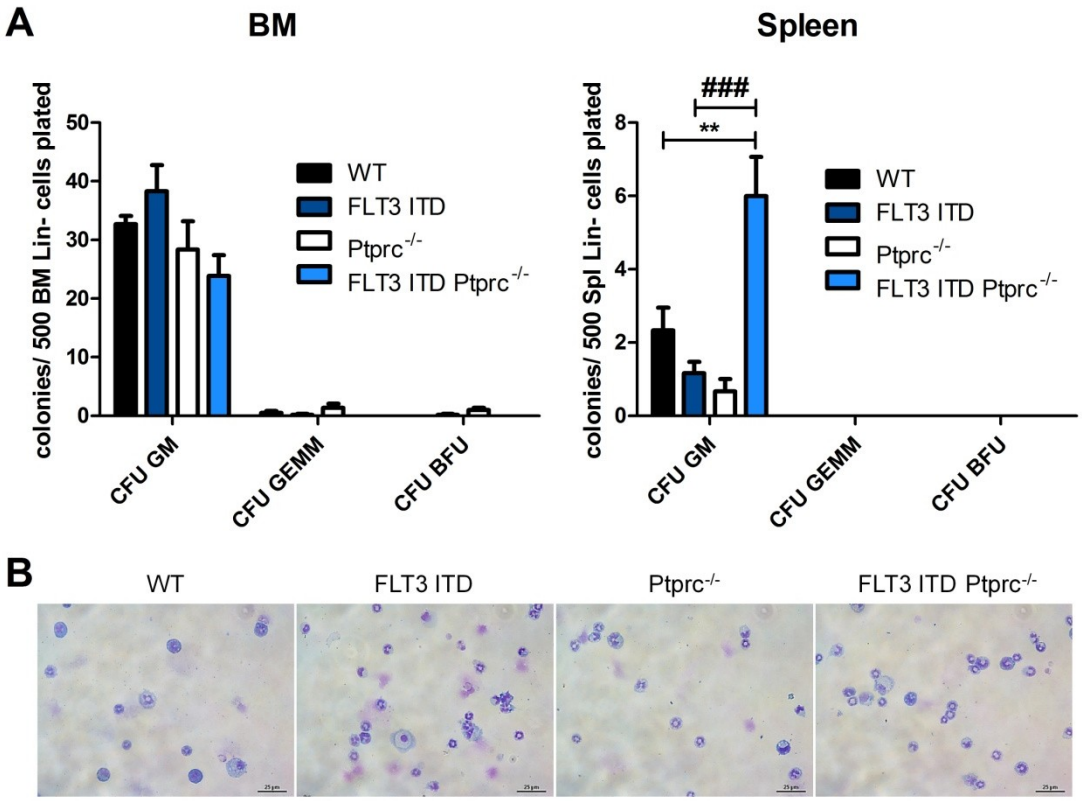

Figure 37. Promotion of clonogenic growth in splenic Lin- cells of FLT3$^{ITD/ITD}$ Ptprc$^{-/-}$ mice. (A) Lin$^-$ BM and spleen cells from 12 - 17 week old WT, FLT3$^{ITD/ITD}$, Ptprc$^{-/-}$ and FLT3$^{ITD/ITD}$ Ptprc$^{-/-}$ mice were plated on M3434 methylcellulose medium (containing SCF-1, IL-3, EPO) and scored for colony formation 7 days later, colony counts of granulocytes/ macrophages (CFU GM), of granulocyte, erythrocyte, monocyte, megakaryocyte (CFU GEMM) and erythroid progenitors (CFU BFU) were shown; n=9. Values are given in mean ± SEM; Colonies were harvested and analyzed by cytospin, (B). Scale bar indicate 25 µm. **p <0.01, ***p <0.001 compared to WT; ###p <0.001 compared to FLT3$^{ITD/ITD}$ mice.

5.2.2.6 Signaling in FLT3$^{ITD/ITD}$ Ptprc$^{-/-}$ mice

Immunoblotting analyses of Lin$^-$ purified BM cells also indicated an aberrant maturation of FLT3 due to the ITD mutation (described in 5.2.1.6). In cells of the FLT3$^{ITD/ITD}$ and FLT3$^{ITD/ITD}$ Ptprc$^{-/-}$ mice predominantly the high-mannose form of FLT3 was detectable, whereas in WT and Ptprc$^{-/-}$ mice both, the high-mannose and complex glycosylated receptor were observed (Figure 38). This result indicated retention of the receptor in the interior of the cell and impaired surface expression. To get information about the activity of FLT3 we next characterized the phosphorylation of FLT3. Phosphorylation of FLT3 Y591 was increased in FLT3$^{ITD/ITD}$ mice which was even more pronounced in FLT3$^{ITD/ITD}$ Ptprc$^{-/-}$ mice compared to Ptprc$^{-/-}$ and WT controls. Phosphorylation of AKT S473 was significantly reduced in mice with single mutation already but much more reduced in FLT3$^{ITD/ITD}$ Ptprc$^{-/-}$ mice compared to WT controls. Src Y416 phosphorylation was

strongly increased in mice carrying FLT3 ITD. In mutated mice ERK1/2 phosphorylation was not altered compared to WT mice.

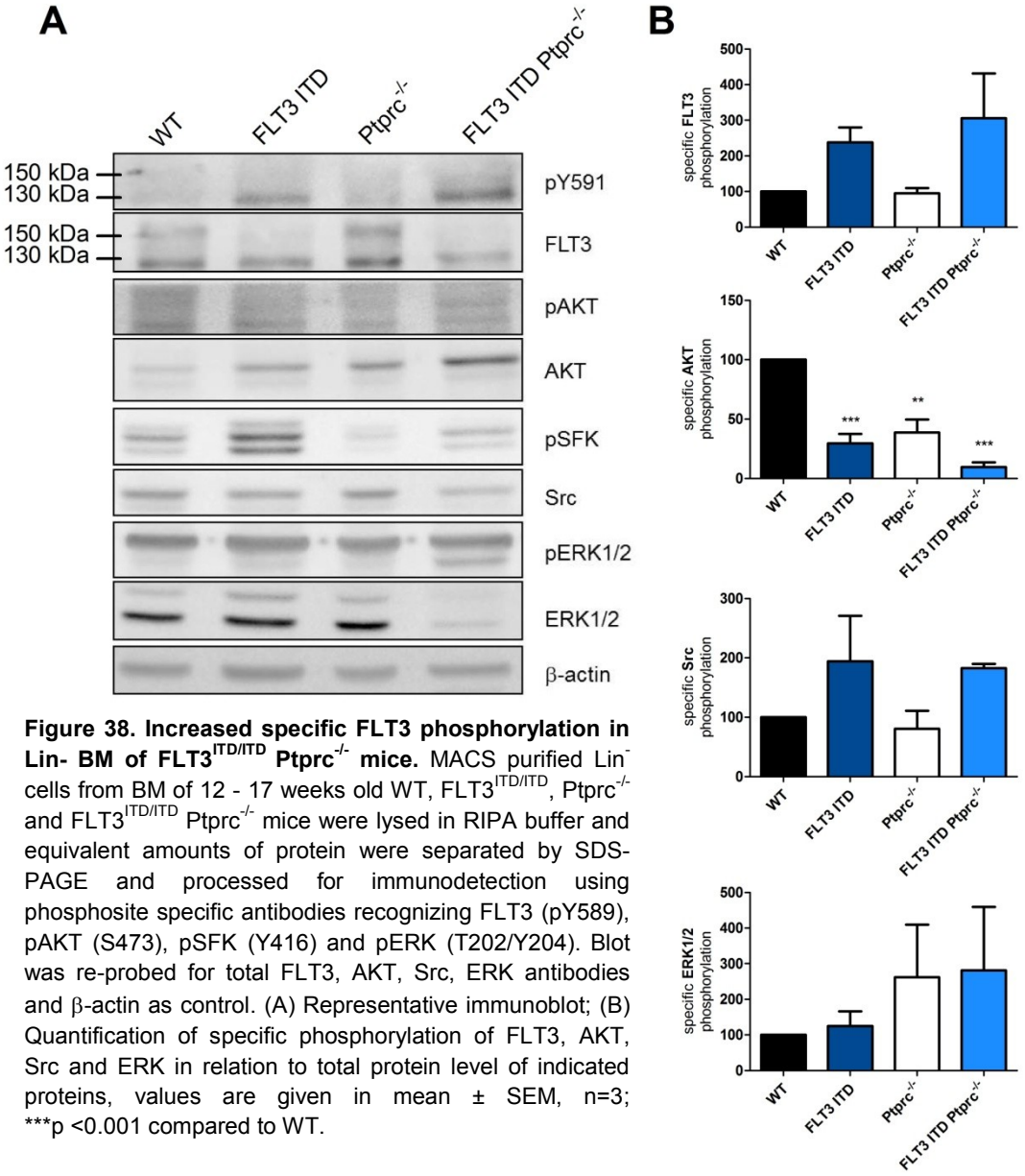

Figure 38. Increased specific FLT3 phosphorylation in Lin- BM of FLT3$^{ITD/ITD}$ Ptprc$^{-/-}$ mice. MACS purified Lin$^-$ cells from BM of 12 - 17 weeks old WT, FLT3$^{ITD/ITD}$, Ptprc$^{-/-}$ and FLT3$^{ITD/ITD}$ Ptprc$^{-/-}$ mice were lysed in RIPA buffer and equivalent amounts of protein were separated by SDS-PAGE and processed for immunodetection using phosphosite specific antibodies recognizing FLT3 (pY589), pAKT (S473), pSFK (Y416) and pERK (T202/Y204). Blot was re-probed for total FLT3, AKT, Src, ERK antibodies and β-actin as control. (A) Representative immunoblot; (B) Quantification of specific phosphorylation of FLT3, AKT, Src and ERK in relation to total protein level of indicated proteins, values are given in mean ± SEM, n=3; ***p <0.001 compared to WT.

Due to the fact that analysis of the FLT3 ITD downstream target STAT5 failed in immunoblotting analyses, immunohistochemical staining of pFLT3 and pSTAT5 was performed. An immunohistochemical analysis in spleen was not possible due to unspecific cross-reactions of the secondary antibody used.

In WT and Ptprc$^{-/-}$ derived liver sections no pFLT3 signal was observed (Figure 39). pFLT3 (Y591) staining revealed an increased level of FLT3 phosphorylation of infiltrated cells in liver of FLT3$^{ITD/ITD}$ Ptprc$^{-/-}$ mice but not in FLT3$^{ITD/ITD}$ mice. Further investigation concerning pSTAT5 level showed that infiltrated cells, positive for FLT3, were also strongly positive for pSTAT5 in FLT3$^{ITD/ITD}$ Ptprc$^{-/-}$ mice. No pSTAT5 positive cells were detected in liver sections of mice harboring a single mutation or WT littermates. Similar

analysis of kidney sections did not show pSTAT5 positive cells in all phenotypes investigated (not shown).

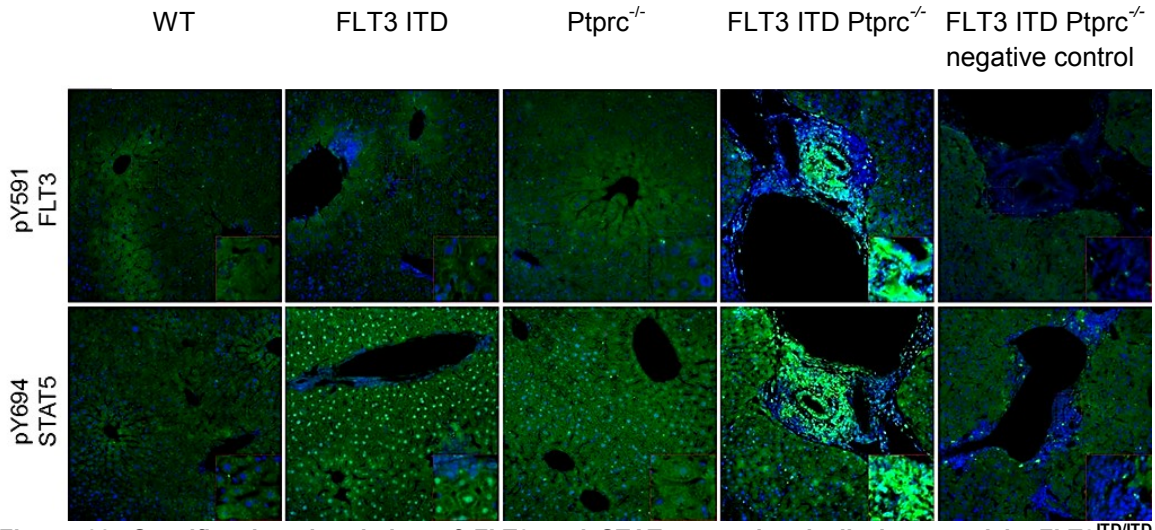

Figure 39. Specific phosphorylation of FLT3 and STAT5 was drastically increased in FLT3$^{ITD/ITD}$ Ptprc$^{-/-}$ mice. Representative images of pFLT3 (Y591, light green, top) and pSTAT5 (Y694, light green, bottom) stained liver sections (4 µm) from WT, FLT3$^{ITD/ITD}$, Ptprc$^{-/-}$ and FLT3$^{ITD/ITD}$ Ptprc$^{-/-}$ mice at the age of 12 - 17 weeks. Samples were co-stained with DAPI. Negative controls were incubated without primary antibody. Magnification 20x. Squares in lower right corner demonstrate 2.5-fold increased part of the respective figure.

5.2.2.7 Impact of Ptprc on bone formation in FLT3$^{ITD/ITD}$ mice

While characterizing histopathology and organ architecture of FLT3$^{ITD/ITD}$ Ptprc$^{-/-}$ mice solid hardening zones were observed in spleen and kidney. H & E staining of spleen and kidney revealed ectopic bone formation zones in FLT3$^{ITD/ITD}$ Ptprc$^{-/-}$ mice (Figure 40 black arrows).

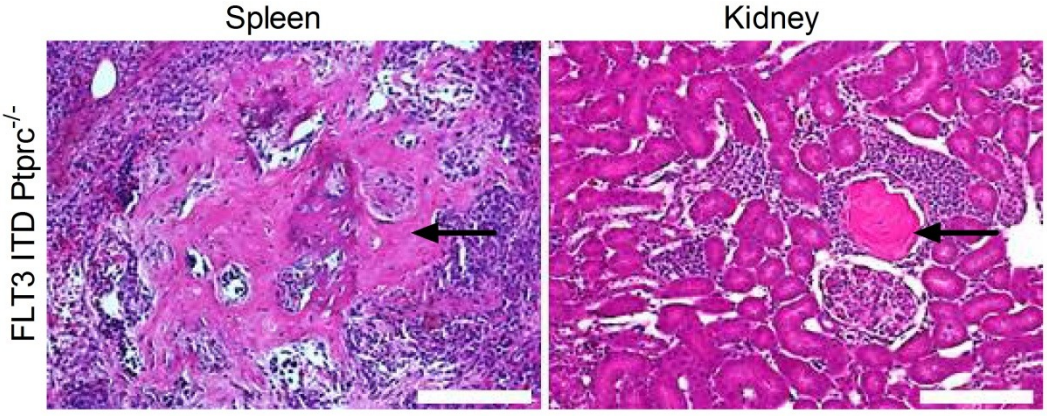

Figure 40. Ectopic bone formation in FLT3$^{ITD/ITD}$ Ptprc$^{-/-}$ mice. Representative images of H & E stained spleen and kidney sections of FLT3$^{ITD/ITD}$ Ptprc$^{-/-}$ mice at the age of 12 - 17 weeks demonstrating ectopic bone formation (black arrow) in peripheral organs. Scale bar indicate 100 µl.

Because of the aberrant bone formation in peripheral organs, we considered that bone formation in these mice may be affected in a more general way. Therefore, the femoral

bone architecture was analyzed. Indeed, a severely different bone structure was observed in H & E stained femur sections of FLT3$^{ITD/ITD}$ Ptprc$^{-/-}$ mice compared to WT controls (Figure 41). Cortical areas of the bone seemed to be completely disorganized and more trabecular-like. Moreover, the normally parallel lamellar structure of the cortex as it is seen in the WT femur was disturbed and wavy. In FLT3$^{ITD/ITD}$ and Ptprc$^{-/-}$ mice the lamellar structure of the cortical bone was still present but the diameter of the femur was increased compared to WT control (compare 4 x magnification). The femoral diameter of FLT3$^{ITD/ITD}$ Ptprc$^{-/-}$ mice was severely increased compared to mice with single mutations or WT controls.

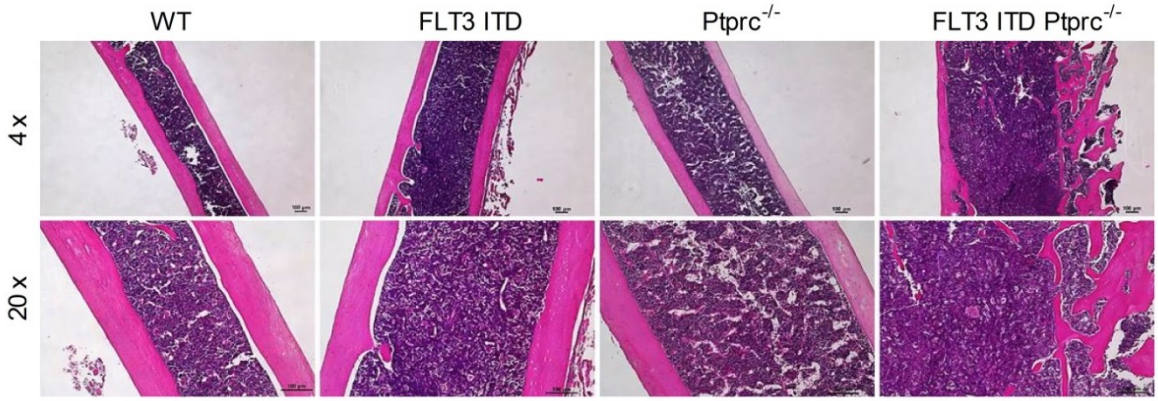

Figure 41. Aberrant bone formation in FLT3$^{ITD/ITD}$ Ptprc$^{-/-}$ mice. Representative images of H & E stained femur slices (decalcified) of 12 - 17 weeks old WT, FLT3$^{ITD/ITD}$, Ptprc$^{-/-}$ and FLT3$^{ITD/ITD}$ Ptprc$^{-/-}$ mice in 4-fold magnification (upper panel) and 20-fold magnification (lower panel) displayed disturbed cortical bone formation in double mutated mice. Scale bar indicates 100 µm.

During bone marrow preparation rough surface structure of bones of FLT3$^{ITD/ITD}$ Ptprc$^{-/-}$ mice was observed. To further investigate the surface and overall bone architecture µCT analysis were performed. Preliminary results demonstrated a strongly increased roughness of femoral surface of FLT3$^{ITD/ITD}$ Ptprc$^{-/-}$ mice compared to mice with single mutation and WT controls which is visualized in the 3D model shown in figure 42A. The roughness angle (µ) is a unit for evaluating the roughness of the bone surface, as described earlier (Hoffmann et al. 2017). The µ value reflects the bone surface roughness. The roughness was increased in FLT3$^{ITD/ITD}$ Ptprc$^{-/-}$ mice compared to mice with single mutation and WT mice. Moreover, FLT3$^{ITD/ITD}$ Ptprc$^{-/-}$ mice displayed decreased femur length as well as bone density but increased bone volume, indicated as cortical thickness index (CTI) compared to mice with single mutation and WT littermates (Figure 42B).

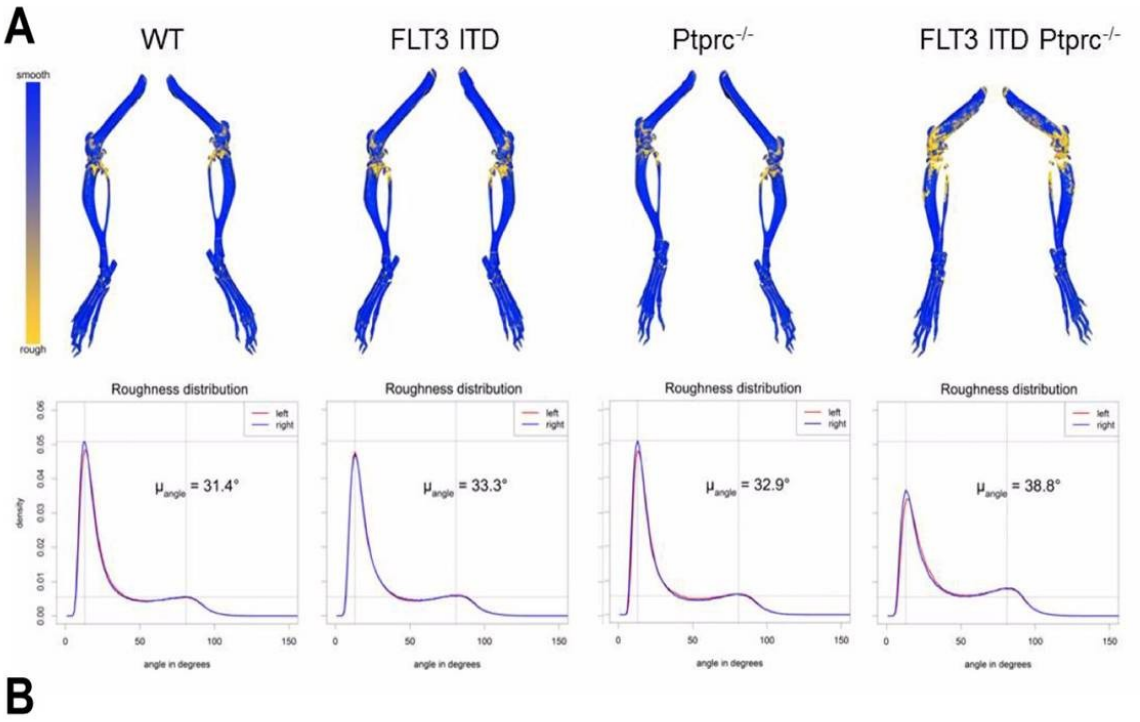

Genotype	Femur length [µm]	Bone density [HU]	Cortical thickness index (CTI)
WT	317.5	4363.3	0.28
FLT3 ITD	289.0	4016.9	0.24
Ptprc$^{-/-}$	304.0	4133.0	0.28
FLT3 ITD Ptprc$^{-/-}$	244.0	3601.2	0.38

Figure 42. Surface analysis and bone formation in FLT3$^{ITD/ITD}$ Ptprc$^{-/-}$ mice. Preliminary micro-CT measurements of WT, FLT3$^{ITD/ITD}$, Ptprc$^{-/-}$ or FLT3$^{ITD/ITD}$ Ptprc$^{-/-}$ mice at the age of 15 weeks were processed to quantify (A) calculated roughness distribution of femoral surface and (B) bone parameters as length of femurs (cortical bone length, left panel), average bone density (in Hounsfield units, middle panel) and average cortical thickness of the femur (cortical thickness index-CTI, right panel). n=1. Analysis of CT data was performed by group of M. T. Figge (Applied Systems Biology, Leibniz Institute for Natural Product Research and Infection Biology, Hans Knöll Institute, Jena, Germany).

An overview about the molecular biological and physiological results obtained from FLT3$^{ITD/ITD}$ mice inactivated for either Ptprj or Ptprc is presented in summarizing table 19. The table shows similar and different responses of Ptprj or Ptprc inactivation in FLT3$^{ITD/ITD}$ mice and in 32D muFLT3 ITD cells.

Table 19. Molecular biological and physiological phenotype due to genetically inactivation of either Ptprj or Ptprc in FLT3 ITD background

	FLT3 ITD Ptprj$^{-/-}$	**FLT3 ITD Ptprc$^{-/-}$**
Cell line based phenotype	- IC_{50} of TKI ↑ - total tyrosine phosphorylation ↓ - STAT5, AKT, Src phosphorylation ↓↓	- total tyrosine phosphorylation ↓ - AKT, Src phosphorylation ↓↓
Physio-logical phenotype	- shortened life span - leukocytosis: • WBC ↑ • myeloid cells ↑ in spleen and peripheral blood - decreased B lymphocytes - extramedullary hematopoiesis • LSK ↑ in spleen • CFU GM ↑ in BM and spleen - increased FLT3 phosphorylation	- drastically shortened life span - splenohepatomegaly - leukocytosis: • WBC ↑↑↑ • myeloid cells ↑↑ in spleen and peripheral blood • monocytosis - anemia: • RBC ↓ • HGB ↓ - drastically reduced of platelets - lack of B and T lymphocytes - extramedullary hematopoiesis: • LSK ↑ in spleen • CFU GM ↑ in spleen • detection of megakaryocytes in spleen - increased FLT3 and STAT5 phosphorylation - bone aberrancies

6. Discussion

6.1 Effect of Ptprj and Ptprc on FLT3 ITD activity in 32D muFLT3 ITD cells

By using stable shRNA expression our group demonstrated previously that shRNA-mediated depletion of the PTP Ptprj and Ptprc in FLT3 ITD expressing 32D cells leads to increased FLT3 phosphorylation and downstream signaling upon ROS quenching (Arora et al. 2011, Godfrey et al. 2012). In order to address the question if Ptprj and Ptprc may affect FLT3 ITD activity and FLT3 ITD-mediated signaling their genes were completely inactivated using CRISPR/Cas9 mediated knockout. In addition, potential overlapping functions of Ptprj and Ptprc were investigated in 32D muFLT3 ITD cells lacking both RPTP.

In contrast to further results of our research group, complete inactivation of either Ptprj or Ptprc or both did not show a regulatory role on FLT3 ITD pY589 phosphorylation. It can be speculated that different Ptprj level result in different regulation of FLT3 ITD activation. It was previously demonstrated in breast cancer cells that activation of Src was dependent on different protein level of Ptprj and correlated with patient prognosis (Spring et al. 2015). Similar regulatory mechanisms of FLT3 ITD phosphorylation by Ptprj may be speculated but has to be investigated further.
Although phosphorylation of FLT3 Y589 was not changed in 32D muFLT3 ITD PTP ko cells compared to 32D muFLT3 ITD cells, the knockout of Ptprj and combinatory knockout of Ptprj and Ptprc in 32D muFLT3 ITD cells resulted in significantly increased IC_{50} of TKI AC220 and strongly increased IC_{50} of PKC412. Elevated kinase activity of FLT3 is known to shift the dose-response curve for TKI towards somewhat lower sensitivity (Tse et al. 2002). Higher IC_{50} values indicate higher tolerance and thereby lower TKI sensitivity. Thus, it can be indirectly concluded that ko of Ptprj as well as combinatorial ko of Ptprj and Ptprc resulted in increased FLT3 ITD activity. This result confirmed the regulatory role of Ptprj on FLT3 ITD in the 32D muFLT3 ITD model cell system. Since the decreased TKI sensitivity of 32D muFLT3 ITD Ptprj ko cells indicated a higher activity of FLT3 ITD it can be speculated that other phosphorylation sites controlling FLT3 ITD kinase activity were regulated by this RPTP. For instance, increased FLT3 Y591 phosphorylation has been demonstrated in 32D huFLT3 cells upon Ptprj downregulation (Arora et al. 2011).

Quenching of cellular ROS by DPI treatment resulted in slightly decreased specific FLT3 phosphorylation in 32D muFLT3 ITD cells and in all PTP ko cell lines. Ptprj has been

demonstrated to be reversibly inactivated by high ROS level in FLT3 ITD positive cells (Godfrey et al. 2012, Jayavelu et al. 2016). The above data were consistent with an oxidation-mediated inactivation of Ptprj. Oxidation susceptibility of Ptprc has been previously demonstrated in other context (Singh et al. 2005). However, own studies indicated no ROS-mediated inactivation of Ptprc in FLT3 ITD positive cells (Godfrey et al. 2012). Since in 32D muFLT3 ITD Ptprj ko cells FLT3 phosphorylation was still decreased upon ROS quenching it can be concluded that either re-activation of Ptprc or of other PTP may affect FLT3 phosphorylation. Reduced FLT3 phosphorylation in cells lacking Ptprj and Ptprc might be due to other PTP, probably SHP-1 and PTP1B, regulating FLT3 ITD activity in ER (Schmidt-Arras et al. 2005, Yudushkin et al. 2007). It may also be speculated that other mechanisms regulate FLT3 phosphorylation. However, in 32D muFLT3 ITD cells genetically inactivated for both RPTP total tyrosine phosphorylation was more decreased than in single PTP ko cells but not further reduced by ROS quenching. Based on this observation it can be speculated that Ptprj and Ptprc were the main oxidation susceptible PTP in 32D cell system or that both RPTP regulate a common target, e.g. Src. It is more likely that the impaired tyrosine phosphorylation was caused by impaired Src activity, which was downregulated due to lack of PTP, irrespective of DPI treatment, than by altered FLT3 ITD activity.

Surprisingly, FLT3 protein level was strongly reduced in all PTP ko cells compared to 32D muFLT3 ITD cells. Consistently, significant decreased FLT3 ITD protein level has been observed in Ptprj ko MV4-11 cells (Sapozhnikova 2017). Decreased protein level of FLT3 can be explained by increased turnover or reduced expression. Reduced TKI sensitivity of FLT3 ITD in response to PTP ko indicated elevated kinase activity. Since turnover of FLT3 ITD is dependent on its activity (Buchwald et al. 2010, Schindler 2010, Oshikawa et al. 2011) it may be speculated that reduced cellular FLT3 ITD protein levels in PTP ko cell lines were due to increased turnover. However, investigation on FLT3 turnover demonstrated no significant changes in Ptprj ko MV4-11 cells (carrying FLT3 ITD) but reduced mRNA level of FLT3 ITD (Sapozhnikova 2017). If the FLT3 ITD mRNA expression in 32D cells, where the receptor is expressed under control of a retroviral promotor, is diminished has to be characterized further.

PTP knockout potentially resulted in further impairment of FLT3 ITD maturation. Since the degree of receptor retention was activity dependent (Choudhary et al. 2009, Schmidt-Arras et al. 2005, Choudhary et al. 2005), this observation may be an indication of increased FLT3 ITD activity in response to Ptprj as well as Ptprc knockout.

Increased receptor activity in PTP ko cells would suggest increased downstream signaling, e.g. elevated FLT3 ITD-mediated STAT5 activation (Choudhary et al. 2005, Choudhary et al. 2007, Choudhary et al. 2009, Schmidt-Arras et al. 2009). Unexpectedly, STAT5 Y694 phosphorylation was significantly reduced in Ptprj and double PTP ko cells and slightly reduced in Ptprc ko cells. Since FLT3 Y589 phosphorylation was not changed in PTP ko cell lines it can be concluded that other factors mediate reduced STAT5 activity. For instance, JAK and SFK have been demonstrated to be important STAT5 activators (Ozawa et al. 2008, Beisenherz-Huss et al. 2001). Src has been reported to be important for FLT3 ITD-mediated STAT5 activation (Leischner et al. 2012). Indeed, phosphorylation of the activating tyrosine residue of Src was drastically downregulated in PTP ko cells. Since Ptprj and Ptprc are reported to be involved in Src activation (Chabot et al. 2009, Spring et al. 2012, Fournier et al. 2016, Gupta and DeFranco 2003), it can be concluded that loss of Src activity was due to RPTP knockout. Decreased STAT5 phosphorylation as well as decreased AKT phosphorylation and reduced total tyrosine phosphorylation in 32D muFLT3 ITD PTP ko cells can be explained by decreased Src activity. Investigation on clonogenic growth demonstrated no change in 32D muFLT3 ITD PTP ko cell lines compared to 32D muFLT3 ITD cells. FLT3 ITD, STAT5 and AKT activity has been reported to contribute to uncontrolled cell proliferation and transforming capacity (Rocnik et al. 2006, Choudhary et al. 2007, Brandts et al. 2005). Unchanged colony formation in 32D muFLT3 ITD PTP ko cells can be explained by unchanged or rather reduced activity of FLT3 ITD, STAT5 and AKT and thus indicated similar transforming capacity of FLT3 ITD in PTP ko cells.

In 32D muFLT3 ITD PTP ko cells signaling analysis revealed no significant change of specific ERK1/2 phosphorylation. In 32D muFLT3 ITD cells ERK1/2 activity was slightly decreased upon DPI treatment. This was presumably mediated by re-activated Ptprj, which directly dephosphorylated tyrosine residue Y204 in ERK1/2 activation loop and thus, resulted in decreased ERK1/2 activity (Sacco et al. 2009). ERK1/2 was not activated by ER-retained high-mannose FLT3 ITD (Schmidt-Arras et al. 2009, Choudhary et al. 2009). Only low activity of ERK1/2 has been observed in 32D FLT3 ITD cells (Mizuki et al. 2000). Strong reduction of ERK1/2 phosphorylation in response to DPI treatment indicates a re-activation of PTP. Since this effect was similar in 32D muFLT3 ITD Ptprj/Ptprc ko cells it can be concluded that further phosphatases regulate ERK1/2 activity. DUSP6, a dual specific phosphatase targeting phosphoserine/ phosphothreonine and phosphotyrosine residues, has been demonstrated to be significantly upregulated in FLT3 ITD expressing cell lines and in AML patient samples with FLT3 ITD mutation (Arora et al. 2012). In addition, it has been reported that DUSP6

negatively regulate ERK1/2 activity (Camps et al. 1998, Dickinson and Keyse 2006). Thus, it is likely that increased DUSP6 activity counteracts ERK1/2 (T202/Y204) phosphorylation in PTP ko cells.

Taken together, there were some hints that Ptprj and Ptprc regulate FLT3 ITD activity in 32D muFLT3 ITD cells. The greatest effects in terms of inactivation of RPTP were observed in terms of Src activity. At present it cannot be differentiated whether the FLT3 ITD activity is directly or indirectly influenced. It can be assumed that in addition to specific effects on FLT3 ITD, other physiological functions are influenced by the two RPTP.

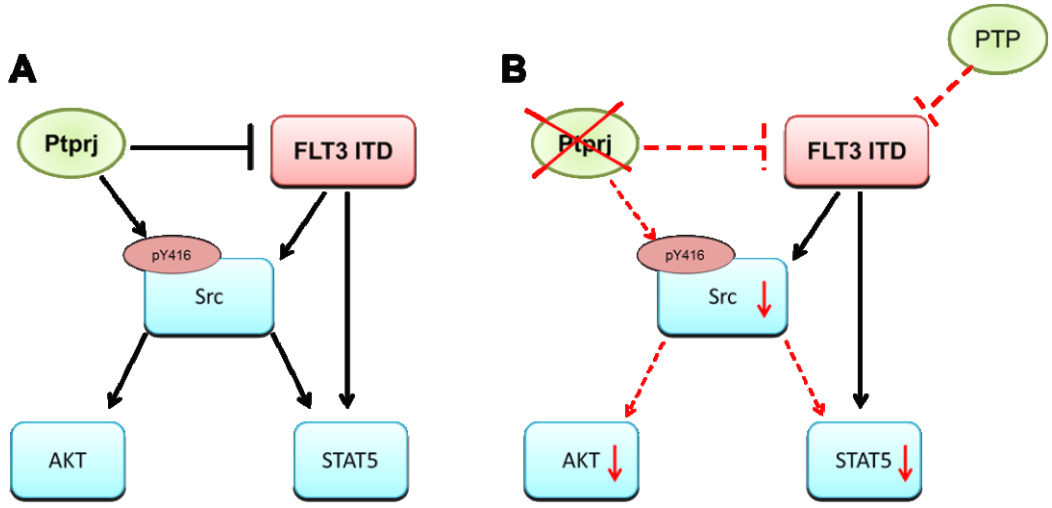

Figure 43. Proposed signaling events in Ptprj expressing (A) and Ptprj deficient (B) 32D muFLT3 ITD cells. Inactivation of Ptprj in 32D muFLT3 ITD cells resulted in decreased Src activity. Decreased Src activity subsequently led to decreased AKT and STAT5 phosphorylation. Phosphorylation of FLT3 ITD was not changed, but maturation was further abrogated.

6.2 Effects of inactivation of Ptprj and Ptprc on hematopoiesis in FLT3$^{ITD/ITD}$ mice

Cell line based studies indicated a possible negative regulatory role of Ptprj for FLT3 ITD activity. To analyze *in vivo* effects of knockout of RPTP Ptprj and Ptprc on FLT3 ITD activity in complex regulated systems, e.g. hematopoiesis, the respective genes were genetically inactivated in FLT3$^{ITD/ITD}$ mice.

6.2.1 Increased disease aggressiveness in FLT3$^{ITD/ITD}$ RPTP ko mice

While life expectancy of Ptprj$^{-/-}$ and Ptprc$^{-/-}$ mice was comparable to WT mice, genetic inactivation of Ptprj or Ptprc in FLT3$^{ITD/ITD}$ mice resulted in shortened survival compared to FLT3$^{ITD/ITD}$ mice. FLT3 ITD knockin mice, created by Gilliland and colleagues were not reported to undergo any alteration in life expectancy (Lee et al. 2007). In contrast, Small and colleagues demonstrated that FLT3 ITD mutation in one allele of FLT3 gene was already sufficient to end in mortality within 6 to 20 months (Li et al. 2008). No change of

life span and viability were reported in Ptprj$^{-/-}$ or Ptprc$^{-/-}$ mice (Trapasso et al. 2006, Byth et al. 1996, Mee et al. 1999), consistent with our own observations. The shortened life time of FLT3$^{ITD/ITD}$ mice with additional knockout of either Ptprj or Ptprc indicated a more progressive FLT3 ITD-driven disease, as it was indeed substantiated by a more detailed characterization and a negative control of FLT3 ITD-induced disease by both PTP.

6.2.2 Augmented myeloproliferative phenotype associated by lack of lymphocytes in FLT3$^{ITD/ITD}$ RPTP ko mice

Several findings indicated an augmented myeloproliferative phenotype in FLT3$^{ITD/ITD}$ mice with additional knockout of one of the investigated RPTP. Splenomegaly and disturbed spleen architecture were observed in FLT3$^{ITD/ITD}$ mice. Enlarged spleen of FLT3 ITD expressing mice has been discussed as consequence of MPN (Li et al. 2008, Lee et al. 2007, Li et al. 2011). Genetic inactivation of Ptprj in FLT3$^{ITD/ITD}$ mice further pronounced this effect leading to splenohepatomegaly, strongly disturbed spleen architecture with expansion of red pulp and excessive infiltration of myeloid cells in peripheral organs, explaining organ enlargement. Since FLT3$^{ITD/ITD}$ Ptprj$^{-/-}$ mice demonstrating an even more aggressive phenotype, e.g. shortened survival, it can be concluded that inactivation of Ptprj results in a more aggressive MPN. Observed organ aberrancies were not reported in mice with systemic Ptprj inactivation (Trapasso et al. 2006).

Similarly, genetic inactivation of Ptprc in FLT3$^{ITD/ITD}$ mice caused a significantly increased spleen and liver weight compared to age-matched FLT3$^{ITD/ITD}$ mice. In addition, the kidneys were significantly increased compared to age-matched WT mice. The severe infiltration of myeloid cells in peripheral organs as well as splenohepatomegaly and nephromegaly indicated a more aggressive form of fatal MPN possibly leading to organ failure and shortened life span of FLT3$^{ITD/ITD}$ Ptprc$^{-/-}$ mice.

Concomitantly, peripheral blood analysis and flow cytometric investigation of spleen revealed significantly increased WBC and myeloproliferative phenotype in FLT3$^{ITD/ITD}$ mice genetically inactivated for Ptprj or Ptprc accompanied by a lack of lymphocytes. More precisely, elevated myeloid CD11b^{+}/Gr-1^{+} population of FLT3$^{ITD/ITD}$ mice was significantly increased in FLT3$^{ITD/ITD}$ mice with additional knockout of RPTP in spleen but not in BM, indicating a monocytic / granulocytic character of MPN. Ligand-mediated activation of FLT3 WT (Gabbianelli et al. 1995) or constitutive activity of FLT3 ITD have been reported to result in an increased monocytic / granulocytic population (Li et al. 2008, Lee et al. 2007). Thus, it can be concluded that reduction of Ptprj or Ptprc strengthens the FLT3 ITD-mediated myeloproliferative effect.

Increased amount of neutrophils associated with reduced number of lymphocytes were observed in response to genetic inactivation of RPTP. Previous studies demonstrated a regulatory role of Ptprc and Ptprj on B cell receptor signaling (Zhu et al. 2008, Skrzypczynska et al. 2016, Zikherman et al. 2012). In addition, an increased B cell population in $Ptprc^{-/-}$ mice has been reported (Byth et al. 1996). In contrast, a decreased fraction of B cells in $FLT3^{ITD/ITD}$ mice has been demonstrated (Lee et al. 2007, Li et al. 2008). Because in $Ptprj^{-/-}$ and $Ptprc^{-/-}$ mice peripheral blood lymphocytes and splenic $CD19^{+}$ population were normal it is likely that the observed lack of B cells in $FLT3^{ITD/ITD}$ mice with additional knockout of Ptprj or Ptprc is mediated by an enhancement of the FLT3 ITD-mediated phenotype. In order to distinguish between the possibilities that the development of B cells is impaired or that B cells are displaced by myeloid cells, further investigations would have to be carried out. A reduced T cell population has been demonstrated in Ptprc knockout mice previously (Byth et al. 1996, Kishihara et al. 1993). This study confirmed the decreased T cell population irrespective of absence or the presence of the FLT3 ITD mutation. On the basis of lack of lymphocytes septic inflammation in response to RPTP inactivation in FLT3 ITD mutated mice can be excluded.

In addition, $FLT3^{ITD/ITD}$ $Ptprc^{-/-}$ mice but any of the age-matched controls demonstrated anemic features, e.g. significantly decreased RBC and HGB, as well as decreased numbers of platelets. These observations indicate a potential negative effect on erythropoiesis or potential negative effect on biogenesis of MEP, the precursors of erythrocytes and platelets. Although FLT3 is not expressed on MEP itself (Gabbianelli et al. 1995) an important role of FLT3 in hematopoiesis of MEP was reported (Boyer et al. 2011).

In $FLT3^{ITD/ITD}$ $Ptprc^{-/-}$ mice increased numbers of LSK cells, containing HSC and MPP, were observed. Igarashi and colleagues showed that MPP contain a cell population of earliest lymphoid progenitors, which differentiate into granulocyte-monocyte-lymphoid progenitor (GMPL), but lack megakaryocyte / erythrocyte lineage potential (Igarashi et al. 2002). It may be speculated that increased numbers of LSK resulted in increased numbers of GMPL and thus, result in impaired biogenesis of MEP as well as differentiated erythrocytes and platelets.

Furthermore, increased numbers of FLT3-positive LSK cells were obtained in $FLT3^{ITD/ITD}$ $Ptprc^{-/-}$ mice. $FLT3^{+}$ MPP cells have been shown to mainly differentiate into lymphoid lineage. These lymphoid–primed MPP cells, called LMPP also have the ability to differentiate into myeloid lineage but lack megakaryocytic / erythrocytic lineage potential

(Adolfsson et al. 2005). Increased amount of LMPP cells within the $FLT3^{+}$ MPP population might additionally explain the decreased RBC and platelet count.
Increased GMPL and LMPP might also contribute to the myeloproliferative phenotype observed in $FLT3^{ITD/ITD}$ $Ptprc^{-/-}$ mice.
As demonstrated previously, expansion of GMP and corresponding decrease of MEP was due to increased FLT3 ITD activity (Lee et al. 2007). Thus, reduced platelets and erythrocytes might be further indications of drastically increased FLT3 ITD activity. However, significantly decreased RBC was observed in $Ptprc^{-/-}$ mice. It cannot be excluded that inactivation of Ptprc itself, which is expressed on all nucleated hematopoietic cells, could also mediate this phenotype irrespective of FLT3 ITD.

6.2.3 Extramedullary hematopoiesis in $FLT3^{ITD/ITD}$ mice genetically inactivated for RPTP

Evaluation of stem cell compartment in $FLT3^{ITD/ITD}$ mice demonstrated increased LSK and myeloid progenitor population (Lee et al. 2007, Li et al. 2008). Inactivation of Ptprj or Ptprc further elevated splenic myeloid progenitor and LSK population, indicating extramedullary hematopoiesis. Thus, RPTP abrogation augments the hematopoietic phenotype of $FLT3^{ITD/ITD}$ mice. In contrast to earlier reports on $Ptprc^{-/-}$ where less HSC were observed in BM but increased amount in spleen (Shivtiel et al. 2008) we could not observe any alteration in LSK population of $Ptprc^{-/-}$ mice. The differences can be explained by usage of two different $Ptprc^{-/-}$ mice. For this study a Ptprc deficient mice lacking exon 9 was used with no Ptprc protein expression. In contrast, Shivtiel and colleagues used an exon 6 lacking $Ptprc^{-/-}$ mice. Due to alternative splicing, low amount of CD45 was still detectable in those mice.
Because of the severe infiltration of hematopoietic stem cells in peripheral organs extramedullary hematopoiesis can be assumed in $FLT3^{ITD/ITD}$ mice genetically inactivated for either Ptprj or Ptprc. Clonal growth of splenic Lin^{-} cells was significantly increased in response to Ptprj or Ptprc inactivation compared to $FLT3^{ITD/ITD}$ mice. Subsequent morphological analysis validated the myeloid character of progenitor cells. Observation of megakaryocytes in spleen in $FLT3^{ITD/ITD}$ $Ptprc^{-/-}$ mice was a further indicator of extramedullary hematopoiesis. Conclusively, our data reveal severe extramedullary hematopoiesis in response to Ptprc knockout in $FLT3^{ITD/ITD}$ mice. Genetic inactivation of Ptprj in $FLT3^{ITD/ITD}$ mice led to extramedullary hematopoiesis as well, but to a lesser extent.
Quantification of FLT3 positive cells among myeloid progenitors and LSK cells showed severely increased amount of FLT3 expressing cells in spleen of $FLT3^{ITD/ITD}$ $Ptprj^{-/-}$ mice and in BM and spleen for $FLT3^{ITD/ITD}$ $Ptprc^{-/-}$ mice, respectively. Therefore, it can be

speculated that extramedullary hematopoiesis and MPN is due to increased FLT3 activity in $FLT3^{ITD/ITD}$ mice genetically inactivated for Ptprj or Ptprc, pointing to an FLT3 ITD-driven development of this phenotype. Activating mutations of FLT3 are known to contribute to leukemic transformation. However, at least one second cooperative mutation impairing hematopoietic differentiation is required for development of an FLT3 ITD-associated AML (Pinheiro et al. 2007, Schessl et al. 2005). Lack of repopulating capacity of CFU in $FLT3^{ITD/ITD}$ mice genetically inactivated for either Ptprj or Ptprc revealed a more aggressive MPN instead of leukemia, confirming the two hit model.

Our data confirmed the FLT3 ITD phenotypes described earlier (Li et al. 2008, Lee et al. 2007). However, different reactions, e.g. survival and disease aggressiveness, of $FLT3^{ITD/ITD}$ mice created by Gilliland group (Lee et al. 2007) and Small group (Li et al. 2008) are currently not understood. It might be due to different ITD sequences used for generation of FLT3 ITD knockin mice. Li and colleagues suggested dependence of MPN aggressiveness in relation to FLT3 ITD expression level or FLT3 ITD activity (Li et al. 2011). This study demonstrated a more aggressive fatal MPN in response of Ptprj or Ptprc inactivation. Thus, it can be concluded, that both phosphatases act antagonistic on FLT3 ITD activity. However, cell autonomous effects could not be excluded.

To further investigate whether observed physiological effects in response to RPTP inactivation were mediated by direct regulation of FLT3 ITD activity, specific phosphorylation of FLT3 ITD and FLT3 ITD downstream targets was analyzed.
Since genetic inactivation of Ptprj in $FLT3^{ITD/ITD}$ mice resulted in significant increased FLT3 Y591 phosphorylation in Lin^- purified BM cells it can be reversely concluded, that Ptprj counteract FLT3 ITD activity. Similar results were obtained in response to Ptprc inactivation in $FLT3^{ITD/ITD}$ mice. Strongly increased FLT3 Y591 phosphorylation was observed in Lin^- BM cells as well as in FLT3 Y591 IHC examination of liver of $FLT3^{ITD/ITD}$ $Ptprc^{-/-}$ mice. Contributing to this, STAT5 phosphorylation was strongly upregulated in FLT3 Y591 phosphorylated liver cells of $FLT3^{ITD/ITD}$ $Ptprc^{-/-}$ mice, indicating an increased FLT3 ITD-mediated signaling. Thus, our results clearly indicate a counteracting role of Ptprc on FLT3 ITD activity.
In addition, abrogation of FLT3 ITD maturation was observed in $FLT3^{ITD/ITD}$ $Ptprc^{-/-}$ mice, similar to *in vitro* observations. Since the retention of the receptor was activity dependent (Choudhary et al. 2009, Schmidt-Arras et al. 2005, Choudhary et al. 2005) this observation is an indication of increased FLT3 ITD activity in response to PTP inactivation.

Similar to *in vitro* signaling analysis AKT S473 phosphorylation was significantly reduced in spleen cells of FLT3 ITD mutated mice as well as in Lin$^-$ purified BM cells compared to WT controls. Significantly decreased AKT S473 phosphorylation in Ptprj or Ptprc knockout animals cannot be explained with our current state of knowledge. It can be speculated that Ptprj and Ptprc or respective substrates regulate AKT activity by so far unknown mechanisms.

In contrast to *in vitro* analysis, phosphorylation of activating tyrosine of Src was significantly increased in splenic cells of FLT3$^{ITD/ITD}$ Ptprj$^{-/-}$ mice. In Lin$^-$ purified BM cells of FLT3$^{ITD/ITD}$ Ptprc$^{-/-}$ mice the tendency of increased Src phosphorylation was observed as well. SFK Fyn, Lyn and Src have been reported to be activated by FL stimulated FLT3 WT and constitutive active FLT3 ITD to contribute to STAT5 activation as well as transforming potential (Chougule et al. 2016, Leischner et al. 2012, Robinson et al. 2005). Therefore, it can be speculated that significantly increased FLT3 ITD activity results in increased phosphorylation of activating tyrosine residue of Src. A probable signaling path of FLT3$^{ITD/ITD}$ Ptprc$^{-/-}$ mice is shown in figure 44.

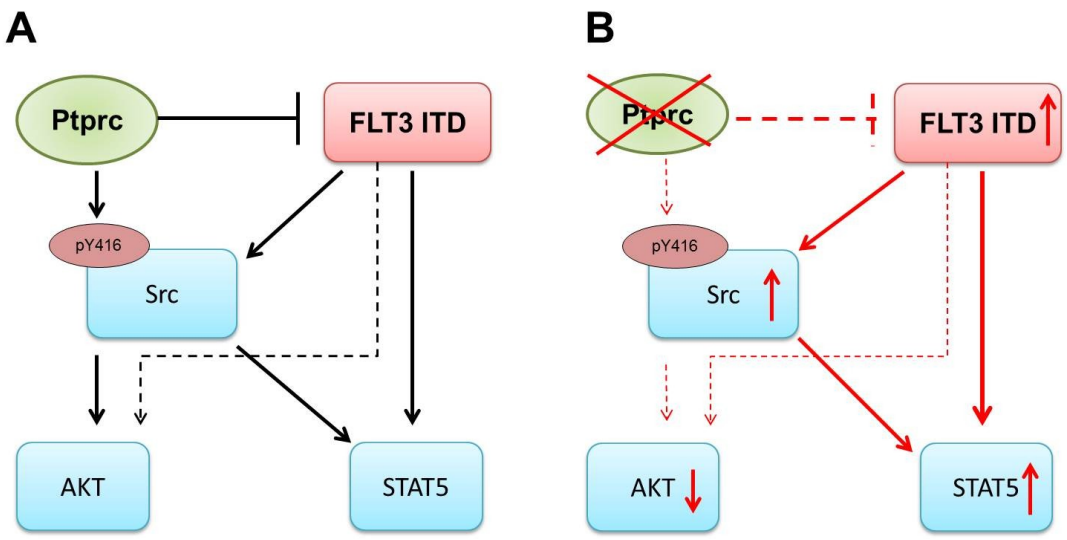

Figure 44. Supposed signaling path in FLT3$^{ITD/ITD}$ and FLT3$^{ITD/ITD}$ Ptprc$^{-/-}$ mice. Supposed FLT3 ITD signaling path in FLT3$^{ITD/ITD}$ mice (A) and FLT3$^{ITD/ITD}$ Ptprc$^{-/-}$ mice (B). Inactivation of Ptprc resulted in increased FLT3 ITD activity which led to increased Src activity and STAT5 phosphorylation. Due to further abrogated FLT3 ITD maturation in Ptprc deficient mice, membrane localized AKT is not accessible anymore for high mannose FLT3 ITD.

Because of experimental difficulties it was not possible to demonstrate STAT5 phosphorylation in FLT3$^{ITD/ITD}$ mice inactivated for Ptprj. But based on the available results, it is justified to speculate that the assumed signaling is also true for FLT3$^{ITD/ITD}$ Ptprj$^{-/-}$ mice. In addition, it cannot be excluded that the effect of Ptprj or Ptprc inactivation on FLT3 ITD is indirect only. Pathways other than the regulatory role of both RPTP on FLT3 ITD could also mediate this phenotype. Since inactivation of Ptprj and Ptprc,

respectively resulted in elevated phosphorylation effects can at least be explained by increased FLT3 ITD activity.

6.2.4 Unexpected role of FLT3 ITD and Ptprc in bone homeostasis

Besides severe alterations in the hematopoietic differentiation profile FLT3$^{ITD/ITD}$ Ptprc$^{-/-}$ mice showed an unexpected bone phenotype. While in FLT3$^{ITD/ITD}$ or in Ptprc$^{-/-}$ mice no obvious alterations in bone formation were observed, inactivation of Ptprc in FLT3$^{ITD/ITD}$ mice resulted in shortened bone length, reduced bone density, increased bone volume and increased surface roughness along with ectopic bone formation in peripheral organs. These preliminary results indicate deregulation of bone metabolism and homeostasis and suggest a role of FLT3 ITD and probably FLT3 in bone formation and metabolism/homeostasis. Bone homeostasis is tightly regulated by balanced activity bone remodeling osteoblasts (OB) and bone resorbing osteoclasts (OC).

It has been demonstrated that HSC regulate mesenchymal stromal cell induction into OB and thereby participating in the formation of this stem cell niche (Jung et al. 2008). Since FLT3$^{ITD/ITD}$ mice genetically inactivated for Ptprc demonstrated MPN with significantly increased HSC population one may speculate that an increased HSC population in FLT3$^{ITD/ITD}$ Ptprc$^{-/-}$ mice may guide mesenchymal differentiation into the osteoblastic lineage. Due to observed extramedullary hematopoiesis ectopic bone formation in peripheral organs could be explained by guided mesenchymal differentiation into osteoblastic lineage and thus subsequent bone formation by OB in peripheral organs.

OC are of hematopoietic origin. OC precursors circulate in the monocyte fraction (Fujikawa et al. 1996). In addition dendritic cells are able to trans-differentiate into OC (Rivollier et al. 2004). FLT3$^{ITD/ITD}$ mice genetically inactivated for Ptprc had significantly increased amounts of myeloid progenitors. Thus, it can be speculated that an increased amount of OC was present which may contribute to cortical porosity.

Ptprc has been identified as a positive regulator of OC activity. Loss of Ptprc led to unregulated OC function associated by impaired bone remodeling (Shivtiel et al. 2008). In contrast, the FL-FLT3-axis is a known negative regulator of the genesis of osteoclasts (Svensson et al. 2016, Voronov and Manolson 2016). Thus, one would expect that in the FLT3$^{ITD/ITD}$ Ptprc$^{-/-}$ mouse model the activated FLT3 signaling and the absence of Ptprc would result in a reduced OC activity and reduced genesis of osteoclasts. However, the observed phenotype of less bone mass indicated either decreased OB activity or increased OC activity or both. Moreover, this unique bone phenotype suggests further functions of Ptprc and FLT3 in bone remodeling.

In Ptprc$^{-/-}$ mice bone aberrancies were reported earlier (Shivtiel et al. 2008). In particular, impaired OC function and increased amount of trabecular structures were observed,

indicating a higher bone volume. In contrast, preliminary results of our own experiments did not reveal aberrant bone structures in mice with single mutation.
It is reasonable to further investigate the previously unrecognized role of FLT3 ITD (and presumably FLT3) because osteoporosis and osteopenia occur frequently in adult AML patients after stem cell transplantation therapy (Ebeling et al. 1999, Schulte et al. 2000). Loss of bone mass was frequently observed early after stem cell transplantation (Massenkeil et al. 2001, Weidner et al. 2017).

6.3 Conclusion and Outlook

FLT3 is considered as an attractive therapeutic target in AML. TKI treatment has been demonstrated to increase patient survival. However, clinical studies of TKI revealed a high susceptibility to mutations for FLT3 ITD and other RTK, leading to TKI resistance. Despite help of approved TKI Midostaurin treatment still about 50% of AML patients have poor prognosis (Levis 2017). Therefore, it is important to identify additional alternative treatment strategies to impair FLT3 ITD activity.
In this study we could demonstrate *in vivo* that Ptprj and Ptprc are naturally occurring antagonists of FLT3 ITD, affecting its activity. Ptprj is a known tumor suppressor gene. In the context of an FLT3 ITD-driven myeloproliferative disease in mice we could confirm anti-tumor activity. It has been previously reported that inhibition of Ptprc negatively affects tumor development (Perron and Saragovi 2018). However, array data demonstrated correlation of low expression level of Ptprj and Ptprc with poor prognosis in FLT3 ITD positive AML patients. We observed aggravated disease progression in FLT3 ITD driven MPN due to Ptprc or Ptprj inactivation. Conversely, activation Ptprc or Ptprj could contribute to better prognosis of AML patients. Till now there are no Ptprj or Ptprc activators in clinical studies. Treatment of FLT3 ITD-positive AML patients with activators of natural occurring antagonists of FLT3 ITD may demonstrate an alternative therapy to TKI treatment. In addition, mutations of FLT3 ITD which affect TKI susceptibility will not affect negative regulatory role of RPTP on FLT3 ITD. It is clear that the complete inactivation of Ptprj and Ptprc in FLT3 ITD mice does not reflect the exact human phenotype. However, these mice are an appropriate model to study the role of the respective phosphatases on FLT3 ITD and corresponding signaling pathways at organismic level.

The novel bone phenotype of $FLT3^{ITD/ITD}$ $Ptprc^{-/-}$ mice is a suitable model to study the role of FLT3 ITD (and presumably FLT3) and Ptprc on bone formation and remodeling. Osteoporosis, osteopenia and loss of bone mass frequently occur in AML patients after stem cell transplantation. Further investigations, which will explore regulatory mechanisms and the role of FLT3 in bone homeostasis, may possibly provide better

treatment approaches. In particular, the mechanism how the disturbed hematopoietic stem cell niche of FLT3 ITD Ptprc$^{-/-}$ mice affects hematopoiesis and bone formation can be characterized. Studies on osteoblast and osteoclast activity and their differentiation capacity of cells derived from FLT3$^{ITD/ITD}$ Ptprc$^{-/-}$ and control mice will provide insight in the *in vivo* role of FLT3 ITD and Ptprc.

7. References

ABU-DUHIER FM, GOODEVE AC, WILSON GA, CARE RS, PEAKE IR AND REILLY JT. 2001. Genomic structure of human FLT3: implications for mutational analysis. British journal of haematology 113: 1076-1077.

ADOLFSSON J, BORGE OJ, BRYDER D, THEILGAARD-MONCH K, ASTRAND-GRUNDSTROM I, SITNICKA E, SASAKI Y AND JACOBSEN SE. 2001. Upregulation of Flt3 expression within the bone marrow Lin(-)Sca1(+)c-kit(+) stem cell compartment is accompanied by loss of self-renewal capacity. Immunity 15: 659-669.

ADOLFSSON J ET AL. 2005. Identification of Flt3+ lympho-myeloid stem cells lacking erythro-megakaryocytic potential a revised road map for adult blood lineage commitment. Cell 121: 295-306.

AGNES F, SHAMOON B, DINA C, ROSNET O, BIRNBAUM D AND GALIBERT F. 1994. Genomic structure of the downstream part of the human FLT3 gene: exon/intron structure conservation among genes encoding receptor tyrosine kinases (RTK) of subclass III. Gene 145: 283-288.

ALONSO A, NUNES-XAVIER CE, BAYON Y AND PULIDO R. 2016. The Extended Family of Protein Tyrosine Phosphatases. Methods Mol Biol 1447: 1-23.

ALONSO A, SASIN J, BOTTINI N, FRIEDBERG I, FRIEDBERG I, OSTERMAN A, GODZIK A, HUNTER T, DIXON J AND MUSTELIN T. 2004. Protein Tyrosine Phosphatases in the Human Genome. Cell 117: 699-711.

ARORA D ET AL. 2012. Expression of protein-tyrosine phosphatases in Acute Myeloid Leukemia cells: FLT3 ITD sustains high levels of DUSP6 expression. Cell communication and signaling : CCS 10: 19.

ARORA D ET AL. 2011. Protein-tyrosine phosphatase DEP-1 controls receptor tyrosine kinase FLT3 signaling. The Journal of biological chemistry 286: 10918-10929.

AUTSCHBACH F, PALOU E, MECHTERSHEIMER G, ROHR C, PIROTTO F, GASSLER N, OTTO HF, SCHRAVEN B AND GAYA A. 1999. Expression of the membrane protein tyrosine phosphatase CD148 in human tissues. Tissue Antigens 54: 485-498.

BALAVENKATRAMAN KK, JANDT E, FRIEDRICH K, KAUTENBURGER T, POOL-ZOBEL BL, ÖSTMAN A AND BÖHMER FD. 2006. DEP-1 protein tyrosine phosphatase inhibits proliferation and migration of colon carcinoma cells and is upregulated by protective nutrients. Oncogene 25: 6319-6324.

BARNEA M, OLENDER T, BEDFORD MT AND ELSON A. 2016. Regulation of receptor-type protein tyrosine phosphatases by their C-terminal tail domains. Biochem Soc Trans 44: 1295-1303.

BEGHINI A, PETERLONGO P, RIPAMONTI CB, LARIZZA L, CAIROLI R, MORRA E AND MECUCCI C. 2000. C-kit mutations in core binding factor leukemias. Blood 95: 726-727.

BEISENHERZ-HUSS C, MUNDT M, HERRALA A, VIHKO P, SCHUBERT A AND GRONER B. 2001. Specific DNA binding and transactivation potential of recombinant, purified Stat5. Molecular and cellular endocrinology 183: 101-112.

BILOTTA A ET AL. 2017. A novel splice variant of the protein tyrosine phosphatase PTPRJ that encodes for a soluble protein involved in angiogenesis. Oncotarget 8: 10091-10102.

BÖHMER F, SZEDLACSEK S, TABERNERO L, ÖSTMAN A AND DEN HERTOG J. 2013a. Protein tyrosine phosphatase structure-function relationships in regulation and pathogenesis. Febs j 280: 413-431.

BÖHMER SA, WEIBRECHT I, SODERBERG O AND BÖHMER FD. 2013b. Association of the protein-tyrosine phosphatase DEP-1 with its substrate FLT3 visualized by in situ proximity ligation assay. PLoS One 8: e62871.

BOYER SW, SCHROEDER AV, SMITH-BERDAN S AND FORSBERG EC. 2011. All hematopoietic cells develop from hematopoietic stem cells through Flk2/Flt3-positive progenitor cells. Cell Stem Cell 9: 64-73.

BOYLE WJ, SIMONET WS AND LACEY DL. 2003. Osteoclast differentiation and activation. Nature 423: 337-342.

BRANDTS CH ET AL. 2005. Constitutive Activation of Akt by Flt3 Internal Tandem Duplications Is Necessary for Increased Survival, Proliferation, and Myeloid Transformation. Cancer research 65: 9643-9650.

BREITENBUECHER F, SCHNITTGER S, GRUNDLER R, MARKOVA B, CARIUS B, BRECHT A, DUYSTER J, HAFERLACH T, HUBER C AND FISCHER T. 2009. Identification of a novel type of ITD mutations located in nonjuxtamembrane domains of the FLT3 tyrosine kinase receptor. Blood 113: 4074-4077.

BUCHWALD M, PIETSCHMANN K, MÜLLER JP, BÖHMER FD, HEINZEL T AND KRAMER OH. 2010. Ubiquitin conjugase UBCH8 targets active FMS-like tyrosine kinase 3 for proteasomal degradation. Leukemia 24: 1412-1421.

BYTH KF, CONROY LA, HOWLETT S, SMITH AJ, MAY J, ALEXANDER DR AND HOLMES N. 1996. CD45-null transgenic mice reveal a positive regulatory role for CD45 in early thymocyte development, in the selection of CD4+CD8+ thymocytes, and B cell maturation. The Journal of experimental medicine 183: 1707-1718.

CAMPS M, NICHOLS A, GILLIERON C, ANTONSSON B, MUDA M, CHABERT C, BOSCHERT U AND ARKINSTALL S. 1998. Catalytic activation of the phosphatase MKP-3 by ERK2 mitogen-activated protein kinase. Science (New York, NY) 280: 1262-1265.

CAROW CE, LEVENSTEIN M, KAUFMANN SH, CHEN J, AMIN S, ROCKWELL P, WITTE L, BOROWITZ MJ, CIVIN CI AND SMALL D. 1996. Expression of the hematopoietic growth factor receptor FLT3 (STK-1/Flk2) in human leukemias. Blood 87: 1089-1096.

CHABOT C, SPRING K, GRATTON JP, ELCHEBLY M AND ROYAL I. 2009. New role for the protein tyrosine phosphatase DEP-1 in Akt activation and endothelial cell survival. Molecular and cellular biology 29: 241-253.

CHARBONNEAU H, TONKS NK, WALSH KA AND FISCHER EH. 1988. The leukocyte common antigen (CD45): a putative receptor-linked protein tyrosine phosphatase. Proceedings of the National Academy of Sciences of the United States of America 85: 7182-7186.

CHOUDHARY C, BRANDTS C, SCHWABLE J, TICKENBROCK L, SARGIN B, UEKER A, BÖHMER FD, BERDEL WE, MÜLLER-TIDOW C AND SERVE H. 2007. Activation mechanisms of STAT5 by oncogenic Flt3-ITD. Blood 110: 370-374.

CHOUDHARY C, MÜLLER-TIDOW C, BERDEL WE AND SERVE H. 2005. Signal transduction of oncogenic Flt3. Int J Hematol 82: 93-99.

CHOUDHARY C ET AL. 2009. Mislocalized activation of oncogenic RTKs switches downstream signaling outcomes. Molecular cell 36: 326-339.

CHOUGULE RA, KAZI JU AND RÖNNSTRAND L. 2016. FYN expression potentiates FLT3-ITD induced STAT5 signaling in acute myeloid leukemia. Oncotarget 7: 9964-9974.

CHU SH, HEISER D, LI L, KAPLAN I, COLLECTOR M, HUSO D, SHARKIS SJ, CIVIN C AND SMALL D. 2012. FLT3-ITD knockin impairs hematopoietic stem cell quiescence/homeostasis, leading to myeloproliferative neoplasm. Cell Stem Cell 11: 346-358.

COHEN P. 2002. Protein kinases--the major drug targets of the twenty-first century? Nat Rev Drug Discov 1: 309-315.

COOPER JA, GOULD KL, CARTWRIGHT CA AND HUNTER T. 1986. Tyr527 is phosphorylated in pp60c-src: implications for regulation. Science (New York, NY) 231: 1431-1434.

CYSTER JG, HEALY JI, KISHIHARA K, MAK TW, THOMAS ML AND GOODNOW CC. 1996. Regulation of B-lymphocyte negative and positive selection by tyrosine phosphatase CD45. Nature 381: 325-328.

DAWES R ET AL. 2006. Altered CD45 expression in C77G carriers influences immune function and outcome of hepatitis C infection. Journal of medical genetics 43: 678-684.

DE LA FUENTE-GARCIA MA, NICOLAS JM, FREED JH, PALOU E, THOMAS AP, VILELLA R, VIVES J AND GAYA A. 1998. CD148 is a membrane protein tyrosine phosphatase present in all hematopoietic lineages and is involved in signal transduction on lymphocytes. Blood 91: 2800-2809.

DESAI DM, SAP J, SILVENNOINEN O, SCHLESSINGER J AND WEISS A. 1994. The catalytic activity of the CD45 membrane-proximal phosphatase domain is required for TCR signaling and regulation. Embo j 13: 4002-4010.

DICKINSON RJ AND KEYSE SM. 2006. Diverse physiological functions for dual-specificity MAP kinase phosphatases. Journal of cell science 119: 4607-4615.

DÖHNER H, WEISDORF DJ AND BLOOMFIELD CD. 2015. Acute Myeloid Leukemia. The New England journal of medicine 373: 1136-1152.

DOMBRET H AND GARDIN C. 2016. An update of current treatments for adult acute myeloid leukemia. Blood 127: 53-61.

DOSIL M, WANG S AND LEMISCHKA IR. 1993. Mitogenic signalling and substrate specificity of the Flk2/Flt3 receptor tyrosine kinase in fibroblasts and interleukin 3-dependent hematopoietic cells. Molecular and cellular biology 13: 6572-6585.

DOWNING JR. 2003. The core-binding factor leukemias: lessons learned from murine models. Current opinion in genetics & development 13: 48-54.

DREXLER HG. 1996. Expression of FLT3 receptor and response to FLT3 ligand by leukemic cells. Leukemia 10: 588-599.

DRUKER BJ ET AL. 2001. Efficacy and safety of a specific inhibitor of the BCR-ABL tyrosine kinase in chronic myeloid leukemia. The New England journal of medicine 344: 1031-1037.

EBELING PR, THOMAS DM, ERBAS B, HOPPER JL, SZER J AND GRIGG AP. 1999. Mechanisms of bone loss following allogeneic and autologous hemopoietic stem cell transplantation. Journal of bone and mineral research : the official journal of the American Society for Bone and Mineral Research 14: 342-350.

ESTEY E AND DÖHNER H. 2006. Acute myeloid leukaemia. Lancet (London, England) 368: 1894-1907.

FABRE JW AND WILLIAMS AF. 1977. Quantitative serological analysis of a rabbit anti-rat lymphocyte serum and preliminary biochemical characterisation of the major antigen recognised. Transplantation 23: 349-359.

FISCHER EH, CHARBONNEAU H AND TONKS NK. 1991. Protein tyrosine phosphatases: a diverse family of intracellular and transmembrane enzymes. Science (New York, NY) 253: 401-406.

FOURNIER P, DUSSAULT S, FUSCO A, RIVARD A AND ROYAL I. 2016. Tyrosine Phosphatase PTPRJ/DEP-1 Is an Essential Promoter of Vascular Permeability, Angiogenesis, and Tumor Progression. Cancer research 76: 5080-5091.

FRÖHLING S, SCHOLL C, GILLILAND DG AND LEVINE RL. 2005. Genetics of myeloid malignancies: pathogenetic and clinical implications. Journal of clinical oncology : official journal of the American Society of Clinical Oncology 23: 6285-6295.

FRÖHLING S ET AL. 2007. Identification of driver and passenger mutations of FLT3 by high-throughput DNA sequence analysis and functional assessment of candidate alleles. Cancer Cell 12: 501-513.

FUJIKAWA Y, QUINN JM, SABOKBAR A, MCGEE JO AND ATHANASOU NA. 1996. The human osteoclast precursor circulates in the monocyte fraction. Endocrinology 137: 4058-4060.

GABAEV I ET AL. 2014. Expression of the human cytomegalovirus UL11 glycoprotein in viral infection and evaluation of its effect on virus-specific CD8 T cells. J Virol 88: 14326-14339.

GABBIANELLI M ET AL. 1995. Multi-level effects of flt3 ligand on human hematopoiesis: expansion of putative stem cells and proliferation of granulomonocytic progenitors/monocytic precursors. Blood 86: 1661-1670.

GAYA A, PIROTTO F, PALOU E, AUTSCHBACH F, DEL POZO V, SOLE J AND SERRA-PAGES C. 1999. CD148, a new membrane tyrosine phosphatase involved in leukocyte function. Leuk Lymphoma 35: 237-243.

GIEBEL B AND PUNZEL M. 2008. Lineage development of hematopoietic stem and progenitor cells. Biological chemistry 389: 813-824.

GILLILAND DG AND GRIFFIN JD. 2002. Role of FLT3 in leukemia. Current opinion in hematology 9: 274-281.

GODFREY R ET AL. 2012. Cell transformation by FLT3 ITD in acute myeloid leukemia involves oxidative inactivation of the tumor suppressor protein-tyrosine phosphatase DEP-1/ PTPRJ. Blood 119: 4499-4511.

GOLUB TR, BARKER GF, LOVETT M AND GILLILAND DG. 1994. Fusion of PDGF receptor beta to a novel ets-like gene, tel, in chronic myelomonocytic leukemia with t(5;12) chromosomal translocation. Cell 77: 307-316.

GRAZIA LAMPUGNANI M ET AL. 2003. Contact inhibition of VEGF-induced proliferation requires vascular endothelial cadherin, beta-catenin, and the phosphatase DEP-1/CD148. J Cell Biol 161: 793-804.

GREENBLATT S ET AL. 2012. Knock-in of a FLT3/ITD mutation cooperates with a NUP98-HOXD13 fusion to generate acute myeloid leukemia in a mouse model. Blood 119: 2883-2894.

GRIFFITH J, BLACK J, FAERMAN C, SWENSON L, WYNN M, LU F, LIPPKE J AND SAXENA K. 2004. The structural basis for autoinhibition of FLT3 by the juxtamembrane domain. Molecular cell 13: 169-178.

GRUNDLER R, MIETHING C, THIEDE C, PESCHEL C AND DUYSTER J. 2005. FLT3-ITD and tyrosine kinase domain mutants induce 2 distinct phenotypes in a murine bone marrow transplantation model. Blood 105: 4792-4799.

GUPTA N AND DEFRANCO AL. 2003. Visualizing lipid raft dynamics and early signaling events during antigen receptor-mediated B-lymphocyte activation. Molecular biology of the cell 14: 432-444.

HALL LR, STREULI M, SCHLOSSMAN SF AND SAITO H. 1988. Complete exon-intron organization of the human leukocyte common antigen (CD45) gene. J Immunol 141: 2781-2787.

HAYAKAWA F, TOWATARI M, KIYOI H, TANIMOTO M, KITAMURA T, SAITO H AND NAOE T. 2000. Tandem-duplicated Flt3 constitutively activates STAT5 and MAP kinase and introduces autonomous cell growth in IL-3-dependent cell lines. Oncogene 19: 624-631.

HAYLOCK DN ET AL. 1997. Increased recruitment of hematopoietic progenitor cells underlies the ex vivo expansion potential of FLT3 ligand. Blood 90: 2260-2272.

HENDRIKS WJ AND PULIDO R. 2013. Protein tyrosine phosphatase variants in human hereditary disorders and disease susceptibilities. Biochim Biophys Acta 1832: 1673-1696.

HIRAYAMA F, LYMAN SD, CLARK SC AND OGAWA M. 1995. The flt3 ligand supports proliferation of lymphohematopoietic progenitors and early B-lymphoid progenitors. Blood 85: 1762-1768.

HJERTSON M, SUNDSTRÖM C, LYMAN SD, NILSSON K AND NILSSON G. 1996. Stem cell factor, but not flt3 ligand, induces differentiation and activation of human mast cells. Experimental hematology 24: 748-754.

HOFFMANN B, SVENSSON CM, STRASSBURGER M, GEBSER B, IRMLER IM, KAMRADT T, PETER SALUZ H AND THILO FIGGE M. 2017. Automated Quantification of Early Bone Alterations and Pathological Bone Turnover in Experimental Arthritis by in vivo PET/CT Imaging. Scientific reports 7: 2217.

HOFMANN M ET AL. 2012. Generation, selection and preclinical characterization of an Fc-optimized FLT3 antibody for the treatment of myeloid leukemia. Leukemia 26: 1228-1237.

HOLMES N. 2006. CD45: all is not yet crystal clear. Immunology 117: 145-155.
HONDA H, INAZAWA J, NISHIDA J, YAZAKI Y AND HIRAI H. 1994. Molecular cloning, characterization, and chromosomal localization of a novel protein-tyrosine phosphatase, HPTP eta. Blood 84: 4186-4194.
HONDA H, SHIBUYA M, CHIBA S, YAZAKI Y AND HIRAI H. 1993. Identification of novel protein-tyrosine phosphatases in a human leukemia cell line, F-36P. Leukemia 7: 742-746.
HOWLADER N NA, KRAPCHO M, MILLER D, BISHOP K, KOSARY CL, YU M, RUHL J, TATALOVICH Z, MARIOTTO A, LEWIS DR, CHEN HS, FEUER EJ, CRONIN KA ,. 2017. SEER Cancer Statistics Review, 1975-2014. https://seercancergov/csr/1975_2014/.
HUDAK S, HUNTE B, CULPEPPER J, MENON S, HANNUM C, THOMPSON-SNIPES L AND RENNICK D. 1995. FLT3/FLK2 ligand promotes the growth of murine stem cells and the expansion of colony-forming cells and spleen colony-forming units. Blood 85: 2747-2755.
IGARASHI H, GREGORY SC, YOKOTA T, SAKAGUCHI N AND KINCADE PW. 2002. Transcription from the RAG1 locus marks the earliest lymphocyte progenitors in bone marrow. Immunity 17: 117-130.
IRIE-SASAKI J ET AL. 2001. CD45 is a JAK phosphatase and negatively regulates cytokine receptor signalling. Nature 409: 349-354.
IULIANO R, LE PERA I, CRISTOFARO C, BAUDI F, ARTURI F, PALLANTE P, MARTELLI ML, TRAPASSO F, CHIARIOTTI L AND FUSCO A. 2004. The tyrosine phosphatase PTPRJ/DEP-1 genotype affects thyroid carcinogenesis. Oncogene 23: 8432-8438.
IULIANO R ET AL. 2003. An adenovirus carrying the rat protein tyrosine phosphatase eta suppresses the growth of human thyroid carcinoma cell lines in vitro and in vivo. Cancer research 63: 882-886.
JACOBSEN M ET AL. 2000. A point mutation in PTPRC is associated with the development of multiple sclerosis. Nature genetics 26: 495-499.
JAYAVELU AK ET AL. 2016. NOX4-driven ROS formation mediates PTP inactivation and cell transformation in FLT3ITD-positive AML cells. Leukemia 30: 473-483.
JETANI H ET AL. 2018. CAR T-cells targeting FLT3 have potent activity against FLT3(-)ITD(+) AML and act synergistically with the FLT3-inhibitor crenolanib. Leukemia.
JULIEN SG, DUBE N, HARDY S AND TREMBLAY ML. 2011. Inside the human cancer tyrosine phosphatome. Nature reviews Cancer 11: 35-49.
JUNG Y ET AL. 2008. Hematopoietic stem cells regulate mesenchymal stromal cell induction into osteoblasts thereby participating in the formation of the stem cell niche. Stem cells (Dayton, Ohio) 26: 2042-2051.
JUSTEMENT LB, CAMPBELL KS, CHIEN NC AND CAMBIER JC. 1991. Regulation of B cell antigen receptor signal transduction and phosphorylation by CD45. Science (New York, NY) 252: 1839-1842.
KANE EV, ROMAN E, CARTWRIGHT R, PARKER J AND MORGAN G. 1999. Tobacco and the risk of acute leukaemia in adults. British journal of cancer 81: 1228-1233.
KAYSER S ET AL. 2009. Insertion of FLT3 internal tandem duplication in the tyrosine kinase domain-1 is associated with resistance to chemotherapy and inferior outcome. Blood 114: 2386-2392.
KEANE MM, LOWREY GA, ETTENBERG SA, DAYTON MA AND LIPKOWITZ S. 1996. The protein tyrosine phosphatase DEP-1 is induced during differentiation and inhibits growth of breast cancer cells. Cancer research 56: 4236-4243.
KELLY LM AND GILLILAND DG. 2002. Genetics of myeloid leukemias. Annual review of genomics and human genetics 3: 179-198.
KELLY LM, LIU Q, KUTOK JL, WILLIAMS IR, BOULTON CL AND GILLILAND DG. 2002. FLT3 internal tandem duplication mutations associated with human acute myeloid leukemias induce myeloproliferative disease in a murine bone marrow transplant model. Blood 99: 310-318.

KIKUSHIGE Y ET AL. 2008. Human Flt3 is expressed at the hematopoietic stem cell and the granulocyte/macrophage progenitor stages to maintain cell survival. J Immunol 180: 7358-7367.

KIM Y, YOON S, KIM SJ, KIM JS, CHEONG JW AND MIN YH. 2012. Myeloperoxidase expression in acute myeloid leukemia helps identifying patients to benefit from transplant. Yonsei Med J 53: 530-536.

KISHIHARA K ET AL. 1993. Normal B lymphocyte development but impaired T cell maturation in CD45-exon6 protein tyrosine phosphatase-deficient mice. Cell 74: 143-156.

KIYOI H AND NAOE T. 2006. Biology, clinical relevance, and molecularly targeted therapy in acute leukemia with FLT3 mutation. Int J Hematol 83: 301-308.

KIYOI H, TOWATARI M, YOKOTA S, HAMAGUCHI M, OHNO R, SAITO H AND NAOE T. 1998. Internal tandem duplication of the FLT3 gene is a novel modality of elongation mutation which causes constitutive activation of the product. Leukemia 12: 1333-1337.

KOCH S, JACOBI A, RYSER M, EHNINGER G AND THIEDE C. 2008. Abnormal localization and accumulation of FLT3-ITD, a mutant receptor tyrosine kinase involved in leukemogenesis. Cells, tissues, organs 188: 225-235.

KOVALENKO M, DENNER K, SANDSTRÖM J, PERSSON C, GROSS S, JANDT E, VILELLA R, BÖHMER F AND ÖSTMAN A. 2000. Site-selective dephosphorylation of the platelet-derived growth factor beta-receptor by the receptor-like protein-tyrosine phosphatase DEP-1. The Journal of biological chemistry 275: 16219-16226.

KUNG C ET AL. 2000. Mutations in the tyrosine phosphatase CD45 gene in a child with severe combined immunodeficiency disease. Nat Med 6: 343-345.

KURAMOCHI S, MATSUDA S, MATSUDA Y, SAITOH T, OHSUGI M AND YAMAMOTO T. 1996. Molecular cloning and characterization of Byp, a murine receptor-type tyrosine phosphatase similar to human DEP-1. FEBS letters 378: 7-14.

LAGUNAS-RANGEL FA, CHAVEZ-VALENCIA V, GOMEZ-GUIJOSA MA AND CORTES-PENAGOS C. 2017. Acute Myeloid Leukemia-Genetic Alterations and Their Clinical Prognosis. International journal of hematology-oncology and stem cell research 11: 328-339.

LE PERA I, IULIANO R, FLORIO T, SUSINI C, TRAPASSO F, SANTORO M, CHIARIOTTI L, SCHETTINI G, VIGLIETTO G AND FUSCO A. 2016. The rat tyrosine phosphatase eta increases cell adhesion by activating c-Src through dephosphorylation of its inhibitory phosphotyrosine residue. Oncogene 35: 5456.

LEE BH ET AL. 2007. FLT3 mutations confer enhanced proliferation and survival properties to multipotent progenitors in a murine model of chronic myelomonocytic leukemia. Cancer Cell 12: 367-380.

LEISCHNER H, ALBERS C, GRUNDLER R, RAZUMOVSKAYA E, SPIEKERMANN K, BOHLANDER S, RONNSTRAND L, GOTZE K, PESCHEL C AND DUYSTER J. 2012. SRC is a signaling mediator in FLT3-ITD- but not in FLT3-TKD-positive AML. Blood 119: 4026-4033.

LEUKEMIA AND LYMPHOMA SOCIETY. 2018. Chimeric Antigen Receptor (CAR) T-Cell Therapy [Online]. http://www.lls.org/treatment/types-of-treatment/immunotherapy/chimeric-antigen-receptor-car-t-cell-therapy. [Accessed 13th March 2018].

LEVIS M. 2017. Midostaurin approved for FLT3-mutated AML. Blood 129: 3403-3406.

LEVIS M ET AL. 2006. Plasma inhibitory activity (PIA): a pharmacodynamic assay reveals insights into the basis for cytotoxic response to FLT3 inhibitors. Blood 108: 3477-3483.

LI L, BAILEY E, GREENBLATT S, HUSO D AND SMALL D. 2011. Loss of the wild-type allele contributes to myeloid expansion and disease aggressiveness in FLT3/ITD knockin mice. Blood 118: 4935-4945.

LI L, PILOTO O, NGUYEN HB, GREENBERG K, TAKAMIYA K, RACKE F, HUSO D AND SMALL D. 2008. Knock-in of an internal tandem duplication mutation into

murine FLT3 confers myeloproliferative disease in a mouse model. Blood 111: 3849-3858.
LIESVELD JLMAL 2010. Acurte Myelogenous Leukemia Williams Hematology, p. Chapter 89.
LYMAN SD AND JACOBSEN SE. 1998. c-kit ligand and Flt3 ligand: stem/progenitor cell factors with overlapping yet distinct activities. Blood 91: 1101-1134.
MACKAREHTSCHIAN K, HARDIN JD, MOORE KA, BOAST S, GOFF SP AND LEMISCHKA IR. 1995. Targeted disruption of the flk2/flt3 gene leads to deficiencies in primitive hematopoietic progenitors. Immunity 3: 147-161.
MAJETI R, BILWES AM, NOEL JP, HUNTER T AND WEISS A. 1998. Dimerization-induced inhibition of receptor protein tyrosine phosphatase function through an inhibitory wedge. Science (New York, NY) 279: 88-91.
MASSENKEIL G, FIENE C, ROSEN O, MICHAEL R, REISINGER W AND ARNOLD R. 2001. Loss of bone mass and vitamin D deficiency after hematopoietic stem cell transplantation: standard prophylactic measures fail to prevent osteoporosis. Leukemia 15: 1701-1705.
MATTHEWS RJ, CAHIR ED AND THOMAS ML. 1990. Identification of an additional member of the protein-tyrosine-phosphatase family: evidence for alternative splicing in the tyrosine phosphatase domain. Proceedings of the National Academy of Sciences of the United States of America 87: 4444-4448.
MATTHEWS W, JORDAN CT, WIEGAND GW, PARDOLL D AND LEMISCHKA IR. 1991. A receptor tyrosine kinase specific to hematopoietic stem and progenitor cell-enriched populations. Cell 65: 1143-1152.
MEE PJ, TURNER M, BASSON MA, COSTELLO PS, ZAMOYSKA R AND TYBULEWICZ VL. 1999. Greatly reduced efficiency of both positive and negative selection of thymocytes in CD45 tyrosine phosphatase-deficient mice. European journal of immunology 29: 2923-2933.
MESHINCHI S AND APPELBAUM FR. 2009. Structural and functional alterations of FLT3 in acute myeloid leukemia. Clinical cancer research : an official journal of the American Association for Cancer Research 15: 4263-4269.
METZELER KH ET AL. 2008. An 86-probe-set gene-expression signature predicts survival in cytogenetically normal acute myeloid leukemia. Blood 112: 4193-4201.
MIZUKI M ET AL. 2000. Flt3 mutations from patients with acute myeloid leukemia induce transformation of 32D cells mediated by the Ras and STAT5 pathways. Blood 96: 3907-3914.
MIZUKI M ET AL. 2003. Suppression of myeloid transcription factors and induction of STAT response genes by AML-specific Flt3 mutations. Blood 101: 3164-3173.
MORI J, WANG YJ, ELLISON S, HEISING S, NEEL BG, TREMBLAY ML, WATSON SP AND SENIS YA. 2012. Dominant role of the protein-tyrosine phosphatase CD148 in regulating platelet activation relative to protein-tyrosine phosphatase-1B. Arterioscler Thromb Vasc Biol 32: 2956-2965.
MORROW DM, XIONG N, GETTY RR, RATAJCZAK MZ, MORGAN D, SEPPALA M, RIITTINEN L, GEWIRTZ AM AND TYKOCINSKI ML. 1994. Hematopoietic placental protein 14. An immunosuppressive factor in cells of the megakaryocytic lineage. Am J Pathol 145: 1485-1495.
MÜLLER JP, PETERMANN A, MAWRIN C AND BÖHMER F-D. 2012. Tumorzellen-Vehikel mit defekten Bremsen. BIOspektrum: 394-397.
NAKAHARA J, SEIWA C, TAN-TAKEUCHI K, GOTOH M, KISHIHARA K, OGAWA M, ASOU H AND AISO S. 2005. Involvement of CD45 in central nervous system myelination. Neuroscience letters 379: 116-121.
NAKAO M, YOKOTA S, IWAI T, KANEKO H, HORIIKE S, KASHIMA K, SONODA Y, FUJIMOTO T AND MISAWA S. 1996. Internal tandem duplication of the flt3 gene found in acute myeloid leukemia. Leukemia 10: 1911-1918.
OLESEN LH, AGGERHOLM A, ANDERSEN BL, NYVOLD CG, GULDBERG P, NORGAARD JM AND HOKLAND P. 2005. Molecular typing of adult acute myeloid leukaemia: significance of translocations, tandem duplications,

methylation, and selective gene expression profiling. British journal of haematology 131: 457-467.
ORTUSO F ET AL. 2013. Discovery of PTPRJ agonist peptides that effectively inhibit in vitro cancer cell proliferation and tube formation. ACS Chem Biol 8: 1497-1506.
OSHIKAWA G, NAGAO T, WU N, KUROSU T AND MIURA O. 2011. c-Cbl and Cbl-b ligases mediate 17-allylaminodemethoxygeldanamycin-induced degradation of autophosphorylated Flt3 kinase with internal tandem duplication through the ubiquitin proteasome pathway. The Journal of biological chemistry 286: 30263-30273.
ÖSTMAN A, HELLBERG C AND BÖHMER FD. 2006. Protein-tyrosine phosphatases and cancer. Nature reviews Cancer 6: 307-320.
ÖSTMAN A, YANG Q AND TONKS NK. 1994. Expression of DEP-1, a receptor-like protein-tyrosine-phosphatase, is enhanced with increasing cell density. Proceedings of the National Academy of Sciences of the United States of America 91: 9680-9684.
OZAWA Y, WILLIAMS AH, ESTES ML, MATSUSHITA N, BOSCHELLI F, JOVE R AND LIST AF. 2008. Src family kinases promote AML cell survival through activation of signal transducers and activators of transcription (STAT). Leukemia research 32: 893-903.
PADUANO F ET AL. 2012. Isolation and functional characterization of peptide agonists of PTPRJ, a tyrosine phosphatase receptor endowed with tumor suppressor activity. ACS Chem Biol 7: 1666-1676.
PALKA HL, PARK M AND TONKS NK. 2003. Hepatocyte growth factor receptor tyrosine kinase met is a substrate of the receptor protein-tyrosine phosphatase DEP-1. The Journal of biological chemistry 278: 5728-5735.
PAPAEMMANUIL E ET AL. 2016. Genomic Classification and Prognosis in Acute Myeloid Leukemia. The New England journal of medicine 374: 2209-2221.
PERRON M AND SARAGOVI H. 2018. Inhibition of CD45 phosphatase activity induces cell cycle arrest and apoptosis of CD45+ lymphoid tumors ex vivo and in vivo. Molecular pharmacology.
PINHEIRO RF, MOREIRA EDE S, SILVA MR, GREGGIO B, ALBERTO FL AND CHAUFFAILLE MDE L. 2007. FLT3 mutation and AML/ETO in a case of Myelodysplastic syndrome in transformation corroborates the two hit model of leukemogenesis. Leukemia research 31: 1015-1018.
PULIDO R AND SANCHEZ-MADRID F. 1992. Glycosylation of CD45: carbohydrate processing through Golgi apparatus is required for cell surface expression and protein stability. European journal of immunology 22: 463-468.
REITER K ET AL. 2018. Tyrosine kinase inhibition increases the cell surface localization of FLT3-ITD and enhances FLT3-directed immunotherapy of acute myeloid leukemia. Leukemia 32: 313-322.
REYA T, MORRISON SJ, CLARKE MF AND WEISSMAN IL. 2001. Stem cells, cancer, and cancer stem cells. Nature 414: 105-111.
RHEINLÄNDER A, SCHRAVEN B AND BOMMHARDT U. 2018. CD45 in human physiology and clinical medicine. Immunol Lett 196: 22-32.
RIVOLLIER A, MAZZORANA M, TEBIB J, PIPERNO M, AITSISELMI T, RABOURDIN-COMBE C, JURDIC P AND SERVET-DELPRAT C. 2004. Immature dendritic cell transdifferentiation into osteoclasts: a novel pathway sustained by the rheumatoid arthritis microenvironment. Blood 104: 4029-4037.
ROBERTS JL ET AL. 2012. CD45-deficient severe combined immunodeficiency caused by uniparental disomy. Proceedings of the National Academy of Sciences of the United States of America 109: 10456-10461.
ROBINSON DR, WU YM AND LIN SF. 2000. The protein tyrosine kinase family of the human genome. Oncogene 19: 5548-5557.
ROBINSON LJ, XUE J AND COREY SJ. 2005. Src family tyrosine kinases are activated by Flt3 and are involved in the proliferative effects of leukemia-associated Flt3 mutations. Experimental hematology 33: 469-479.

ROCNIK JL, OKABE R, YU JC, LEE BH, GIESE N, SCHENKEIN DP AND GILLILAND DG. 2006. Roles of tyrosine 589 and 591 in STAT5 activation and transformation mediated by FLT3-ITD. Blood 108: 1339-1345.

ROSNET O ET AL. 1996. Human FLT3/FLK2 receptor tyrosine kinase is expressed at the surface of normal and malignant hematopoietic cells. Leukemia 10: 238-248.

ROSNET O, MARCHETTO S, DELAPEYRIERE O AND BIRNBAUM D. 1991. Murine Flt3, a gene encoding a novel tyrosine kinase receptor of the PDGFR/CSF1R family. Oncogene 6: 1641-1650.

ROSNET O, SCHIFF C, PEBUSQUE MJ, MARCHETTO S, TONNELLE C, TOIRON Y, BIRG F AND BIRNBAUM D. 1993. Human FLT3/FLK2 gene: cDNA cloning and expression in hematopoietic cells. Blood 82: 1110-1119.

RUIVENKAMP CA ET AL. 2002. Ptprj is a candidate for the mouse colon-cancer susceptibility locus Scc1 and is frequently deleted in human cancers. Nature genetics 31: 295-300.

SACCO F, TINTI M, PALMA A, FERRARI E, NARDOZZA AP, HOOFT VAN HUIJSDUIJNEN R, TAKAHASHI T, CASTAGNOLI L AND CESARENI G. 2009. Tumor suppressor density-enhanced phosphatase-1 (DEP-1) inhibits the RAS pathway by direct dephosphorylation of ERK1/2 kinases. The Journal of biological chemistry 284: 22048-22058.

SALLMYR A, FAN J, DATTA K, KIM KT, GROSU D, SHAPIRO P, SMALL D AND RASSOOL F. 2008. Internal tandem duplication of FLT3 (FLT3/ITD) induces increased ROS production, DNA damage, and misrepair: implications for poor prognosis in AML. Blood 111: 3173-3182.

SANJANA NE, SHALEM O AND ZHANG F. 2014. Improved vectors and genome-wide libraries for CRISPR screening. Nature methods 11: 783-784.

SAPOZHNIKOVA V. 2017. Activation of agonistic RPTP DEP-1 (CD148) to control FLT3-ITD. Master Thesis, Friedrich-Schiller University.

SATO T, FURUKAWA K, AUTERO M, GAHMBERG CG AND KOBATA A. 1993. Structural study of the sugar chains of human leukocyte common antigen CD45. Biochemistry 32: 12694-12704.

SCHESSL C ET AL. 2005. The AML1-ETO fusion gene and the FLT3 length mutation collaborate in inducing acute leukemia in mice. J Clin Invest 115: 2159-2168.

SCHINDLER K. 2010. Biogenese des Wildtyp- und onkogenen Flt3-Proteins Diplom Diplomarbeit, Friedrich-Schiller Universität Jena.

SCHLENK RF ET AL. 2008. Mutations and treatment outcome in cytogenetically normal acute myeloid leukemia. The New England journal of medicine 358: 1909-1918.

SCHMIDT-ARRAS D, BÖHMER SA, KOCH S, MÜLLER JP, BLEI L, CORNILS H, BAUER R, KORASIKHA S, THIEDE C AND BÖHMER FD. 2009. Anchoring of FLT3 in the endoplasmic reticulum alters signaling quality. Blood 113: 3568-3576.

SCHMIDT-ARRAS DE, BÖHMER A, MARKOVA B, CHOUDHARY C, SERVE H AND BÖHMER FD. 2005. Tyrosine phosphorylation regulates maturation of receptor tyrosine kinases. Molecular and cellular biology 25: 3690-3703.

SCHNEBLE N, MULLER J, KLICHE S, BAUER R, WETZKER R, BOHMER FD, WANG ZQ AND MULLER JP. 2017. The protein-tyrosine phosphatase DEP-1 promotes migration and phagocytic activity of microglial cells in part through negative regulation of fyn tyrosine kinase. Glia 65: 416-428.

SCHNITTGER S ET AL. 2002. Analysis of FLT3 length mutations in 1003 patients with acute myeloid leukemia: correlation to cytogenetics, FAB subtype, and prognosis in the AMLCG study and usefulness as a marker for the detection of minimal residual disease. Blood 100: 59-66.

SCHULTE C, BEELEN DW, SCHAEFER UW AND MANN K. 2000. Bone loss in long-term survivors after transplantation of hematopoietic stem cells: a prospective study. Osteoporosis international : a journal established as result of cooperation between the European Foundation for Osteoporosis and the National Osteoporosis Foundation of the USA 11: 344-353.

SEITA J AND WEISSMAN IL. 2010. Hematopoietic stem cell: self-renewal versus differentiation. Wiley interdisciplinary reviews Systems biology and medicine 2: 640-653.

SELL S. 2005. Leukemia: stem cells, maturation arrest, and differentiation therapy. Stem cell reviews 1: 197-205.

SENIS YA ET AL. 2009. The tyrosine phosphatase CD148 is an essential positive regulator of platelet activation and thrombosis. Blood 113: 4942-4954.

SHIVTIEL S ET AL. 2008. CD45 regulates retention, motility, and numbers of hematopoietic progenitors, and affects osteoclast remodeling of metaphyseal trabecules. The Journal of experimental medicine 205: 2381-2395.

SINGH DK, KUMAR D, SIDDIQUI Z, BASU SK, KUMAR V AND RAO KV. 2005. The strength of receptor signaling is centrally controlled through a cooperative loop between Ca2+ and an oxidant signal. Cell 121: 281-293.

SKRZYPCZYNSKA KATARZYNA M, ZHU JING W AND WEISS A. 2016. Positive Regulation of Lyn Kinase by CD148 Is Required for B Cell Receptor Signaling in B1 but Not B2 B Cells. Immunity.

SMALL D ET AL. 1994. STK-1, the human homolog of Flk-2/Flt-3, is selectively expressed in CD34+ human bone marrow cells and is involved in the proliferation of early progenitor/stem cells. Proceedings of the National Academy of Sciences of the United States of America 91: 459-463.

SMITH SM, LE BEAU MM, HUO D, KARRISON T, SOBECKS RM, ANASTASI J, VARDIMAN JW, ROWLEY JD AND LARSON RA. 2003. Clinical-cytogenetic associations in 306 patients with therapy-related myelodysplasia and myeloid leukemia: the University of Chicago series. Blood 102: 43-52.

SPRING K, CHABOT C, LANGLOIS S, LAPOINTE L, TRINH NT, CARON C, HEBDA JK, GAVARD J, ELCHEBLY M AND ROYAL I. 2012. Tyrosine phosphorylation of DEP-1/CD148 as a mechanism controlling Src kinase activation, endothelial cell permeability, invasion, and capillary formation. Blood 120: 2745-2756.

SPRING K, FOURNIER P, LAPOINTE L, CHABOT C, ROUSSY J, POMMEY S, STAGG J AND ROYAL I. 2015. The protein tyrosine phosphatase DEP-1/PTPRJ promotes breast cancer cell invasion and metastasis. Oncogene 34: 5536-5547.

STEINER M 2017. SYNIMMUNE GmbH Initiates First-in-Human Study of Fc-Optimized Antibody FLYSYN for the Treatment of Acute Myeloid Leukemia

STIREWALT DL AND RADICH JP. 2003. The role of FLT3 in haematopoietic malignancies. Nature reviews Cancer 3: 650-665.

STONE JD, CONROY LA, BYTH KF, HEDERER RA, HOWLETT S, TAKEMOTO Y, HOLMES N AND ALEXANDER DR. 1997. Aberrant TCR-mediated signaling in CD45-null thymocytes involves dysfunctional regulation of Lck, Fyn, TCR-zeta, and ZAP-70. J Immunol 158: 5773-5782.

STONE RM ET AL. 2017. Midostaurin plus Chemotherapy for Acute Myeloid Leukemia with a FLT3 Mutation. The New England journal of medicine 377: 454-464.

STOPP S. 2009. Einfluss der Protein-Tyrosin-Phosphatasen DEP-1 und CD45 auf das Tyrosin-Phosphorylierungsmuster der Rezeptor-Tyrosinkinase FLT3. Diplomarbeit, Friedrich-Schiller-University.

STREULI M, KRUEGER NX, THAI T, TANG M AND SAITO H. 1990. Distinct functional roles of the two intracellular phosphatase like domains of the receptor-linked protein tyrosine phosphatases LCA and LAR. Embo j 9: 2399-2407.

SVENSSON CM, HOFFMANN B, IRMLER IM, STRASSBURGER M, FIGGE MT AND SALUZ HP. 2017. Quantification of arthritic bone degradation by analysis of 3D micro-computed tomography data. Scientific reports 7: 44434.

SVENSSON MN, ERLANDSSON MC, JONSSON IM, ANDERSSON KM AND BOKAREWA MI. 2016. Impaired signaling through the Fms-like tyrosine kinase 3 receptor increases osteoclast formation and bone damage in arthritis. J Leukoc Biol 99: 413-423.

SZVETKO AL, JONES A, MACKENZIE J, TAJOURI L, CSURHES PA, GREER JM, PENDER MP AND GRIFFITHS LR. 2009. An investigation of the C77G and

C772T variations within the human protein tyrosine phosphatase receptor type C gene for association with multiple sclerosis in an Australian population. Brain research 1255: 148-152.

TAKAHASHI K, MERNAUGH RL, FRIEDMAN DB, WELLER R, TSUBOI N, YAMASHITA H, QUARANTA V AND TAKAHASHI T. 2012. Thrombospondin-1 acts as a ligand for CD148 tyrosine phosphatase. Proceedings of the National Academy of Sciences of the United States of America 109: 1985-1990.

TAKAHASHI S. 2011. Downstream molecular pathways of FLT3 in the pathogenesis of acute myeloid leukemia: biology and therapeutic implications. Journal of hematology & oncology 4: 13.

TAKAHASHI T, TAKAHASHI K, ST JOHN PL, FLEMING PA, TOMEMORI T, WATANABE T, ABRAHAMSON DR, DRAKE CJ, SHIRASAWA T AND DANIEL TO. 2003. A mutant receptor tyrosine phosphatase, CD148, causes defects in vascular development. Molecular and cellular biology 23: 1817-1831.

TAN J, TOWN T, MORI T, WU Y, SAXE M, CRAWFORD F AND MULLAN M. 2000. CD45 opposes beta-amyloid peptide-induced microglial activation via inhibition of p44/42 mitogen-activated protein kinase. The Journal of neuroscience : the official journal of the Society for Neuroscience 20: 7587-7594.

TANGYE SG, WU J, AVERSA G, DE VRIES JE, LANIER LL AND PHILLIPS JH. 1998. Negative regulation of human T cell activation by the receptor-type protein tyrosine phosphatase CD148. J Immunol 161: 3803-3807.

TAUTZ L, CRITTON DA AND GROTEGUT S. 2013. Protein tyrosine phosphatases: structure, function, and implication in human disease. Methods Mol Biol 1053: 179-221.

TCHILIAN EZ, WALLACE DL, DAWES R, IMAMI N, BURTON C, GOTCH F AND BEVERLEY PC. 2001a. A point mutation in CD45 may be associated with an increased risk of HIV-1 infection. AIDS (London, England) 15: 1892-1894.

TCHILIAN EZ, WALLACE DL, WELLS RS, FLOWER DR, MORGAN G AND BEVERLEY PC. 2001b. A deletion in the gene encoding the CD45 antigen in a patient with SCID. J Immunol 166: 1308-1313.

THOMAS M, SHACKELFORD D, RALPH S AND TROWBRIDGE I. 1987. Structural studies of T200 glycoprotein and the IL-2 receptor. J Recept Res 7: 133-155.

THOMAS ML. 1989. The leukocyte common antigen family. Annu Rev Immunol 7: 339-369.

THOMAS ML, BARCLAY AN, GAGNON J AND WILLIAMS AF. 1985. Evidence from cDNA clones that the rat leukocyte-common antigen (T200) spans the lipid bilayer and contains a cytoplasmic domain of 80,000 Mr. Cell 41: 83-93.

THOMAS ML AND BROWN EJ. 1999. Positive and negative regulation of Src-family membrane kinases by CD45. Immunol Today 20: 406-411.

THUDE H, HUNDRIESER J, WONIGEIT K AND SCHWINZER R. 1995. A point mutation in the human CD45 gene associated with defective splicing of exon A. European journal of immunology 25: 2101-2106.

TONKS NK. 2006. Protein tyrosine phosphatases: from genes, to function, to disease. Nat Rev Mol Cell Biol 7: 833-846.

TONKS NK, CHARBONNEAU H, DILTZ CD, FISCHER EH AND WALSH KA. 1988. Demonstration that the leukocyte common antigen CD45 is a protein tyrosine phosphatase. Biochemistry 27: 8695-8701.

TRAPASSO F ET AL. 2006. Genetic ablation of Ptprj, a mouse cancer susceptibility gene, results in normal growth and development and does not predispose to spontaneous tumorigenesis. DNA Cell Biol 25: 376-382.

TRAPASSO F, IULIANO R, BOCCIA A, STELLA A, VISCONTI R, BRUNI P, BALDASSARRE G, SANTORO M, VIGLIETTO G AND FUSCO A. 2000. Rat protein tyrosine phosphatase eta suppresses the neoplastic phenotype of retrovirally transformed thyroid cells through the stabilization of p27(Kip1). Molecular and cellular biology 20: 9236-9246.

TRAPASSO F ET AL. 2004. Restoration of receptor-type protein tyrosine phosphatase eta function inhibits human pancreatic carcinoma cell growth in vitro and in vivo. Carcinogenesis 25: 2107-2114.

TROWBRIDGE IS, OSTERGAARD HL AND JOHNSON P. 1991. CD45: a leukocyte-specific member of the protein tyrosine phosphatase family. Biochim Biophys Acta 1095: 46-56.

TROWBRIDGE IS, RALPH P AND BEVAN MJ. 1975. Differences in the surface proteins of mouse B and T cells. Proceedings of the National Academy of Sciences of the United States of America 72: 157-161.

TROWBRIDGE IS AND THOMAS ML. 1994. CD45: an emerging role as a protein tyrosine phosphatase required for lymphocyte activation and development. Annu Rev Immunol 12: 85-116.

TSE KF, ALLEBACH J, LEVIS M, SMITH BD, BÖHMER FD AND SMALL D. 2002. Inhibition of the transforming activity of FLT3 internal tandem duplication mutants from AML patients by a tyrosine kinase inhibitor. Leukemia 16: 2027-2036.

TSUCHIDA R ET AL. 2014. BMP4/Thrombospondin-1 loop paracrinically inhibits tumor angiogenesis and suppresses the growth of solid tumors. Oncogene 33: 3803-3811.

ULLRICH A AND SCHLESSINGER J. 1990. Signal transduction by receptors with tyrosine kinase activity. Cell 61: 203-212.

VALK PJ ET AL. 2004. Prognostically useful gene-expression profiles in acute myeloid leukemia. The New England journal of medicine 350: 1617-1628.

VARDIMAN JW ET AL. 2009. The 2008 revision of the World Health Organization (WHO) classification of myeloid neoplasms and acute leukemia: rationale and important changes. Blood 114: 937-951.

VERSTRAETE K AND SAVVIDES SN. 2012. Extracellular assembly and activation principles of oncogenic class III receptor tyrosine kinases. Nature reviews Cancer 12: 753-766.

VORONOV I AND MANOLSON MF. 2016. Editorial: Flt3 ligand-friend or foe? Journal of leukocyte biology 99: 401-403.

WANG Y, GUO W, LIANG L AND ESSELMAN WJ. 1999. Phosphorylation of CD45 by casein kinase 2. Modulation of activity and mutational analysis. The Journal of biological chemistry 274: 7454-7461.

WANG Y ET AL. 2018. Targeting FLT3 in acute myeloid leukemia using ligand-based chimeric antigen receptor-engineered T cells. Journal of hematology & oncology 11: 60.

WEIDNER H ET AL. 2017. Myelodysplastic syndromes and bone loss in mice and men. Leukemia 31: 1003-1007.

WEIJLAND A, NEUBAUER G, COURTNEIDGE SA, MANN M, WIERENGA RK AND SUPERTI-FURGA G. 1996. The purification and characterization of the catalytic domain of Src expressed in Schizosaccharomyces pombe. Comparison of unphosphorylated and tyrosine phosphorylated species. European journal of biochemistry 240: 756-764.

WHITEFORD JR, XIAN X, CHAUSSADE C, VANHAESEBROECK B, NOURSHARGH S AND COUCHMAN JR. 2011. Syndecan-2 is a novel ligand for the protein tyrosine phosphatase receptor CD148. Molecular biology of the cell 22: 3609-3624.

XU Z AND WEISS A. 2002. Negative regulation of CD45 by differential homodimerization of the alternatively spliced isoforms. Nat Immunol 3: 764-771.

YAMAMOTO Y ET AL. 2001. Activating mutation of D835 within the activation loop of FLT3 in human hematologic malignancies. Blood 97: 2434-2439.

YUDUSHKIN IA, SCHLEIFENBAUM A, KINKHABWALA A, NEEL BG, SCHULTZ C AND BASTIAENS PI. 2007. Live-cell imaging of enzyme-substrate interaction reveals spatial regulation of PTP1B. Science (New York, NY) 315: 115-119.

ZHANG S, FUKUDA S, LEE Y, HANGOC G, COOPER S, SPOLSKI R, LEONARD WJ AND BROXMEYER HE. 2000. Essential role of signal transducer and activator of

transcription (Stat)5a but not Stat5b for Flt3-dependent signaling. The Journal of experimental medicine 192: 719-728.

ZHAO M, KIYOI H, YAMAMOTO Y, ITO M, TOWATARI M, OMURA S, KITAMURA T, UEDA R, SAITO H AND NAOE T. 2000. In vivo treatment of mutant FLT3-transformed murine leukemia with a tyrosine kinase inhibitor. Leukemia 14: 374-378.

ZHU JW, BRDICKA T, KATSUMOTO TR, LIN J AND WEISS A. 2008. Structurally distinct phosphatases CD45 and CD148 both regulate B cell and macrophage immunoreceptor signaling. Immunity 28: 183-196.

ZIKHERMAN J, DOAN K, PARAMESWARAN R, RASCHKE W AND WEISS A. 2012. Quantitative differences in CD45 expression unmask functions for CD45 in B-cell development, tolerance, and survival. Proceedings of the National Academy of Sciences of the United States of America 109: E3-12.

8. Appendices

8.1 Ehrenwörtliche Erklärung

Hiermit erkläre ich,

dass mir die Promotionsordnung der Medizinischen Fakultät der Friedrich-Schiller-Universität bekannt ist,

dass ich die Dissertation selbst angefertigt habe und alle von mir benutzten Hilfsmittel, persönlichen Mitteilungen und Quellen in meiner Arbeit angegeben sind,

mich folgende Personen bei der Auswahl und Auswertung des Materials sowie bei der Herstellung des Manuskripts unterstützt haben: PD Jörg P. Müller, Prof. Frank-D-Böhmer,

dass die Hilfe eines Promotionsberaters nicht in Anspruch genommen wurde und dass Dritte weder unmittelbar noch mittelbar geldwerte Leistungen von mir für Arbeiten erhalten haben, die im Zusammenhang mit dem Inhalt der vorgelegten Dissertation stehen,

dass ich die Dissertation noch nicht als Prüfungsarbeit für eine staatliche oder andere wissenschaftliche Prüfung eingereicht habe und

dass ich die gleiche, eine in wesentlichen Teilen ähnliche oder eine andere Abhandlung nicht bei einer anderen Hochschule als Dissertation eingereicht habe.

Ort, Datum Unterschrift des Verfassers

8.2 Figures